NASA Tech Briefs

Official Publication of the
National Aeronautics and
Space Administration
Volume 16 Number 4

Transferring Technology
to Industry and
Government
April 1992

SUPERCONDUCTIVITY:
The State Of The Art

TO-5 RELAY

The Unforgettable Maglatch TO-5

- Non-destructive memory
- Low power consumption
- Inherently bi-stable pulse operation
- CMOS compatible Centigrid® version

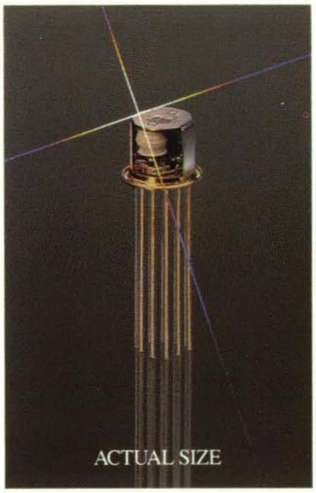

The Maglatch TO-5. It's a legend in its own time. The little magnetic latching relay that just won't forget. It can't. Because once you set it with a brief pulse of coil voltage, it simply stays in that state until reset. Even if the system loses power.

In applications where power drain is critical, the Maglatch TO-5 is unbeatable. Since no holding power is needed, it uses less energy than any other type of relay on the market.

The Maglatch's inherently low intercontact capacitance gives it high isolation and low insertion loss up through UHF, making it ideal for RF switching applications. And its tiny footprint makes it ideal for high density printed circuit boards.

The Maglatch TO-5 comes in commercial/industrial versions as well as military versions qualified to "L," "M" and "P" levels of MIL-R-39016. And now it comes in a CMOS compatible version as well. This version can be driven directly with CMOS level signals, with no outside amplification. That cuts down on the number of components and connections, for even greater system reliability.

The Maglatch TO-5. It's the world's smallest relay with indestructible memory. Call or write today for complete information.

TELEDYNE RELAYS
Innovations In Switching Technology

Home Office, 12525 Daphne Avenue, Hawthorne, CA 90250 • Telephone: 213-777-0077 • FAX: 213-779-9161

U.S. REGIONAL SALES OFFICES: EASTERN: (908) 272-0020, **SOUTHEAST:** (407) 682-9044, **NORTH CENTRAL:** (708) 529-1060, **CENTRAL:** (214) 348-0898, **WESTERN:** (408) 978-8899.
OVERSEAS: GERMANY, 0611-7636-0, **ENGLAND:** (081) 571-9596, **FRANCE:** 47-61-08-08, **BELGIUM:** (02) 673-99-88, **JAPAN:** (3) 3797-6956.

Circle Reader Action No. 348

INTRODUCING GENERIC CADD 6.0

FULL-TIME CADD AVAILABLE FOR PART-TIME WORK.

UPGRADES AVAILABLE

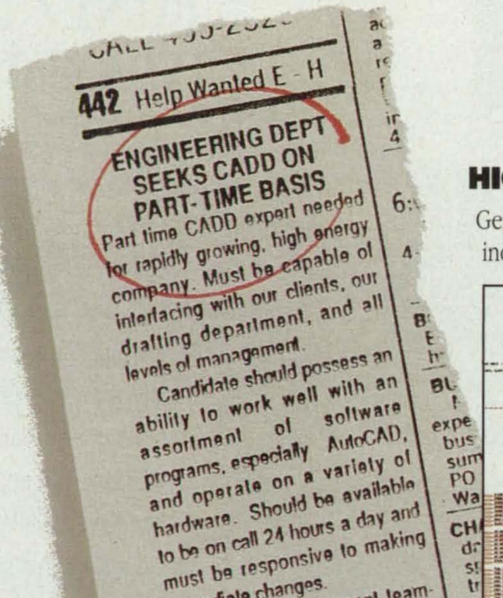
CALL 455-2525

442 Help Wanted E - H

ENGINEERING DEPT SEEKS CADD ON PART-TIME BASIS

Part time CADD expert needed for rapidly growing, high energy company. Must be capable of interfacing with our clients, our drafting department, and all levels of management.

Candidate should possess an ability to work well with an assortment of software programs, especially AutoCAD, and operate on a variety of hardware. Should be available to be on call 24 hours a day and must be responsive to making immediate changes.

We offer a pleasant team-oriented work atmosphere in a modern well-equipped facility, opportunity for advancement and a host of benefits. Send resumes and work samples to:

PreCision Manufacturing
11911 34th Avenue
Seattle, WA 98011
206/487-2233

EXECUTIVE DIRECTOR

Generic CADD® 6.0 is a feature-rich computer-aided design and drafting tool for those who want high-end performance at a reasonable price. It's ideal for the busy engineer or designer who may require CADD just part of the time. Today, Generic CADD offers more power than ever.

IMPORT AUTOCAD FILES DIRECTLY

With Generic CADD 6.0 you can easily import 2D files from AutoCAD®-based designers and drafting departments. Plus, its fast DXF In/Out feature lets you work with a myriad of popular CAD, CAM, CAE and GIS software.

NEW FEATURES AND EASE OF USE

Generic CADD 6.0 has a new macro programming language to help you eliminate repetitive commands. Or even create new features. A multi-view option lets you split the screen into windows, each having a different zoom factor. Its bill-of-material generator builds parts lists and reports. And thanks to extensive online help and all-new tutorial, you'll be productive in just hours.

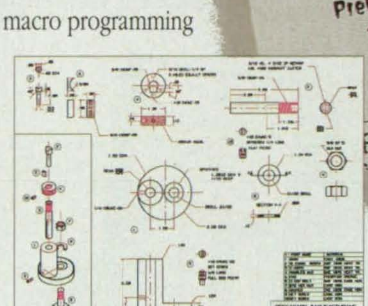

Produce professional drawings from initial concepts to finished production blueprints.

HIGHLY COMPATIBLE

Generic CADD 6.0 runs on standard desktop PCs, including XTs, ATs, 386s and even laptops. Plus, it works with leading word processors, desktop publishers and draw and paint programs. Such as WordPerfect, PageMaker and CorelDraw.

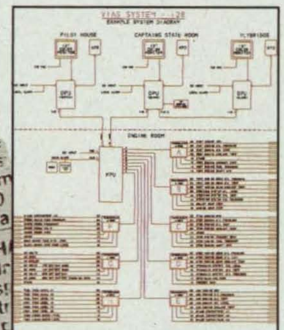

Easily generate process flow, system diagrams and schematics.

PRICED RIGHT—EVEN FOR PART-TIME WORK

At $495, you can easily justify the cost of Generic CADD 6.0, even if you use it only part of the time. It's so affordable every engineer can have a copy.

For more information or the name of a Generic CADD retailer near you, call us at

1-800-228-3601, Ext. 803.

PC MAGAZINE EDITORS' CHOICE
December 17, 1991
Generic CADD 5.0

"For pure ease of use, power, and speed at a reasonable price, Generic CADD is hard to beat."
PC Magazine 12/17/91

AUTODESK

Circle Reader Action No. 420


LabWindows
Instrument Library
TEAC

1. Install Data Acquisition Board
2. Turn on Computer
3. Launch LabWindows

When you start LabWindows®, you'll have all the software you need to develop your data acquisition and control system. LabWindows is a data acquisition, data analysis, and graphical presentation system – all in one. And it's backed by a complete line of plug-in boards and SCXI signal conditioning modules.

The Choice for Data Acquisition
With LabWindows, you can use any National Instruments plug-in board ranging from low-cost to high performance. Select from A/D, D/A, digital I/O, timing I/O, or DSP boards for the PC/XT/AT/EISA and IBM PS/2. And now, with our *DAQ Designer*™ system configuration software tool, you can easily determine the best plug-in boards and signal conditioning products for your application.

If you're ready to launch your data acquisition development, *Take a Look at LabWindows.*

For a **free** LabWindows Demo disk and your **free** copy of DAQ Designer call us at **(512) 794-0100** or **(800) 433-3488** (U. S. and Canada)

NATIONAL INSTRUMENTS®
The Software is the Instrument®

6504 Bridge Point Parkway
Austin, TX 78730-5039
Fax: (512) 794-8411

BRANCH OFFICES AUSTRALIA 03 879 9422 • **BELGIUM** 02 757 00 20 • **CANADA** 519 622 9310 • **DENMARK** 45 76 73 22 • **FRANCE** 1 48 65 33 70 • **GERMANY** 089 714 50 93 **ITALY** 02 48301892 • **JAPAN** 03 37881921 • **NETHERLANDS** 01720 45761 • **NORWAY** 03 846866 • **SPAIN** 91 896 0675 • **SWEDEN** 08 98 49 70 • **SWITZERLAND** 056 45 58 80 • **U.K.** 0635 523545

Circle Reader Action No. 681

2048 x 2048 Pixel, 12-Bit Digital CCD Camera

Photometrics introduces the world's first **2048 x 2048 pixel CCD camera** with a direct digital output and 12 bits per pixel (4096 gray levels). This ultra-high resolution camera interfaces directly to Macintosh II, 286/386 AT bus computers, or VME-based systems.

This camera features:

- A scientific-grade CCD image sensor with 2048 x 2048 pixels (Eastman Kodak KAF-4200)
- Thermoelectrically cooled camera head providing 12-bit dynamic range (4096 gray levels per pixel)
- A direct digital interface, plug-in programmable controller for Macintosh II, 286/386 AT bus, or VME computers
- Software for camera control, image acquisition, and calibration

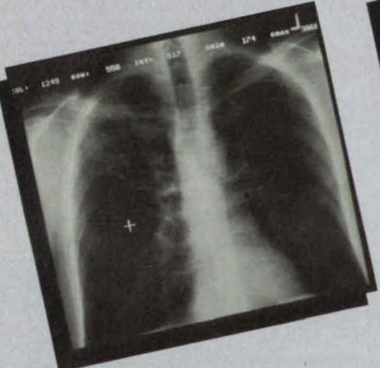

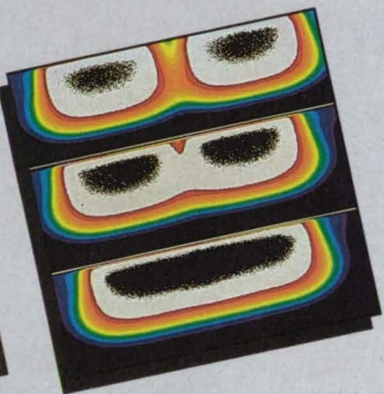

This camera can be used for high-resolution, low light applications including x-ray imaging and densitometry. (Image on right courtesy of the Medical College of Georgia.)

This new Photometrics camera is ideal for use in film digitization, electron and optical microscopy, medical diagnostic imaging (with phosphor screens), photodigitization, color separation, densitometry, and other applications demanding high resolution and high dynamic range.

Photometrics has a complete line of cooled CCD cameras from 512 x 512 to 2048 x 2048 pixels with 12, 14, or 16 bits per pixel. For end-user and OEM applications assistance, please call **(602) 889-9933.**

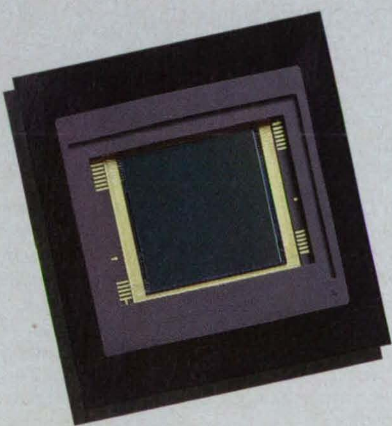

KAF-4200 CCD
(2048 x 2048 pixels)

Photometrics
World Leader in High Performance CCD Imaging

Circle Reader Action No. 562

Also in Europe: Photometrics GmbH, Sollner Str. 61
D-8000 München 71, Germany, Telefax: 0 89-79-97-15, Telephone: 0 89-79-95-80
ARGENTINA: Laser Optics S.A., tel: 01-466-754 ■ **FRANCE:** Sofretec, tel: 1-34-23-30-00
ISRAEL: New Technology RK Ltd., tel: 03-324181 ■ **JAPAN:** Seki Technotron Corp., tel: 03-3820-1712
KOREA: Eusung International Corp., tel: 02-785-1368 ■ **TAIWAN:** Gorman Co., Ltd. tel: 02-392-3170
SINGAPORE: Astro Scientific Centre, tel: 567-4163

Photometrics, Ltd.
3440 East Britannia Drive • Tucson, Arizona 85706
FAX: (602) 573-1944 • Telephone: (602) 889-9933

NASA Tech Briefs
Transferring Technology to Industry and Government

April 1992
Volume 16 Number 4 ABP BPA

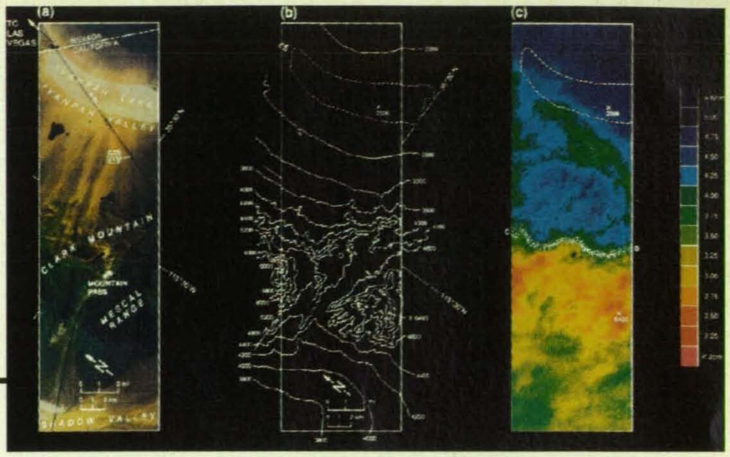

Photo courtesy JPL

Measurements of atmospheric water vapor by NASA's AVIRIS spectrometer are turned into high-resolution maps useful in meteorology, climatology, and agriculture. The figure above illustrates the results of airborne mapping in a desert area in eastern California. Computed column abundances of water vapor (right) were compared with a composite three-wavelength image (left) and a topographical map (middle). The column abundances were found to conform to topography and to decrease with surface elevation. *See the tech brief on page 55.*

SPECIAL FEATURE

TECHNICAL SECTION

DEPARTMENTS

On The Cover: Reflected differential interference contrast photomicrograph highlights the surface details of the high-temperature superconducting ceramic $Bi_2Sr_2CaCu_2O_x$. This material is being widely investigated due to its unusually high critical temperature for superconductivity. To learn how NASA is applying such superconductors to space projects, turn to page 12.
(Photomicrograph courtesy Michael W. Davidson, Florida State University)

Jet Propulsion Laboratory researchers have produced an optical phase-locked loop (page 40) that achieves a phase-error variance of less than .05 mrad$_2$ with a narrow band loop. The system offers applications in fiber optic communications, navigation, and scientific instrumentation. Photo courtesy JPL

NASA Tech Briefs, ISSN 0145-319X, USPS 750-070, copyright © 1992 in U.S., is published monthly by Associated Business Publications Co., Ltd., 41 E. 42nd St., New York, NY 10017-5391. The copyrighted information does not include the (U. S. rights to) individual tech briefs which are supplied by NASA. Editorial, sales, production and circulation offices at 41 East 42nd Street, New York, NY 10017-5391. Subscription for non-qualified subscribers in the U.S., Panama Canal Zone, and Puerto Rico, $75.00 for 1 year; $125.00 for 2 years; $200.00 for 3 years. Single copies $10.00. Foreign subscriptions one-year U.S. Funds $150.00. Remit by check, draft, postal, express orders or VISA, MasterCard, and American Express. Other remittances at sender's risk. Address all communications for subscriptions or circulation to NASA Tech Briefs, 41 East 42nd Street, New York, NY 10017-5391. Second-class postage paid at New York, NY and additional mailing offices.

POSTMASTER: please send address changes to NASA Tech Briefs, 41 E. 42nd Street, Suite 921, New York, NY 10017-5391.

NASA Tech Briefs

Official Publication of
National Aeronautics and
Space Administration

ABP BPA

NASA Tech Briefs:

Published by .... **Associated Business Publications**
Editor-in-Chief/Publisher .... **Bill Schnirring**
Associate Publisher/Editor .... **Joseph T. Pramberger**
Managing Editor .... **R.J. Laer**
Associate Editor .... **Sarah L. Gall**
Technical Advisor .... **Dr. Robert E. Waterman**
Production Manager .... **Rita Nothaft**
Traffic Manager .... **James E. Cobb**
Art Director .... **Pierre Granier**
Marketing Director .... **Wayne Pierce**
Assistant Circulation Manager .... **Nipa Joshi**
Advertising Coordinator .... **Daniel Murphy**
Telecommunications Specialist .... **Evelyn Mars**
Reader Service Manager .... **Sylvia Valentin**

Briefs & Supporting Literature:
Provided to National Aeronautics and Space Administration by
International Computers & Telecommunications, Inc.,
NY, NY with assistance from **Logical Technical Services**, NY, NY
Technical/Managing Editor .... **Ted Selinsky**
Art Director .... **Luis Martinez**
Administrator .... **Elizabeth Texeira**
Chief Copy Editor .... **Lorne Bullen**
Staff Writers/Editors .... **Dr. James Boyd, Dr. Larry Grunberger, Dr. Theron Cole, Jordan Randjelovich, George Watson, Oden Browne**
Graphics .... **Zinaida Gimpeleva, Vernald Gillman, Pamela Baynham, Charles Sammartano**
Editorial & Production .... **Bill Little, Ivonne Valdes, Susan Kyu Oh, Frank Ponce**

NASA:
NASA Tech Briefs are provided by the National Aeronautics and Space Administration, Technology Utilization Division, Washington, DC:
Administrator .... **Richard H. Truly**
Assistant Administrator for Commercial Programs .... **John G. Mannix**
Deputy Assistant Administrator(Programs) .... **Frank E. Penaranda**
Deputy Director TU Division(Publications Manager) .... **Leonard A. Ault**
Manager, Technology Utilization Office, NASA Center
For AeroSpace Information .... **Walter M. Heiland**

Associated Business Publications
41 East 42nd Street, Suite 921, New York, NY 10017-5391
(212) 490-3999 FAX (212) 986-7864
President .... **Bill Schnirring**
Executive Vice President .... **Frank Nothaft**
Vice President/Chief Operating Officer .... **Domenic A. Mucchetti**
Operations Manager .... **Rita Nothaft**
Controller .... **Felecia Lahey**
Trade Show Manager .... **Justina Cardillo**
Systems Analyst .... **Patrick Wolfert**

Advertising:
New York Office: (212) 490-3999 FAX (212) 986-7864

Account Executive (NY,NJ,OH,MI) .... **Brian Clerkin** at (201) 366-2751
Account Executive (VA,DC,MD,DE,WV) .... **John D. Floyd, CBC** at (215) 399-3265
Account Executive .... **Debby Crane** at (201) 967-9838
Regional Manager (Midwest) .... **Paul Lesher, CBC** at (312) 296-2040
Account Executive (Northwest) .... **Bill Hague** at (206) 858-7575
Regional Sales Manager (South) .... **Douglas Shaller** at (212) 490-3999
Account Executives (Eastern MA,NH,ME,RI) .... **Paul Gillespie** at (508) 429-8907; **Bill Doucette** at (508) 429-9861
Account Executives (Western MA,CT,VT) .... **George Watts** at (413) 253-9881
Account Executives (Calif.,AZ,NV,NM)
for Area Codes 602/702/505 **Paul Sanacore**
for Area Codes 213/818/805/619/714 **Tom Stillman, Robert D'Alexander**
for Area Codes 408/415/916/209/707/801 **Ron Hall** at (310) 372-2744

NTBM-Research Center
Account Supervisor .... **Lourdes Del Valle**

GRAFTOOL™

"is the best choice..." and "...delivers on all accounts."

Reprinted with permission from PC Magazine, March 26, 1991, Copyright ©1989 Ziff Communications Co. and PC Magazine, November 13, 1990 ©Ziff Communications Co.

PC MAGAZINE EDITORS' CHOICE
March 26, 1991
Graftool, Version 3.3

Presentation graphics and analysis for scientific users.

Your technical data requires more muscle and sophistication than basic business graphics and plotting packages can provide. It's simply a matter of using the right tool for the job. In addition to publication-quality graphics, you need powerful analysis tools and capabilities such as Graftool's ■ Intelligent Data Cursor™ to read out data points on curves & surfaces ■ Linear & non-linear curve-fitting ■ Unlimited zoom & rotation ■ Multiple axes in linear, log, or probability scales ■ Advanced data handling, allowing over 268,000,000 data points ■ Powerful scientific spreadsheet which can directly read your Lotus or ASCII files ■ Unrestricted placement of graphs & text ■ Direct compatibility with Microsoft Word & WordPerfect.

With Graftool, all this power and flexibility purr quietly under the hood, while pop-up menus and push-buttons bring an ease of use previously unheard of in scientific software. Just "point & process" with increased productivity and greater understanding.

GRAFTOOL – the right tool for your technical solutions.

GRAFTOOL $495.

- Interactive demo available
- Academic discounts.

3-D VISIONS

Call Toll Free for Details

1-800-729-4723

2780 Skypark Drive, Torrance, CA 90505

Circle Reader Action No. 392

An engineering
improve eve

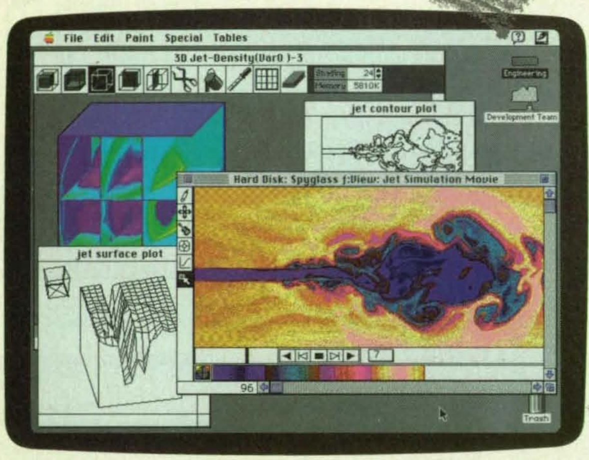

Engineering looks at R&D

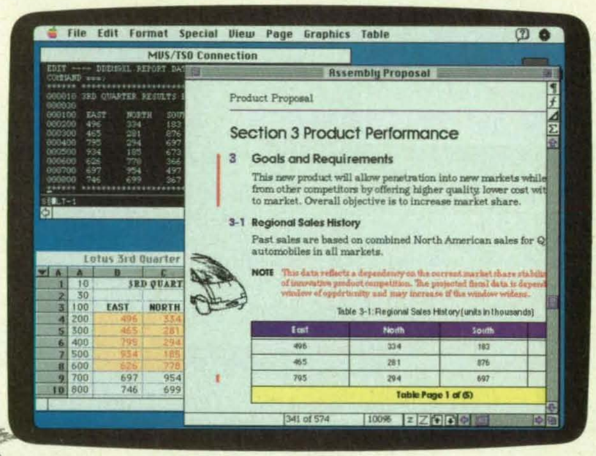

Engineering looks at Marketing

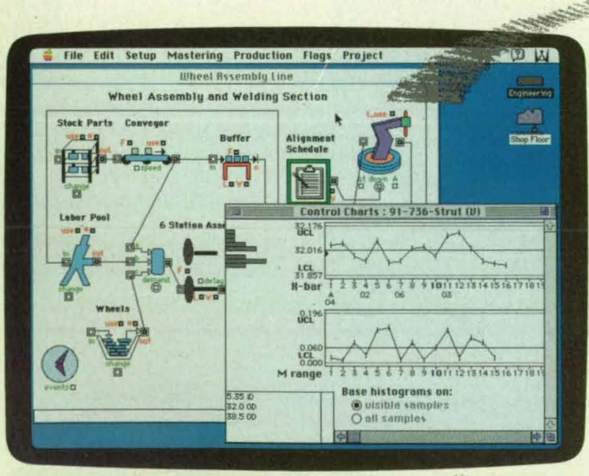

Engineering looks at Manufacturing

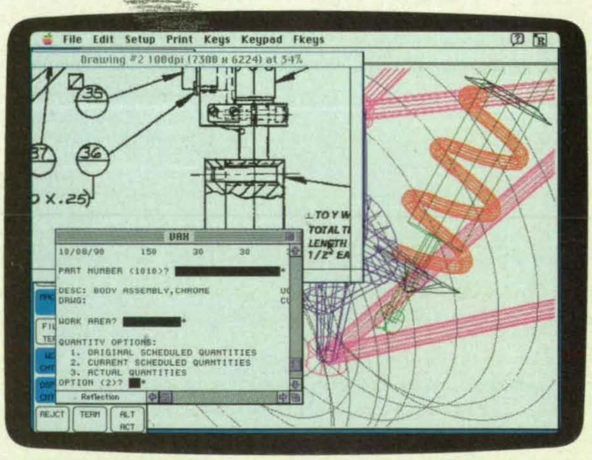

Manufacturing looks at Engineering

(SCREEN, UPPER LEFT) Engineering and scientific data visualized with Spyglass software. (SCREEN, UPPER RIGHT) Shown in background: sales history is captured locally on the Macintosh from an IBM host using 3270 terminal emulation, and then cut and paste into Lotus 1-2-3 for Macintosh. Shown in foreground: data is placed in a table format using FrameMaker, a technical publishing package by Frame Technology. (SCREEN, BOTTOM LEFT) In background: Extend by Imagine That simulates the processes on the shop floor. In foreground: Shop floor data is analyzed using Applied Stat by Applied Statistics, a statistical process control program. (SCREEN, BOTTOM RIGHT) In background: ACCESS-150, a terminal emulation program by EDS, allows the Macintosh to front-end Unigraphics software. Also, Optix, a document management package from Blueridge Technologies, shows a scanned working drawing. In foreground: MANMAN, an integrated MRP II system from Ask Computer Systems, Inc., is running on a remote VAX host.

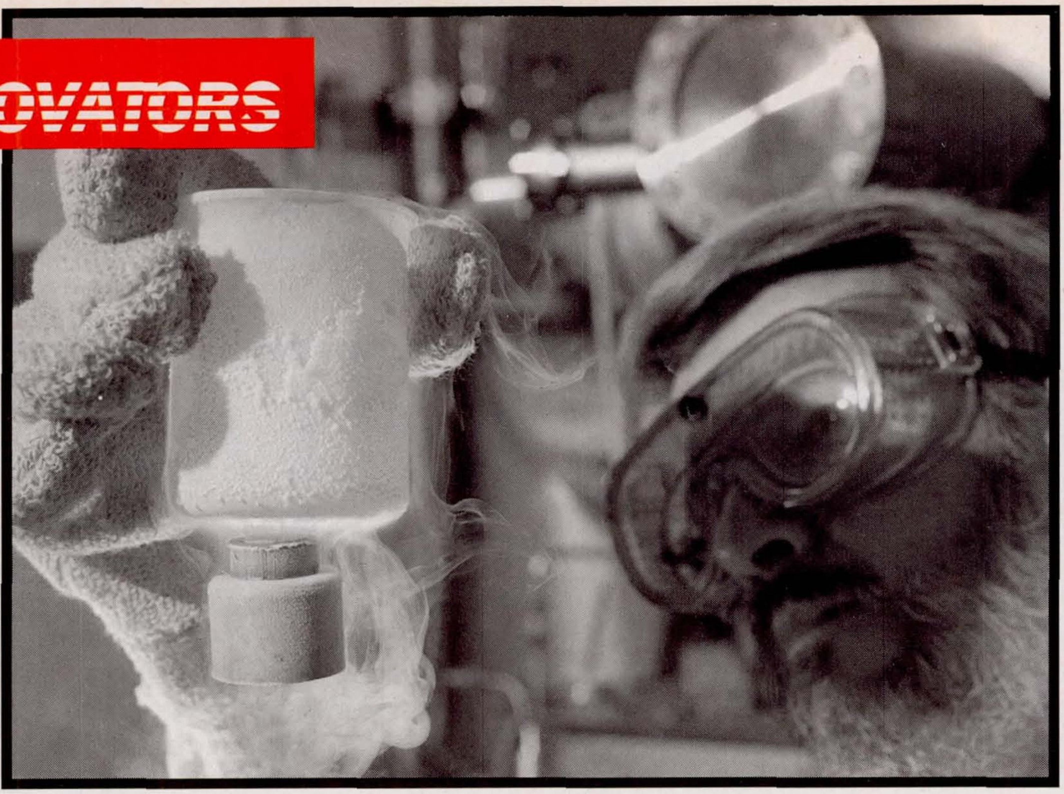

Palmer Peters, a Marshall Space Flight Center researcher, investigates high-temperature superconductors for bearings applications.

"Super" Ceramics Take Off

In the five years since the discovery of high-temperature superconductors (HTS), NASA researchers have aggressively pursued their potential to revolutionize space science. Projects at NASA field centers are incorporating superconductors into communications devices, remote sensors, cryogenic systems, and propulsion and power systems that promise to extend mission life and dramatically improve system performance. Several space-qualified devices and experiments are ready for launch this year. Meanwhile, basic research into the nature and fabrication of HTS materials continues to expand the range of both space- and ground-based applications.

High-temperature superconductors offer zero electrical resistance at temperatures above 77 K, allowing use of inexpensive liquid nitrogen rather than liquid helium as a coolant. The naturally cold space environment coupled with the materials' reduced cryogenic requirements make space an attractive environment for pioneering their use. Further, studies indicate that the technology's high development costs will be offset by significant benefits to space missions.

"You always have to weigh the expense and difficulty (of using high-temperature superconductors) against the gains in performance and knowledge," said Robert Romanofsky, a research engineer at NASA's Lewis Research Center. "It's frequently worthwhile for NASA missions because of their one-of-a-kind nature."

Successful fabrication of HTS thin films, particularly of the ceramic $YBa_2Cu_3O_{7-x}$, has laid the groundwork for numerous signal processing applications. The program at NASA Lewis focuses on integrating thin-film microwave devices into space communications systems. The technology has the potential to improve performance while sharply reducing system volume and mass: HTS phase shifters offer reduced circuit loss with HTS switches; miniaturized microstrip filters can substitute for bulky waveguide filters with no loss in efficiency; and HTS can improve amplifier sensitivity.

Lewis engineers have fabricated a prototype antenna array that significantly reduces heat loss. "A phased array antenna employing superconductors might be used to relay messages from a land rover on Mars to a satellite," said Romanofsky.

A receiver built at Johnson Space Center will be integrated with a Lewis-developed antenna for an experiment relaying signals from a ground station through the Advanced Communication Technology Satellite to an HTS antenna/receiver system in a shuttle payload bay. The system offers high sensitivity, low noise, and broad bandwidth.

Space-qualified microwave devices developed at Lewis and the Jet Propulsion Laboratory will fly aboard the Naval Research Laboratory's High-Temperature Superconductivity Space Experiment (HTSSE). Intended to demonstrate the viability of HTS materials in a microgravity environment, Phase I will carry experiments submitted by 20 organizations. JPL has provided an HTS filter for the HTSSE-1, scheduled for launch later this year, and is producing with Lewis an X-band hybrid HTS/semiconductor receiver for the experiment's second phase. JPL also is developing local oscillators, mixers, and broad bandwidth detectors.

Two of NASA's Centers for the Commercial Development of Space (CCDSs) also are involved in HTS development. In July, the Consortium for Materials Development for Space at the University of Alabama will fly an experiment on STS-46, in which samples of partially oxidized superconductors from industrial and academic sources will be monitored to determine how to achieve the sharpest transition at orbital temperature. And the University of Houston's Space Vacuum Epitaxy Center plans to send an experiment investigating the growth of HTS thin films on the second flight of NASA's Wake Shield Facility.

Improving sensitivity and reducing noise in space-based sensors is the goal of Goddard Space Flight Center investigators. They have employed HTS technology in the development of in-frared bolometers designed for thermal emission spectroscopy on outer planet missions. Transition-edge, kinetic inductance, and, most recently, magnetic susceptibility bolometers have been prototyped and found to offer progressively better performance in terms of improved signal-to-noise ratio and ability to identify atmospheric molecules.

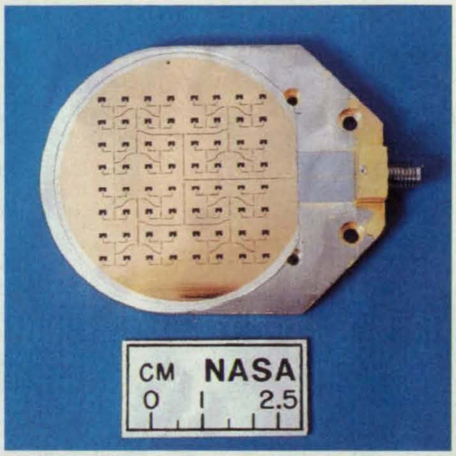

A 64-element superconducting microstrip antenna, tested at NASA Lewis, operates at 30 GHz with a 2 dB higher gain than standard antennas at 70 K.

Researchers hope the bolometers will benefit the data-gathering ability of the 1996 Cassini mission to Saturn and Titan. "Better detectors exist but require large amounts of liquid helium impossible to take on such long-term missions," said Goddard's John Brasunus. "We hope to optimize the new devices to detect longer wavelengths."

HTS may also benefit cryogenics, the technology now required for its own use. The ceramic superconductors are ideal for cryogenic applications because they are excellent electrical conductors and, unlike metals, extremely poor heat conductors. Electrical leads fashioned from HTS materials can reduce the heat load in systems intended to cool space-based sensors, thereby reducing liquid helium evaporation and extending mission life. Stephanie Wise, an aerospace technologist at Langley Research Center, hopes to test the viability of this application with HTS wire strips launched aboard the Comet service module in 1995. Using $YBa_2Cu_3O_{7-x}$ for the sensor leads on the SAFIRE (Spectroscopy of the Atmosphere by Far Infrared Emission) mission later in this decade could extend the mission's life by more than five percent. According to Wise, there is commercial interest in the circuitry, perhaps for ground-based cryocoolers.

Engineering Challenge

Despite their unique electrical, thermal, and mechanical properties, current HTS materials pose numerous engineering challenges. A significant barrier to wider application is their limited power handling: high current densities heat the materials above critical temperature, resulting in loss of superconductivity. Research at NASA Lewis and elsewhere addressing the fundamental character of high-temperature superconductors seeks to resolve engineering and fabrication difficulties while looking for new and better materials.

Early and continued success with HTS thin films on a variety of substrates contrasts with slower progress in the development of bulk solids and wire, which are needed for applications with high current density or critical magnetic field requirements such as power and propulsion systems. NASA recently approved a Phase II Small Business Innovation Research (SBIR) grant to Creare Inc. for the ground-demonstration of a passively-cooled HTS power transmission line, the feasibility of which was demonstrated in Phase I.

"At present, HTS power transmission lines are cost-effective only for moving large amounts of power over long distances," said Paul Aron, deputy chief of the Photovoltaics Branch at NASA Lewis. "Such a line could deliver power generated by a space-borne nuclear power plant to a manned space facility, or across the surface of the moon." Power delivered by HTS lines may one day be efficiently stored as magnetic energy in a ring of HTS material.

Recent progress in bulk solid fabrication has fueled investigation into HTS bearings. Goddard researchers are investigating the merits of HTS passive magnetic bearings based on the perfect diamagnetism of superconductors, known as the Meissner effect. Researcher Yuri Flom expects the bearings, which operate without physical contact, to provide "high-speed, frictionless, reliable, long-duration, and maintenance-free service in hostile environments." Potential applications include flywheels, canned pumps for cryogenics, beam choppers, and textile spindles.

Rudolf Decher of the Marshall Space Flight Center is working on high-thrust bearings to replace rolling element bearings in rocket engine turbopumps to eliminate maintenance downtime. The HTS bearings would likely be used in conjunction with hydrostatic bearings, which would take over after liftoff.

Also exploiting the magnetic characteristics of HTS materials are Johnson Center researchers developing HTS magnetic phased-array antennas for attraction/repulsion systems. These could be used for space vehicle docking, pushing a satellite out of a shuttle bay, or as a tetherless astronaut rescue system.

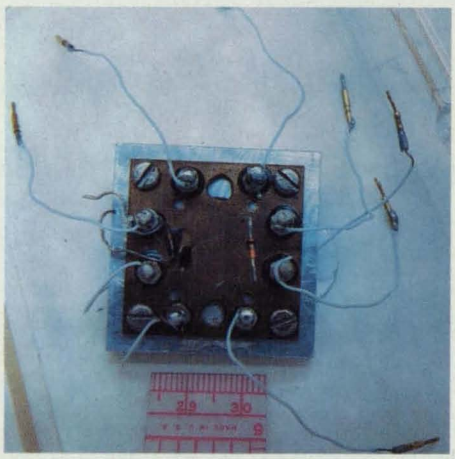
This bolometer, developed at the Goddard Space Flight Center for interplanetary missions, uses an HTS thin film to detect temperature increases due to absorbed infrared radiation.

"The amount of energy you can store in a superconductor has increased ten-fold in the last few years," said chief technologist Kumar Krishen. "I expect that many applications will become cost-effective on the ground."

This September, Krishen will serve as program chairman of the third annual World Congress on Superconductivity in Munich, Germany. NASA is co-sponsoring the event, at which 24 nations will discuss the current status and future prospects of HTS technology. ❑

For more information about NASA's superconductivity research, contact Martin M. Sokoloski, Program Manager, NASA Headquarters, Washington, DC 20546.

Now you can and not get

Introducing new RISC System/6000 POWERstation

If you're interested in open systems but don't want to suffer the slings and arrows of outrageous prices, IBM is about to hit you where you live. The RISC System/6000™ POWERstation 220 gives you more wallop for your money, while delivering a hefty 25.9 SPECmarks.™ That's compared to the SUN IPC's™ 13.4 SPECmarks and the DEC5000's™ 17.8.

Model	Entry Grayscale Workstation**	Entry 8-bit Color Workstation†
IBM 220W	$7,185	$9,995
HP 705/710	$8,415	$14,065

Scientists see stars. CASE users can start with a grayscale workstation with a paging disk for just $7,185. If it's CAD clout you're after, you can get a workstation specially outfitted for mechanical design—with 2D color graphics and 400MB of fixed disk storage—for only $9,995. All models in the POWERstation 220 series come with two expansion

*In Canada, call 1 800 465-1234. **16MB, Paging Disk, Display, Operating System, Graphical User Interface. †16MB, 400MB Disk, Display, Operating System, Graphical User Interface.

get more clout, clobbered.

and POWERservers that pack more punch for less.

slots and upgradable components. And industry-standard memory upgrades and add-ons for both are affordable, so growing won't be a pain.

Striking a blow for business. The POWERserver 220 is great for commercial UNIX® solutions, too. You can configure it as a commercial server, to give your business the speed, muscle and openness of UNIX, for only $9,715. And the POWERserver 220 is as expandable as all our other models.

IBM is in your corner. Nobody else delivers the knockout support of IBM. An IBM customer engineer can install your machines, configure your network and integrate all your systems, whether they're made by IBM or not. And IBM Credit Corporation has flexible financing packages to meet your needs. Get hit with the details. Call your IBM marketing representative or Business Partner. For literature, call 1 800 IBM-6676, ext. 769.*

And, for those who decide to shop for UNIX solutions elsewhere, a word of advice. Duck.

The RISC System/6000
For the Power Seeker.

IBM®

New Product Ideas

New Product Ideas are just a few of the many innovations described in this issue of *NASA Tech Briefs* and having promising commercial applications. Each is discussed further on the referenced page in the appropriate section in this issue. If you are interested in developing a product from these or other NASA innovations, you can receive further technical information by requesting the TSP referenced at the end of the full-length article or by writing the Technology Utilization Office of the sponsoring NASA center (see page 18). NASA's patent-licensing program to encourage commercial development is described on page 18.

Tool Changer for Robot

A mechanism allows a robot to change tools on the end of its arm. It needs no additional electrical or pneumatic energy to make or break the connection.
(See page 71)

Probe and Drogue for Quick Attachment and Detachment

This mechanism attaches and detaches parts quickly and locks them together positively. It accommodates a large alignment error when parts are brought together.
(See page 88)

Laterally Coupled Distributed-Feedback Lasers

This design can be fabricated in fewer steps than prior laser designs of this type. The new design was demonstrated in single mode at 9,054 Å.
(See page 24)

Fastener for Hot, Oxidizing Environments

This threaded fastener is designed for service at extremely high temperatures in oxidizing atmosphere. The fastener is made from a ceramic-coated composite material.
(See page 84)

Expandable Compartmental Storage

A new storage cabinet has racks that hold articles in net compartments. The stored articles are visible and quickly accessible.
(See page 79)

Lightweight, High-Yield Photocathode

A commercially produced quartz cloth increases the electric current emitted by an aluminum photocathode. At 4 kV, current increased by a factor 667.
(See page 33)

Ferroelectric/Optoelectronic Memory/Processor

A proposed nonvolatile analog memory and data processor could perform massively parallel inner-product or matrix-vector computations at high speed, using optical inputs. Practical applications would include optical computing, recognition of patterns, neural networks, and other operations with ultradense memories.
(See page 28)

Axial-Loading Circumferential Dovetail Turbine-Blade Mount

Here the blades are mounted in the rotor disk in axial direction. The new configuration allows circumferentially longer and therefore stronger dovetail joints.
(See page 77)

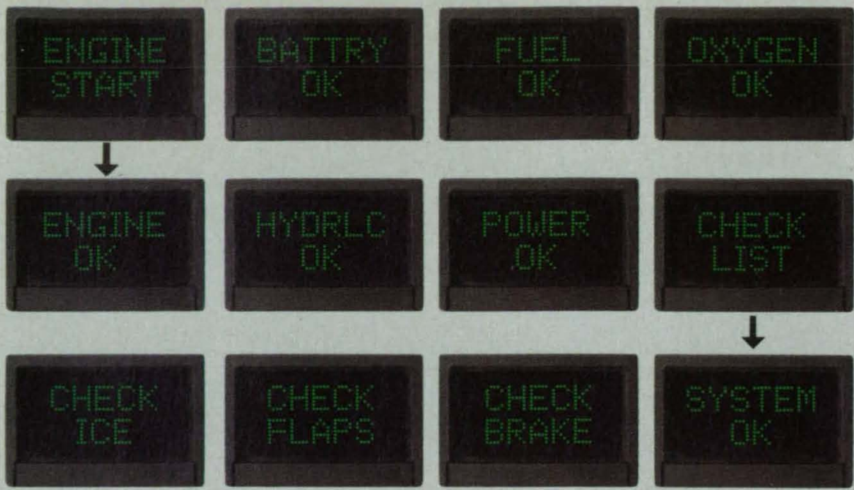

1

2

3

AN APPLICATIONS EXAMPLE.
While the following example is for aircraft, it could apply to any air, land, sea or space system.

SEQUENCE ONE: The four-pushbutton display reads "ENGINE START," "BATTERY OK," "FUEL OK," OXYGEN OK." The operator selects "ENGINE START."

SEQUENCE TWO: The four-pushbutton display now changes to read "ENGINE OK," "HYDRLC OK," "POWER OK," "CHECK LIST." The operator selects "CHECK LIST."

SEQUENCE THREE: The four-pushbutton display now reads "CHECK ICE," "CHECK FLAPS," "CHECK BRAKE," "SYSTEM OK." In this manner, the designer can program in as many sequences as required.

Design flexibility: The programmable display system.

Vivisun Series 2000, now the leading programmable display pushbutton system, interfaces the operator with the host computer. The user-friendly LED dot-matrix displays can display any graphics or alpha-numerics and are available in green, red or amber. They can efficiently guide the operator through any complex sequence with no errors and no wasted time.

They also simplify operator training as well as control panel design. One Vivisun Series 2000 programmable display system can do the work of 50 or more dedicated switches. In short, Vivisun Series 2000 gives the design engineer more control over the design.

Contact us today.

AEROSPACE OPTICS INC.
3201 Sandy Lane, Fort Worth, Texas 76112
(817) 451-1141 • Telex 75-8461 • Fax (817) 654-3405

Vivisun Series 2000 programmable displays. The intelligent communications system.

SERIES
VIVISUN 2000™

HOW YOU CAN BENEFIT FROM NASA's TECHNOLOGY UTILIZATION SERVICES

If you're a regular reader of TECH BRIEFS, then you're already making use of one of the low-and no-cost services provided by NASA's Technology Utilization (TU) Network. But a TECH BRIEFS subscription represents only a fraction of the technical information and applications/engineering services offered by the TU Network as a whole. In fact, when all of the components of NASA's Technology Utilization Network are considered, TECH BRIEFS represents the proverbial tip of the iceberg.

We've outlined below NASA's TU Network—named the participants, described their services, and listed the individuals you can contact for more information relating to your specific needs. We encourage you to make use of the information, access, and applications services offered by NASA's Technology Utilization Network.

How You Can Access Technology Transfer Services At NASA Field Centers:

Technology Utilization Officers & Patent Counsels—Each NASA Field Center has a Technology Utilization Officer (TUO) and a Patent Counsel to facilitate technology transfer between NASA and the private sector.

If you need further information about new technologies presented in *NASA Tech Briefs*, request the Technical Support Package (TSP). If a TSP is not available, you can contact the Technology Utilization Officer at the NASA Field Center that sponsored the research. He can arrange for assistance in applying the technology by putting you in touch with the people who developed it. If you want information about the patent status of a technology or are interested in licensing a NASA invention, contact the Patent Counsel at the NASA Field Center that sponsored the research. Refer to the NASA reference number at the end of the Tech Brief.

Ames Research Ctr.
Technology Utilization Officer:Geoffrey S. Lee
Mail Code 223-3
Moffett Field, CA 94035
(415) 604-4044
Patent Counsel:
Darrell G. Brekke
Mail Code 200-11
Moffett Field, CA 94035
(415) 604-5104

Lewis Research Center
Technology Utilization Officer: Anthony F. Ratajczak
Mail Stop 7-3
21000 Brookpark Road
Cleveland, OH 44135
(216) 433-2225
Patent Counsel:
Gene E. Shook
Mail Code LE-LAW
21000 Brookpark Road
Cleveland, OH 44135
(216) 433-5753

John C. Stennis Space Center
Technology Utilization Officer: Robert Barlow
Code HA-30
Stennis Space Center, MS 39529
(601) 688-2042

John F. Kennedy Space Center
Technology Utilization Officer: James A. Aliberti
Mail Stop PT-PMO-A
Kennedy Space Center, FL 32899
(407) 867-3017
Patent Counsel:
Bill Sheehan
Mail Code PT-PAT
Kennedy Space Center, FL 32899
(407) 867-2544

Langley Research Ctr.
Technology Utilization Officer: Joseph J. Mathis, Jr.
Head, TU & AO Office
Mail Stop 200
10 West Taylor Road,
Hampton, VA 23665-5225
(804) 864-2484
Patent Counsel:
Dr. George F. Helfrich
Mail Stop 143
9A Ames Road,
Hampton, VA 23665-5225
(804) 864-3221

Goddard Space Flight Center
Technology Utilization Officer: Donald S. Friedman
Mail Code 702.1
Greenbelt, MD 20771
(301) 286-6242
Patent Counsel:
R. Dennis Marchant
Mail Code 204
Greenbelt, MD 20771
(301) 286-7351

Jet Propulsion Lab.
NASA Resident Office
Technology Utilization Officer: Arif Husain
Mail Stop 180-801
4800 Oak Grove Drive
Pasadena, CA 91109
(818) 354-4862
Patent Counsel:
Thomas H. Jones
Mail Code 180-801
4800 Oak Grove Drive
Pasadena, CA 91109
(818) 354-5179
Technology Utilization Mgr. for JPL: Dr. Norman L. Chalfin
Mail Stop 156-211
4800 Oak Grove Drive
Pasadena, CA 91109
(818) 354-2240

George C. Marshall Space Flight Center
Technology Utilization Officer: Ismail Akbay
Code AT01
Marshall Space Flight Center, AL 35812
(205) 544-2223
Fax (205) 544-3151
Patent Counsel:
Robert L. Broad, Jr.
Mail Code CC01
Marshall Space Flight Center, AL 35812
(205) 544-0021

Lyndon B. Johnson Space Center
Technology Utilization Officer: Dean C. Glenn
Mail Code IC-4
Houston, TX 77058
(713) 483-3809
Patent Counsel:
Edward K. Fein
Mail Code AL3
Houston, TX 77058
(713) 483-4871

NASA Headquarters
Technology Utilization Officer: Leonard A. Ault
Code CU
Washington, DC 20546
(703) 557-5598
Assistant General Counsel for Patent Matters: Robert F. Kempf, Code GP
Washington, DC 20546
(202) 453-2424

How You Can Utilize NASA's Regional Technology Transfer Centers (RTTCs) — A nationwide network offering a broad range of technical services, including computerized access to over 100 million documents worldwide.

You can contact NASA's network of RTTCs for assistance in solving a specific technical problem or meeting your information needs. The "user friendly" RTTCs are staffed by technology transfer experts who provide computerized information retrieval from one of the world's largest banks of technical data. Data bases, ranging from NASA's own data base to Chemical Abstracts and INSPEC, are accessible through the six RTTCs located throughout the nation. The RTTCs also offer technical consultation services and/or linkage with other experts in the field. You can obtain more information about these services by calling or writing the nearest RTTC. User fees are charged for information services.

REGIONAL TECHNOLOGY TRANSFER CENTERS (RTTCs)

RTTC Directors

NORTHEAST
Dr. William Gasko
Center tor Technology Commercialization
Massachusetts Technology Park
100 North Drive
Westborough, MA 01581
(508) 870-0042

MID-ATLANTIC
Ms. Lani S. Hummel
University of Pittsburgh
823 William Pitt Union
Pittsburgh, PA 15260
(412) 648-7000

SOUTHEAST
Mr. J. Ronald Thornton
Southern Technology Application Center
University of Florida
College of Eng.
Box 24
One Progress Boulevard
Alachua, FL 32615
(904) 462-3913
(800) 354-4832 (FL only)
(800) 225-0308 (toll-free US)

MID-CONTINENT
Dr. Helen B. Dorsey
Texas A&M University
237 Wisenbaker Engineering Research Center
College Station, TX 77843-3041
(409) 847-9217

MID-WEST
Dr. Joseph W. Ray
Great Lakes Technology Transfer Center
25000 Great Northern Corp. Center
Suite 450
Columbus, OH 44070-5310
(216) 734-0094

FAR-WEST
Mr. Robert Stark
Western Research Applications Center
University of Southern California
3716 South Hope Street,
Suite 200
Los Angeles, CA 90007-4344
(213) 743-6132
(800) 642-2872 (CA only)
(800) 872-7477 (toll-free US)

If you are interested in information, applications, research, training, and services relating to satellite and aerial data for Earth resources, contact NASA's transfer point for earth observing technology: **Technology Application Center, University of New Mexico, 2808 Central, S.E., Albuquerque, NM 87131-6031; Dr. Stan Morain, Director (505) 277-3622.**

If you represent a public sector organization with a particular need, you can contact NASA's Application Team for technology matching and problem solving assistance. Staffed by professional engineers from a variety of disciplines, the Application Team works with public sector organizations to identify and solve critical problems with existing NASA technology. **Technology Application Team, Research Triangle Institute, P.O. Box 12194, Research Triangle Park, NC 27709; *Dr. Doris Rouse, Director,* (919) 541-6980**

A Shortcut To Software: **COSMIC®**—For software developed with NASA funding, contact COSMIC, NASA's Computer Software Management and Information Center. New and updated programs are announced in the Computer Programs section. COSMIC publishes an annual software catalog. For more information call or write: **COSMIC®**, 382 East Broad Street, Athens, GA 30602 *John A. Gibson, Director,* (404) 542-3265; FAX (404) 542-4807.

If You Have a Question..**NASA Center For AeroSpace Information** can answer questions about NASA's Technology Utilization Network and its services and documents. The CASI staff supplies documents and provides referrals. Call, write or use the feedback card in this issue to contact: **NASA Center For AeroSpace Information,** Technology Utilization Office, P.O. Box 8757, Baltimore, MD 21240-0757. *Walter M. Heiland, Manager,* (410) 859-5300, Ext. 245.

Electronic Components and Circuits

Infrared Multiple-Quantum-Well Phototransistor

Photocurrent would be amplified, and dark current would be suppressed.

NASA's Jet Propulsion Laboratory, Pasadena, California

A proposed npn $Al_xGa_{1-x}As$ phototransistor would incorporate a multiple-quantum-well (MQW) infrared photodetector. This internal MQW photodetector would have n-doped contacts and would be embedded between the p-doped base region and the n-doped collector region of the transistor (see figure). The heterostructure of the transistor would be such that the gap between the valence and conduction electron-energy bands would be greater in the emitter than in the base. As a consequence, the electric field at the junction between the emitter and the base would block the hole current, thereby reducing the dark current. Moreover, the quantum-well barriers would be made relatively thick to reduce quantum tunneling between the quantum wells, thereby reducing the dark current further.

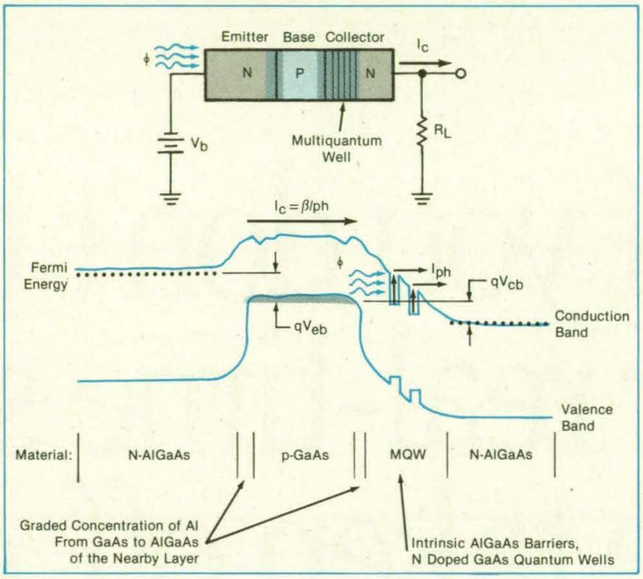

The $Al_xGa_{1-x}As$ **Infrared Phototransistor** would include a multiple-quantum-well detector in its base/collector region.

The incident radiation would excite electrons in the base/collector junction. The resulting change in the charge of the base would alter the potential across the base/emitter junction, causing the emitter to inject electrons into the base. Provided that the lifetime of the injected electrons in the base exceeded the time of transit of these electrons across the base, normal transistor action would produce current gain. With an applied bias and the base contact floating, the photogenerated carriers would contribute a photocurrent I_{ph} in the collector. The total collector current, I_c, would be given by

$$I_c = (1+\beta)I_{ph}$$

where the transistor gain, β, would be of the order of 100.

By making the MQW long (preferably at least one characteristic length for the absorption of photons of the wavelength of interest), it would increase the quantum detection efficiency. It would allow the base region to be kept small — a requirement for achieving high transistor gain. The high electric field in the collector/base junction portion of the MQW region would rapidly sweep the photoexcited electrons from the junction, increasing the response. The coupling of radiation to the phototransistor could be enhanced by directing the radiation along the MQW detector with a diffraction grating or other device to match the selection rule of the intersubband transitions in the quantum wells.

This work was done by Shmuel I. Borenstain of Caltech for **NASA's Jet Propulsion Laboratory**. *For further information, Circle 78 on the TSP Request Card. NPO-17980*

Channelized-Coplanar-Waveguide PIN-Diode Switches

Isolation exceeds 20 dB, while insertion loss is less than 1 dB.

Lewis Research Center, Cleveland, Ohio

As part of a NASA effort to develop coplanar waveguide (CPW) into a viable alternative to microstrip for microwave and millimeter-wave circuits, three different positive/intrinsic/negative (PIN-diode) reflective CPW switches have been demonstrated. The first switch includes a series-mounted diode to bridge a gap in the center strip conductor of the CPW. The second switch includes a pair of diodes to short the center strip conductor to the ground planes. The third switch includes a diode to switch between a band-pass filter and a notch filter.

The top part of the figure shows the layout and an equivalent electrical circuit of the series-mounted diode switch. The equivalent circuit of the series gap is represented by the capacitive circuit. When the diode is forward biased, the coupling capacitor, C_c, is shorted by the low impedance of the diode, permitting the radio-frequency signal to propagate unattenuated. The isolation of the switch is determined by the high impedance of the reverse-biased diode and C_c. Because the impedance of the coupling capacitor decreases with in-

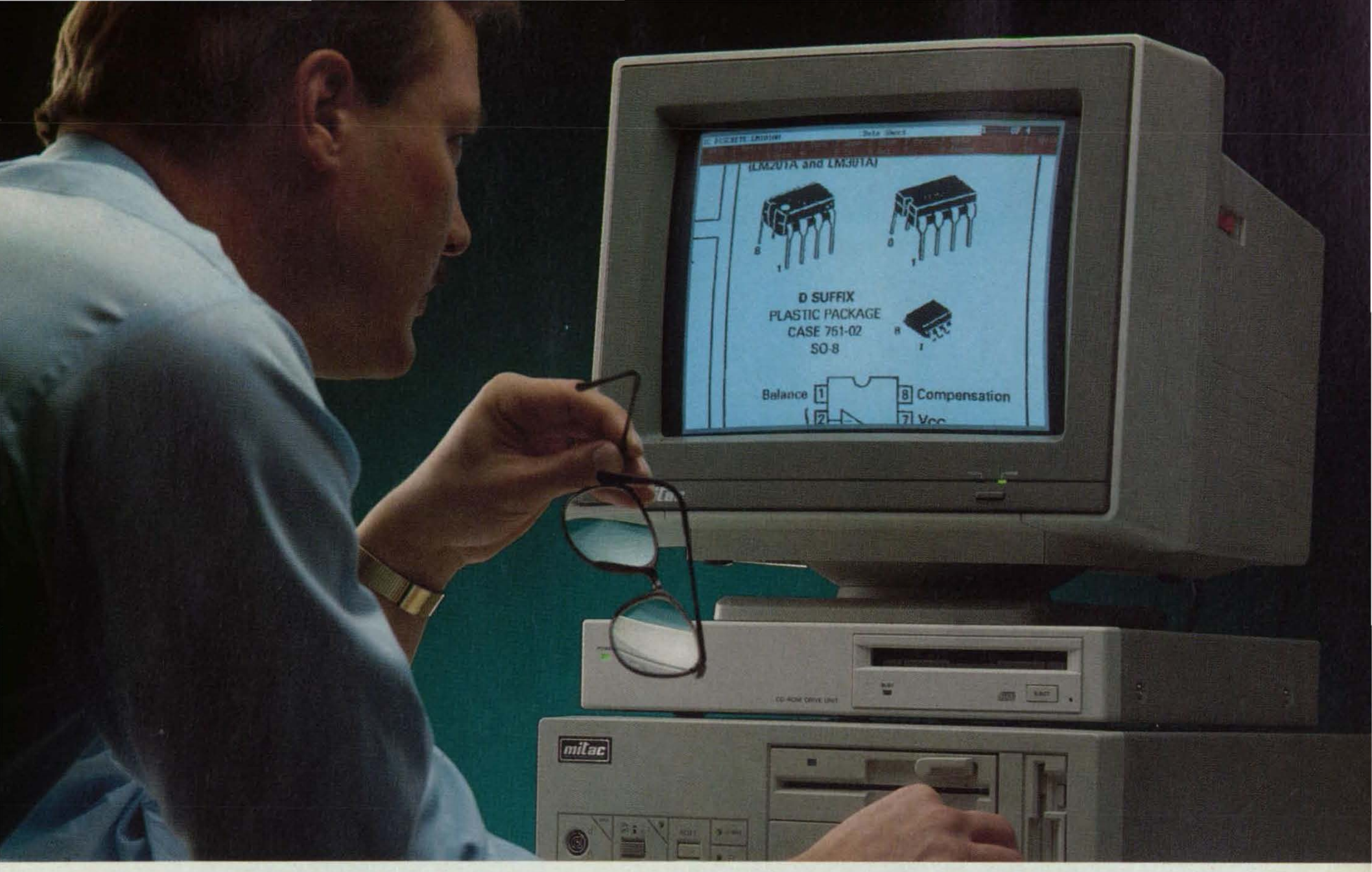

D SUFFIX
PLASTIC PACKAGE
CASE 751-02
SO-8
Balance
Compensation
mitac

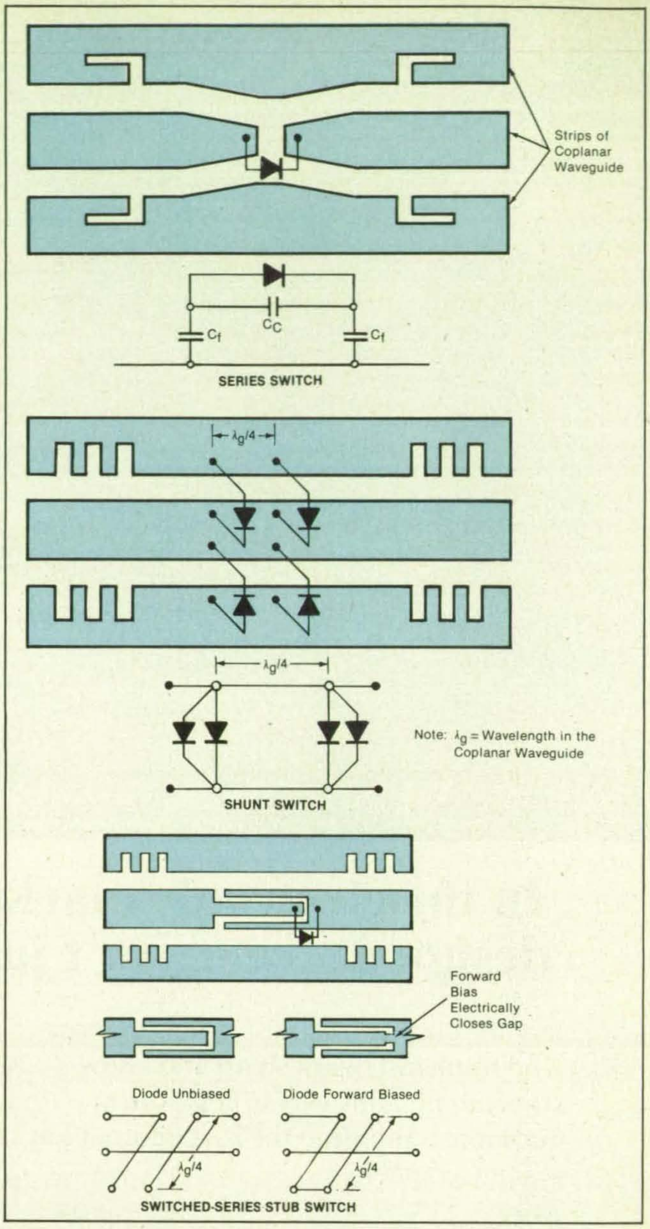

CPW PIN-Diode Switches have been built in these three configurations.

creasing frequency, the isolation deteriorates at higher frequencies. Therefore, this switch is limited to use at lower frequencies, or else matching circuits must be used to resonate-out the coupling capacitance in the "off" state.

The middle part of the figure illustrates the shunt-mounted diode switch. When the diodes are forward-biased, the slots are loaded by the low impedance of the diode. This low impedance presents an effective short circuit to the radio-frequency signal, which is, therefore, reflected. Additional pairs of diodes spaced a quarter wavelength apart can be used to increase the isolation of the switch.

A switched filter is illustrated at the bottom of the figure. A diode is used to switch between an open-circuit-terminated series stub and a short-circuit-terminated series stub. For a stub one-quarter wavelength long, this is equivalent to switching between a band-pass filter and a notch filter. Because of the high Q (the ratio of reactance to resistance) of the notch filter, very-narrow-band, high-isolation switches can be made.

All three switches have been fabricated with beam-lead PIN diodes and tested. The measured isolation for each switch was greater than 20 dB, and the insertion loss was less than 1 dB.

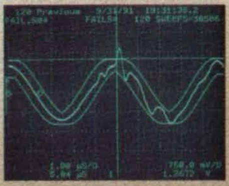

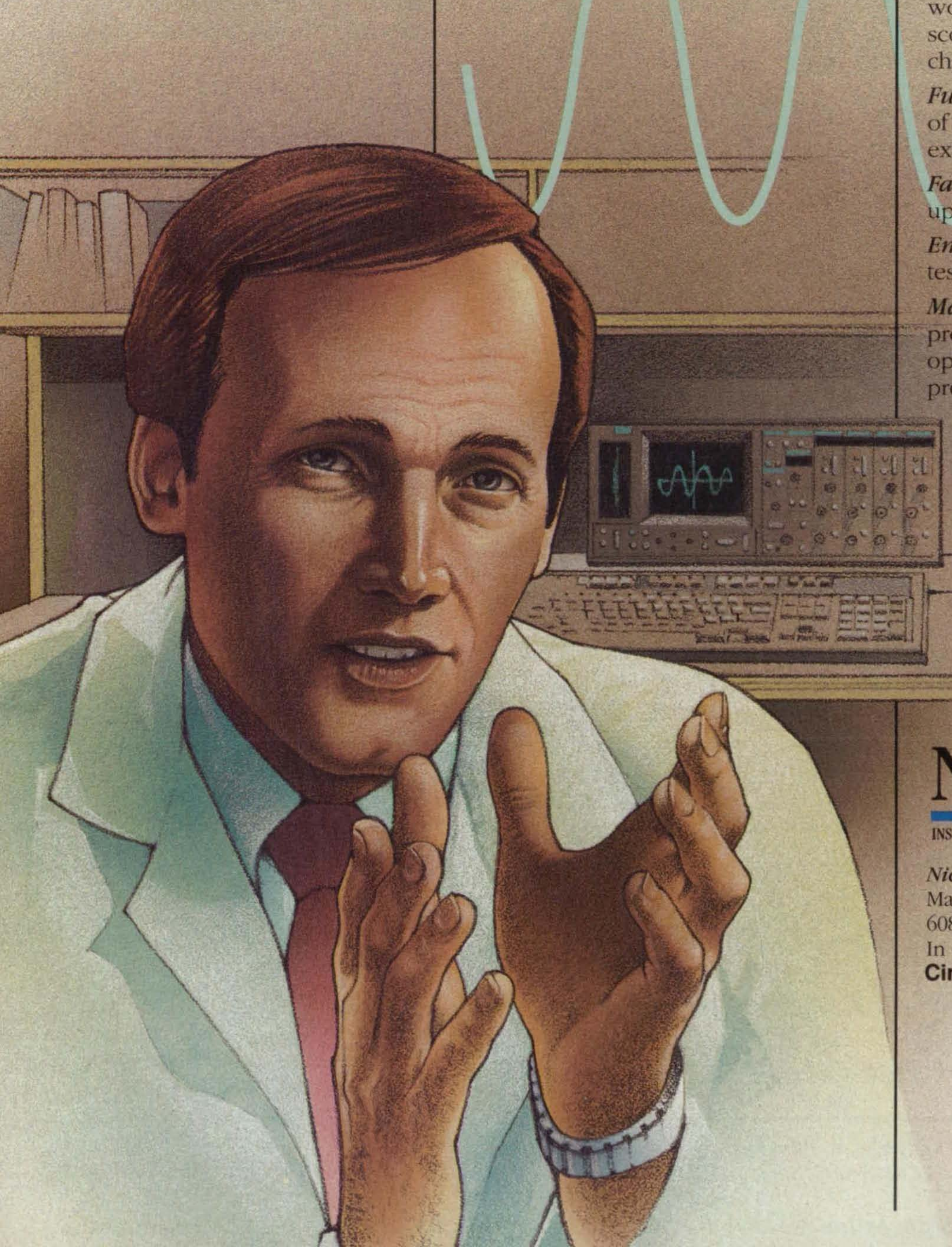

This work was done by G. E. Ponchak of **Lewis Research Center** *and R. N. Simons of Case Western Reserve University. Further information may be found in NASA TM-102289 [N90-11943], "Channelized Coplanar Waveguide Pin-Diode Switches."*

Copies may be purchased [prepayment required] from the National Technical Information Service, Springfield, Virginia 22161, Telephone No. (703) 487-4650. Rush orders may be placed for an extra fee by calling (800) 336-4700.
LEW-15080

Laterally Coupled Distributed-Feedback Lasers

Gratings would be located laterally (instead of longitudinally) next to ridge waveguides.

NASA's Jet Propulsion Laboratory, Pasadena, California

Distributed-feedback semiconductor lasers of a proposed design called "laterally coupled" would feature Bragg gratings located on the top surfaces next to the sides of the ridge waveguides that overlie the gain regions of the laser resonators. The figure shows a proposed laterally coupled distributed-feedback laser along with (1) a distributed-feedback laser of prior design in which the Bragg grating is located underneath the ridge waveguide, and (2) a laser of related prior design called "distributed Bragg reflector," in which the Bragg reflector is located at one end of the ridge waveguide.

Both of the prior designs involve disadvantages. Distributed-Bragg-grating lasers have more-complicated shapes, and, therefore, more steps are needed to fabricate them. The fabrication of distributed-feedback lasers is simpler, but undesirable scattering occurs at the discontinuities between the Bragg gratings and the overlying layers of the laser structures.

In comparison with the devices of both prior designs, the proposed laterally coupled devices could be fabricated in fewer steps. The scattering would also be sup-

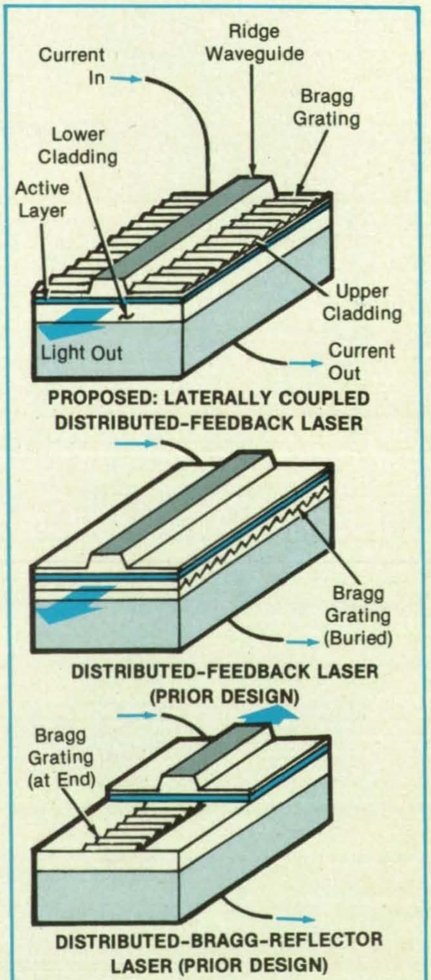

A **Laterally Coupled Distributed-Feedback Laser** offers advantages over lasers of two related prior designs.


USA

pressed. In a laterally coupled distributed-feedback laser, the gratings would interact with the lateral evanescent electromagnetic fields, producing the feedback that would support oscillation in a single mode.

By etching the ridge waveguide and grating separately, precise control over the grating depth is achieved, yielding precise control over the amount of grating coupling. A single-mode laterally coupled DFB laser has been demonstrated operating single-mode at 9054 Å wavelength based on this structure.

This work was done by Robert J. Lang and Siamak Forouhar of Caltech, and Richard C. Tiberio and George Porkolab of Cornell University for **NASA's Jet Propulsion Laboratory**. *For further information, Circle 142 on the TSP Request Card.*

Inquiries concerning rights for the commercial use of this invention should be addressed to the Patent Counsel, NASA Resident Office-JPL [see page 18]. Refer to NPO-18393.

Ferroelectric/Optoelectronic Memory/Processor

A planar memory array would perform massively parallel analog computations.

NASA's Jet Propulsion Laboratory, Pasadena, California

A proposed hybrid optoelectronic non-volatile analog memory and data processor would comprise a planar array of microscopic photosensitive ferroelectric capacitors. The processor could perform massively parallel inner-product or matrix•vector computations in real time and at high speed, using optical matrix or vector inputs. Alternatively, the processor could serve as an analog memory array addressable by an optical contactless gate for serial readout. Processors of this type would overcome the electronic crosstalk and the limitations on the number of input/output contacts inherent in electronic implementations of large interconnection arrays. They could be used in general optical computing, recognition of patterns, artificial neural networks, and other applications that require massively parallel input/output operations with ultradense memories.

The processor would be fabricated on a silicon substrate. The microscopic ferroelectric capacitor that constitutes each memory element would include a metal electrode on the substrate, an intermediate layer of ferroelectric material, and a transparent outer electrode (see figure). The remanent electric polarization of the ferroelectric material would be the analog representation of the content of the memory element.

Multiplication or readout of the content would be based on the fact that illumination of a ferroelectric material with photons of energy near its bandgap gives rise to a photocurrent proportional to the product of the remanent polarization and the intensity of the light. The photogenerated charge carriers would move along the internal electric field generated by the remanent polarization, contributing to the overall photocurrent and to the photogenerated electromotive force.

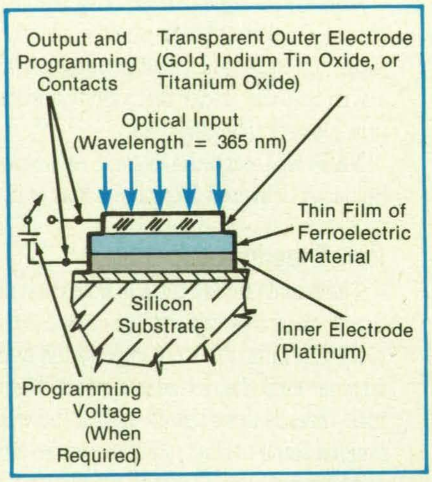

A Photosensitive Ferroelectric Memory Element would put out a current proportional to the optical input and to the remanent polarization of the ferroelectric material. An array of such elements would constitute an ultradense memory and optoelectronic processor.

Suppose, for example, that each element of memory represents one element of a pattern. The remembered pattern could be compared with the illuminating pattern by summing the outputs of all the elements, thereby effectively taking the inner product of the two patterns. As an example of another mode of operation, one could illuminate the array with a pattern that represents a column vector and obtain a matrix•vector product by summing the output currents of the elements in each row.

Each memory element could be programmed with the desired remanent polarization by applying a voltage for a specific time. Typically, for a programming voltage of < 5 V, the programming time would range from 100 ns to 1 ms, depend-

ing on the desired analog level. A dynamic analog resolution of 10 bits should be achievable. Memory elements could be as small as 10 by 10 μm. Output current densities could range from about 0.1 to 10 $\mu A/cm^2$ for incident optical signals from about 0.1 to 10 mW/cm^2.

This work was done by Sarita Thakoor and Anilkumar P. Thakoor of Caltech for **NASA's Jet Propulsion Laboratory.** *For further information, Circle 81 on the TSP Request Card.*

In accordance with Public Law 96-517, the contractor has elected to retain title to this invention. Inquiries concerning rights for its commercial use should be addressed to

Edward Ansell
Director of Patents and Licensing
Mail Stop 305-6
California Institute of Technology
1201 East California Boulevard
Pasadena, CA 91125

Refer to NPO-18222, volume and number of this NASA Tech Briefs *issue, and the page number.*

$Al_xGa_{1-x}As$ Single-Quantum-Well Surface-Emitting Lasers

Powers and external differential quantum efficiencies exceed those of prior devices configured similarly.

NASA's Jet Propulsion Laboratory, Pasadena, California

The figure illustrates a surface-emitting solid-state laser that contains an edge-emitting $Al_{0.08}Ga_{0.92}As$ single-quantum-well (SQW) active layer sandwiched between graded-index-of-refraction separate-confinement-heterostructure (GRINSCH) layers of $Al_xGa_{1-x}As$ and that includes etched 90° mirrors and 45° facets to direct the edge-emitted beam perpendicularly to the top surface. The lasers of this type resemble the ones described in the preceding article, "Pseudomorphic-$In_xGa_{1-x}As$ Surface-Emitting Lasers" (NPO-18243), with the principal exception of the distribution of materials in the GRINSCH and SQW layers.

Like the lasers described in the preceding article, these lasers take full advantage of the well-developed edge-emitting Fabry–Perot laser technology. The structures, materials, and processes for the fabrication of lasers of both types are compatible with those of other optoelectronic devices. Consequently, these lasers are suitable for incorporation into optoelectronic integrated circuits for photonic computing; e.g., optoelectronic neural networks.

Prototype lasers like the one shown in the figure were fabricated from a wafer grown by metal-organic vapor-phase epitaxy on a (100) n^+ GaAs substrate with an n^+ GaAs buffer layer. The GaAs and $Al_xGa_{1-x}As$ layers were grown by use of trimethylgallium, trimethylaluminum, and arsine. Sources of p and n doping were diethyl zinc and silane, respectively, in hydrogen. The $Al_{0.08}Ga_{0.92}As$ active layer was 90 Å thick. The two GRINSCH layers, each 1,400 Å thick, were made by linearly grading the mole fraction, x, of AlAs from 0.2 to 0.6. The upper and lower cladding layers were 1.5-μm-thick $Al_{0.6}Ga_{0.4}As$, p- and n-doped, respectively. A cap layer of p^+ GaAs 0.2 μm thick was grown on top to facilitate the formation of an ohmic contact.

The wafer thus produced was subjected

This **Surface-Emitting Solid-State Laser** features output power and external differential quantum efficiency greater than those of other GRINSCH SQW lasers with 45° output-beam deflectors.

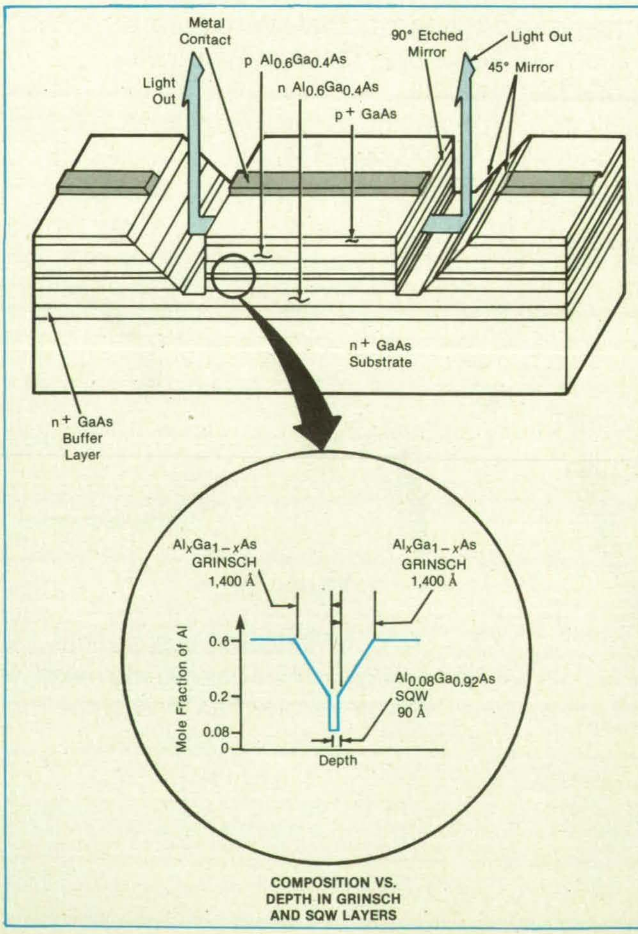

Our DMP™-160 Series Does the Work of Four Plotters, a Scanner and a Night Shift.

FREE $50 IN PENS when you purchase any large-format HI pen plotter. Windows™ Driver now available.

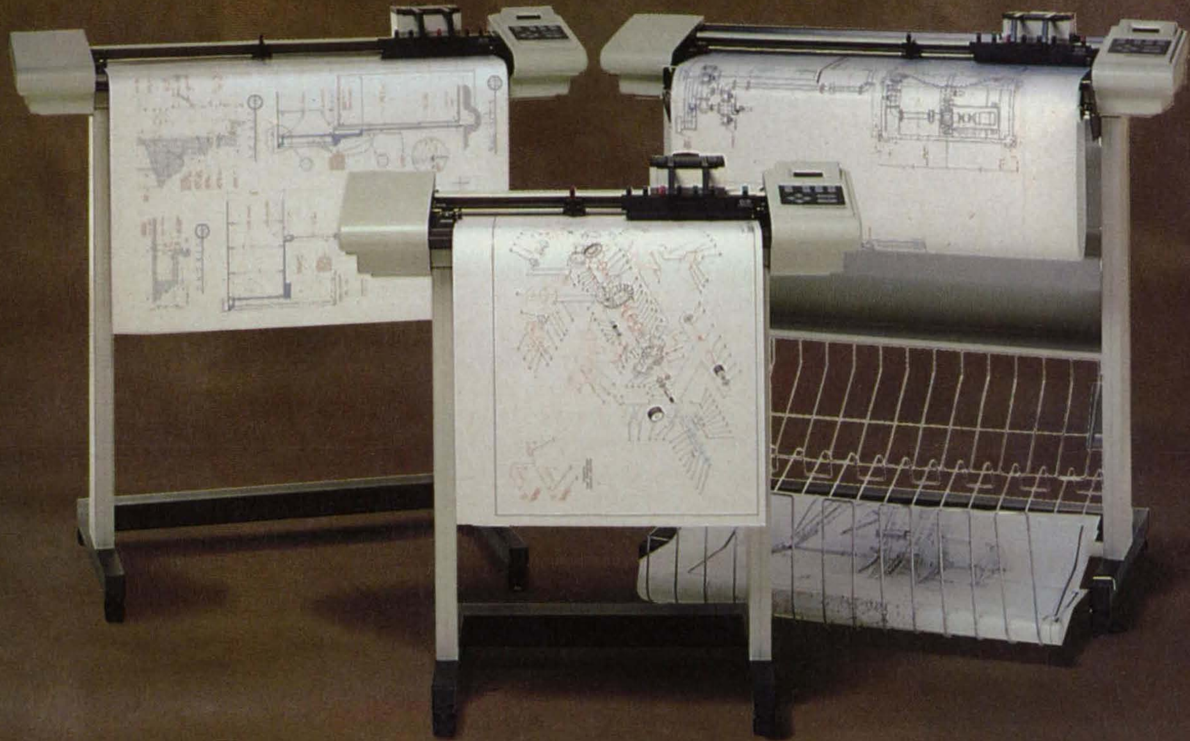

Never before has one family of plotters done so much, so fast, and so well. Our D- and E-size plotters are the only ones that include the new, highly-compact HP-GL/2 plot language and 512K standard memory. That's the equivalent of 2 MB on other plotters. And they're the only ones that can be expanded to 4 MB. So instead of tying up you and your computer during long or multiple plots, our new plotters

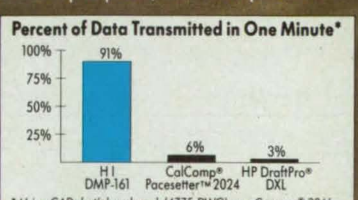

release your equipment 15 to 30 times faster than the competition.

Increased AutoCAD® Productivity. These new plotters arrive AutoCAD ready with ADI® drivers which allow you to immediately harness the full productivity features of the DMP-160 Series.

Set-It-and-Forget-It Unattended Plotting. Our DMP-162R E-size plotter comes with 1MB of memory and an automatic rollfeed and cutting system—ideal for network, multi-user or heavy plotting requirements. This workhorse does it all: Configures your plotter directly from your PC or Macintosh® with our Hot-To-Plot™ programs. Stores up to four different user configurations. Uses a pen grouping feature for up to eight times the pen life. And cuts and gathers plots in a catch-basket for immediate access. Just load a 150' roll of D- or E-size paper, push a few buttons and go back to work. Or go home.

Turn Your Plotter Into a Scanner. Only Houston Instrument offers the optional SCAN-CAD™ accessory and software that allows any DMP-160 Series plotter to double as an affordable, large format scanner.

Every Decision Should Be This Easy.™ See the new DMP-160 Series today. And find out what it's like to go home early at night. For information, or the name of your local dealer, contact Houston Instrument today at 1-800-444-3425.

HOUSTON INSTRUMENT®
A Summagraphics Company

Circle Reader Action No. 550

to ion-beam etching to produce the 90° Fabry–Perot-mirror surfaces and the 45° output-beam-deflecting mirror surfaces. The mirror surfaces were positioned to define laser cavities ~500 μm long, and the resulting broad surface-emitting lasers were patterned by use of photoresist into laser stripes 100 μm wide. Ohmic metal contacts were then applied.

In tests, the lasers exhibited a threshold current of 300 mA, a peak output power of 380 mW, and an external differential quantum efficiency of 17 percent without coating of the mirror facets. The threshold current is comparable to, or lower than, previously reported threshold currents, while the output power and external differential quantum efficiency exceed those previously reported for surface-emitting lasers configured similarly. The performance could be improved by decreasing the distance between the 90° and 45° mirror surfaces, by smoothing these surfaces (e.g., by wet chemical and dry etching or by chemically-assisted ion-beam etching), and by applying highly reflective coats to the 45° mirror surfaces.

This work was done by Jae H. Kim of Caltech for **NASA's Jet Propulsion Laboratory**. *For further information, Circle 50 on the TSP Request Card.*

This invention is owned by NASA, and a patent application has been filed. Inquiries concerning nonexclusive or exclusive license for its commercial development should be addressed to the Patent Counsel, NASA Resident Office-JPL [see page 18]. Refer to NPO-18281.

"Forback" dc-to-dc Converters

Features of older converter circuits are combined to obtain advantages and eliminate disadvantages.

Goddard Space Flight Center, Greenbelt, Maryland

Dc-to-dc power-converter circuits of a configuration called "forback" resemble circuits of standard configurations called "forward," "flyback," and "Cúk" (see Figure 1). The forback circuit, which employs minor modifications to existing topologies, combines some of the advantages, while eliminating some of the disadvantages, of the older circuits.

The unique features of the forback configuration are best explained by reference to the isolated version illustrated in Figure 2. As in the Cúk circuit, the secondary winding of the transformer is coupled capacitively to the rectifier and filter circuit. As in the forward circuit, energy is delivered to the secondary while the switching transistor is in the conducting portion of the operating cycle. As in the flyback circuit, energy that is stored in the core of the transformer during the transistor-conduction period is released to a capacitor during the transistor-nonconduction period. Thus, energy is transmitted to the secondary side of the transformer during both the transistor-conduction and the transistor-nonconduction periods of the operating cycle.

The relationships among voltages and currents in the forback configuration are such as to enforce volt-second balance on the core of the transformer. Although the portion of the forback circuit on the primary side of the transformer is similar to that of the forward circuit, the flyback arrangement of the capacitively coupled secondary winding eliminates the need for the reset winding that is used in the forward circuit to return energy stored in the

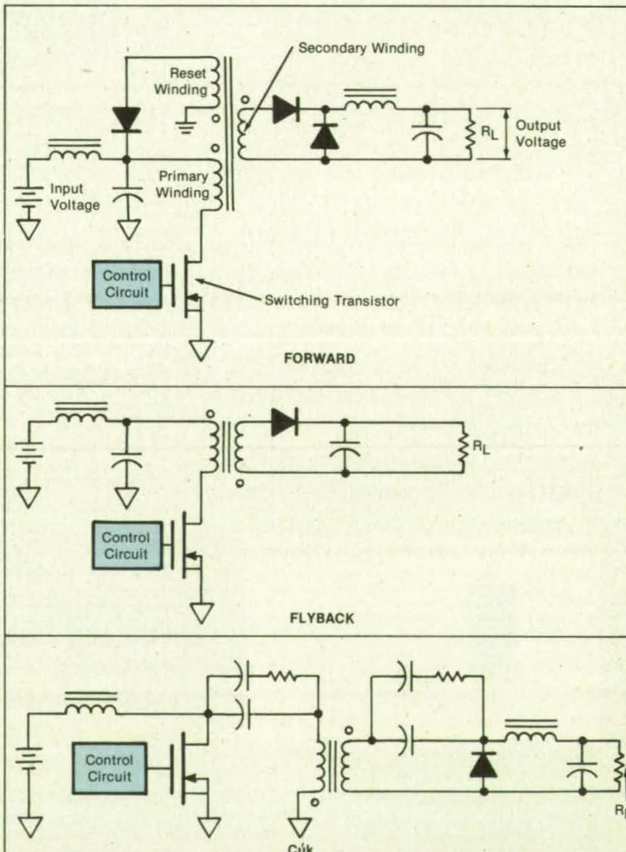

Figure 1. These **dc-to-dc Converter Circuits** are the predecessors of the forback circuit.

core to the primary side. The voltage stresses on the switching transistor of the forback are less than those in a similar Cuk circuit that includes the same capacitively coupled network on the secondary side of the transformer.

This work was done by Alan T. Lukemire of **Goddard Space Flight Center**. *For further information, Circle 102 on the TSP Request Card.*
GSC-13404

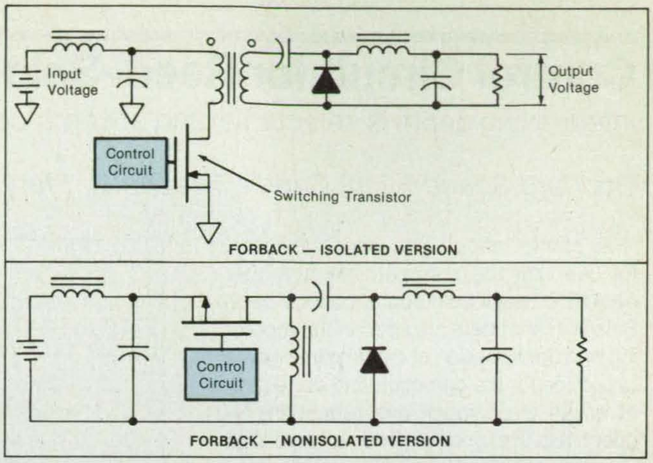

Figure 2. The **Forback Circuit** contains numbers and types of components similar to those of its predecessors. In addition to the isolated version discussed din the text, there is also a nonisolated version.

Lightweight, High-Yield Photocathode

Quartz cloth multiplies electron current.

NASA's Jet Propulsion Laboratory, Pasadena, California

A layer of Astroquartz (or equivalent) cloth woven from quartz thread is an essential part of a high-yield photocathode. Such a photocathode is desirable in applications in which low power consumption is required.

In an experiment (see figure), a piece of Astroquartz material with an aluminum backing was placed on a grounded metallic plate. The aluminum backing was in direct electrical contact with the metallic plate and thus also at ground potential. A positively biased wire-mesh grid was placed 1 cm above the quartz cloth, resulting in a strong electric field in the region between the grid and the cloth.

When the cloth was illuminated with ultraviolet light (to which the quartz cloth was semitransparent), photoelectrons were produced at the aluminum backing surface. The photoelectrons were accelerated by the electric field. When the high-energy electrons collided with the quartz cloth, electron multiplication occurred via the generation of secondary electrons at the surface of the cloth. These secondary electrons were accelerated by the strong electric field and were ejected into space.

In the experiment, the ratio between the total current emitted from the aluminum surface covered by the quartz cloth and the current emitted by the aluminum surface alone was measured at various applied voltages. For example, at a potential of 2.0 kV, the total current emitted from the surface covered by quartz cloth was 2.66 times as large; at 4.0 kV, it was 667 times as large.

This work was done by Philip L. Leung and Stephen B. Gabriel of Caltech and Ralph F. Wuerker of the University of California at Los Angeles for **NASA's Jet Propulsion Laboratory**. *For further information, Circle 58 on the TSP Request Card.*
NPO-18226

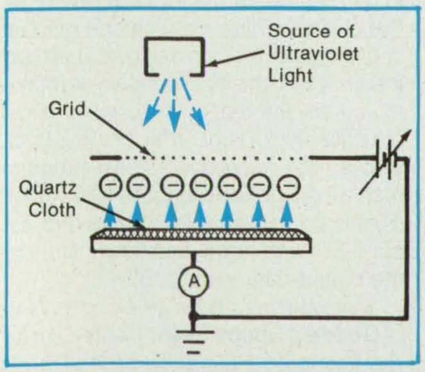

Quartz Cloth Multiplies the Electron Current emitted by an aluminum photocathode sensitive to ultraviolet light when placed in an external steady-state electric field.

Control Circuit for Reed-Solomon Encoder

Interleaving depth is selectable, and accommodation to the input data rate is automatic.

Goddard Space Flight Center, Greenbelt, Maryland

A control circuit has been designed for use with the commercially available AHA4610 Reed–Solomon encoder. Reed–Solomon encoders are used in the recording and transmission of digital data signals to provide for the detection and correction of errors in playback and reception, respectively. The control circuit is needed to select the depth of interleaving and to synchronize the input and output blocks of data and parity bits with suitable clock signals. By use of data buffers, the input and output data streams can be fed into and out of the encoder at the internal clock rate of the encoder. The internal clock rate of the encoder, the data rate of the source of data, and the data rate of the destination equipment can all differ from each other. The control circuit adapts automatically to any input data rate from 0 to 80 Mb/s.

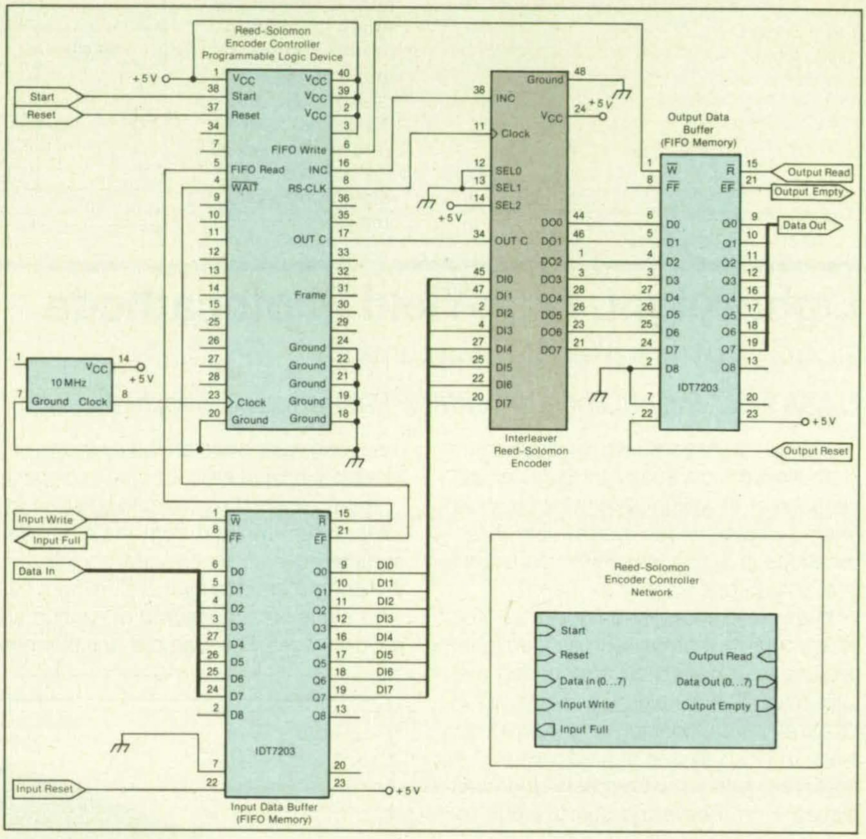

This **Control Circuit** provides synchronizing and control signals for a Reed-Solomon encoder. With the control circuit, the encoder can operate with asynchronous input and output data streams at rates up to 80 Mb/s.

The control circuit (see figure) includes two first-in/first-out (FIFO) memory chips as data buffers and one programmable logic device, which acts as a network controller. The particular encoder provides a (255,223) Reed–Solomon code and can be programmed to interleave at any depth from one to eight. This means, for example, that when operated at a design interleaving depth of five, the input data are encoded in blocks of 1,115 bytes, along with 160 bytes of parity data, to produce code blocks of 1,275 bytes, capable of correcting an error burst up to 80 bytes long.

The control circuit selects the interleaving depth by holding the three selecting lines (SEL0, SEL1, and SEL2) of the interleaving portion of the Reed–Solomon encoder at the appropriate logic levels. The control circuit provides the 10-MHz internal-clock (INC) signal, which corresponds to a data rate of 80 Mb/s. Data present on the input pins of the interleaver (DI0 through DI7) are clocked into the interleaver when INC goes high. INC must remain high during the input data block (1,115 bytes at an interleaving depth of five).

After a delay of one clock period, the data present on lines DI0 through DI7 are routed through the interleaver and appear on the output data lines of the interleaver (DO0 through DO7). The output signal OUTC goes high to indicate that data on the output lines are valid. A new byte appears on the output every clock cycle during an input block.

Once the correct number of input bytes have been clocked in, INC must be brought low. One clock cycle later, OUTC goes low, indicating that subsequent data on the output lines will be parity bytes. The interleaver must then be clocked the required number of times to put out all the parity bytes for the given interleaving depth.

The network-controller portion of the control circuit provides all the data-management and control signals for the encoder. These include the following signals: "start," "reset," "input write," "output read," "input full," "output empty," "data in (0...7)," and "data out (0...7)."

When "reset" is high and "start" is low, clocking the system for a minimum of 32*n* clock periods (where *n* is the interleaving depth) clears the interleaver. Bringing "reset" to low and taking "start" high for at least two clock periods starts the operation of the control network.

Data fed into the circuit from the source by use of the "input write" line are stored in the input FIFO. As long as the "input full" line is high, data can be written into the FIFO. When data are put into the input FIFO, the network controller automatically produces the control signals needed to manage flow of data from the input FIFO, through the encoder, out of the encoder, and into the output FIFO.

When data are written into the output FIFO, the "output empty" line goes high. This indicates that data are now available to be read out of the FIFO by use of the "output read" line. Data can be read out of the system as long as "output empty" is high. Thus, the input data are asynchronous from the output data, with the output data blocks larger than the input data blocks. The network-controller programmable logic device produces INC and the signals on the input FIFO read and output FIFO write lines, and it synchronizes the output data with OUTC.

This work was done by Douglas Ross of **Goddard Space Flight Center**. *For further information, Circle 15 on the TSP Request Card.*
GSC-13342

Books and Reports

These reports, studies, handbooks are available from NASA as Technical Support Packages (TSP's) when a Request Card number is cited; otherwise they are available from the National Technical Information Service.

Mathematical Modeling of a Nuclear/Thermionic Power Source

Lifetime and performance are predicted, taking into account swelling of fuel elements.

A report discusses mathematical modeling for prediction of the performance and lifetime of a spacecraft power source that is an integrated combination of a nuclear-fission reactor and thermionic converters. The core of the reactor is an array of 176 closely packed thermionic fuel elements, each of which consists primarily of a cylindrical housing that contains 6 thermionic converters with UO_2 fuel inside. The converters within each thermionic fuel element are electrically connected in series. The nuclear reaction is controlled by cylindrical control drums that surround the reactor vessel and by seven shutdown rods in the core. The reactor is cooled by a pumped liquid metal that is, in turn, cooled by a heat-pipe radiator. Electrical power of 100 kW at 100 V is extracted by a series/parallel network in which the total of 1,056 thermionic converters are connected in 4 parallel strings, within each of which 264 converters are connected in series.

The principal cause of degradation and ultimate failure is considered to be short-circuiting of the emitters to the collectors in the thermionic converters, caused by swelling of the UO_2 fuel pellets. Accordingly, to conduct this study, a detailed mathematical model of the nuclear reaction, thermal conditions in the core, and thermionic performance was combined with a mathematical model of swelling of the fuel. The inputs required for the model included the geometries of the reactor, coolant loop, and radiator; the drop in temperature in the coolant loop; the average emitter temperature; the pressure of the cesium in each of five radial zones; the relative-power-density profile of the reactor; and the particular series/parallel electrical configuration (which could be the one described above or a different one).

The computer code that implements the model is started with all of the inputs. First, it calculates temperatures of the emitters and collectors and the performances of the converters, and it adjusts the thermal power and the temperatures in the reactor to obtain the specified electrical output power and voltage. Next, time is stepped forward, and the model calculates the distortion of the emitter during the time step on the basis of the temperature, power density, consumption of fuel, and fraction of volume of fuel occupied by voids. Damage to the radiator by meteoroids and debris is also estimated. The effects of the distortion of the emitter and of the degraded performance of the radiator are used to derive a new set of temperatures of emitters and collectors to deliver the desired electrical output. These calculations are repeated over many time steps until the emitters have distorted so much as to cause shorting in so many converters that the system can no longer deliver the required power. At that point, the system is deemed to have failed.

Applying this analysis to the specific 100-kW reactor, it was found that in the worst-case scenario, initial shorting would begin after 4 years and the system would last another 2 years. In a nominal scenario, the first short would occur after about 8 years, and the system would fail about 2.3 years later.

This work was done by Jan W. Vandersande and Richard C. Ewell of Caltech for **NASA's Jet Propulsion Laboratory**. *To obtain a copy of the report, "Lifetime Performance Predictions for In-Core Thermionic Converters," Circle 146 on the TSP Request Card.*
NPO-18312

Bilevel Shared Control of a Remote Robotic Manipulator

Teleoperator and autonomous modes would be blended, each overcoming deficiencies of the other.

NASA's Jet Propulsion Laboratory, Pasadena, California

A proposed concept for the control of a remote robotic manipulator calls for a blend of autonomous and teleoperator (hand-control or other commands from the human operator) control modes. The concept is called "bilevel shared control" because it calls for a two-level hierarchical control system that would accept commands in both modes at both levels, sharing control between the two modes in such a way that each mode would overcome some of the deficiencies of the other. The concept is particularly applicable to a robotic system characterized by a long communication delay between the local (operator's control) site and the remote (robotic-manipulator) site or to a robotic system intended to function partly autonomously, with occasional intervention by the operator.

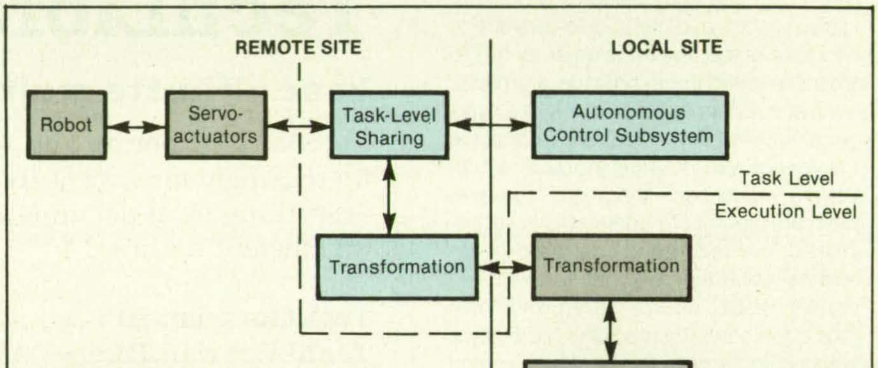

In **Bilevel Shared Control**, both task-level and execution-level functions would be performed at local and remote sites, both types of functions sharing both autonomous and teleoperative inputs.

Recent articles in *NASA Tech Briefs* described aspects of multilevel hierarchical control. To recapitulate: The control hierarchy ranges from larger digital processors and the associated software at the highest (task-planning) level down through smaller digital processors with lower-level software and possibly some digital/analog interface circuitry at intermediate (partly planning, partly reflex-action) levels, to more digital/analog interface circuitry, control actuators, and sensors at the lowest (execution) level. In bilevel shared control, such a hierarchy would be simplified to only the high (task) level and the low (execution) level.

In a bilevel shared-control system, functions at both levels would be performed at both the local and remote sites (see figure). At the local site, a planning algorithm would generate task-level autonomous commands, which would be transmitted to the remote site. At the same time, the operator would acquire (1) visual information about the remote manipulator and its surroundings through television displays and (2) tactile information about the contact and inertial forces on the manipulator via a force-reflecting hand controller. In response to this sensory information, the operator would generate teleoperative commands to correct the movements of the manipulator.

The autonomous commands to be generated by the planning algorithm would include the specification of (1) a coordinate system (called the "task" coordinate system) attached to the remote manipulator and (2) high-level task trajectories in this coordinate system. A hybrid position/force scheme would be used to represent low-level tasks in terms of simpler motion and force trajectories specified in the sets of orthogonal motion and force coordinates that would constitute the task coordinate system. To blend the autonomous and teleoperative control modes, it would be necessary to transform the teleoperative commands from the hand-controller (local) coordinate system to the task (remote) coordinate system. Part of this transformation would be performed locally and part remotely: the part of the transformation that involves the robot-joint angles would best be done remotely where communication delays were significant because the angle information would, thereby, be less outdated.

At the execution level, the commanded trajectories could come directly from the autonomous part, the teleoperator part, or a mixture of the two. For this purpose, it is necessary only that the servocontroller be capable of tracking the commanded motion and/or force trajectories in a stable fashion. To reduce the detrimental effects of communication delays, whenever such delays were significant, integration of teleoperator and autonomous commands would be allowed only along directions of motion, while forces would be controlled autonomously. The integration would be effected by determining when and how the two types of commands may be mixed, and performing the mixing process in software via a mixing matrix, the entries of which would reflect the relative weight given to each teleoperative and autonomous input.

This work was done by Samad A. Hayati and Subramanian T. Venkataraman of Caltech for **NASA's Jet Propulsion Laboratory**. *For further information, Circle 80 on the TSP Request Card.*

This invention is owned by NASA, and a patent application has been filed. Inquiries concerning nonexclusive or exclusive license for its commercial development should be addressed to the Patent Counsel, NASA Resident Office-JPL [see page 18]. Refer to NPO-17800.

Bandwidth-Synthesizing FM Radar

Resolution would be increased by a factor of *N*.

NASA's Jet Propulsion Laboratory, Pasadena, California

A proposed frequency-modulation (FM) radar system would use sawtooth-waveform linear frequency sweeps and a return-signal-processing scheme in which samples of signals from *N* consecutive sweep periods would be combined in such a way as to multiply the range resolution by a factor of *N*. This system could be regarded as synthesizing a bandwidth of *N* times that of its transmitted signal in the sense that to increase the resolution of an ordinary radar system in which consecutive samples are not combined, it is necessary to increase the bandwidth of the transmitted signal by the same factor. The bandwidth-synthesizing scheme would likely be used in FM radar altimeters.

Figure 1 shows time and frequency relationships among the sawtooth transmitted signal, the sawtooth return signal, and a theoretical single linear sweep of *N* times the actual bandwidth, *B*. The bandwidth-synthesizing effect would depend on coherency in the phase of the transmitted sawtooth FM and on coherent Nyquist sampling and phase detection in the processing of the return signal. Under these conditions, samples obtained in *N* consecutive linear frequency sweeps over bandwidth *B* would be indistinguishable from the ambiguous (with respect to frequency) samples that, in principle, would be obtained by sampling coherently from the single linear sweep over bandwidth *NB*. The ambiguity would be caused by the analog reconstruction of the broader sweep from a sampling frequency many times as small as the broader bandwidth, *NB*.

In one version of the system, illustrated in Figure 2, the transmitted sawtooth FM sweep would be produced at an intermediate frequency of *B* by a memory and a digital-to-analog converter controlled by a timing signal from a master oscillator.

The intermediate frequency (IF) of *B* is chosen because it would ease the handling of the signal in the voltage domain rather than in the complex in-phase/quadrature domain. The resultant IF FM signal would contain sweeps from a frequency of *B* to a frequency of 2*B*, repeated with a period *T*. There would be *N* sweeps, making the total duration of the waveform *NT*.

The IF FM signal would be mixed in a radio-frequency transceiver with a carrier signal generated by frequency multiplication from the master oscillator. The output of this mixing operation would be band-pass-filtered and transmitted to the target. In essentially the reverse of the transmission process, the return signal would be radio-frequency-demodulated to IF in the transceiver. The IF return signal would be sampled at a rate of 4*B*, and the frequency of the samples would be shifted by *B* to produce IF demodulated in-phase and quadrature (IQ) samples. The IQ samples would then be subsampled at a rate of *B*.

Subsequent digital processing would imitate arithmetic in the complex plane: Complex conjugate samples of the *NT*, *NB* linear frequency sweep would be multiplied by the IF demodulated IQ samples. A fast Fourier transform (FFT) of size *NTB* would be applied to the complex products. Each FFT coefficient would then correspond to a sample taken at a time resolution of 1/*NB*. The associated range resolution would be *c*/2*NB* (where *c* is the speed of light), which is *N* times that of a conventional radar of bandwidth *B*.

This work was done by Chialin Wu of Caltech for **NASA's Jet Propulsion Laboratory**. *For further information, Circle 161 on the TSP Request Card.*
NPO-18142

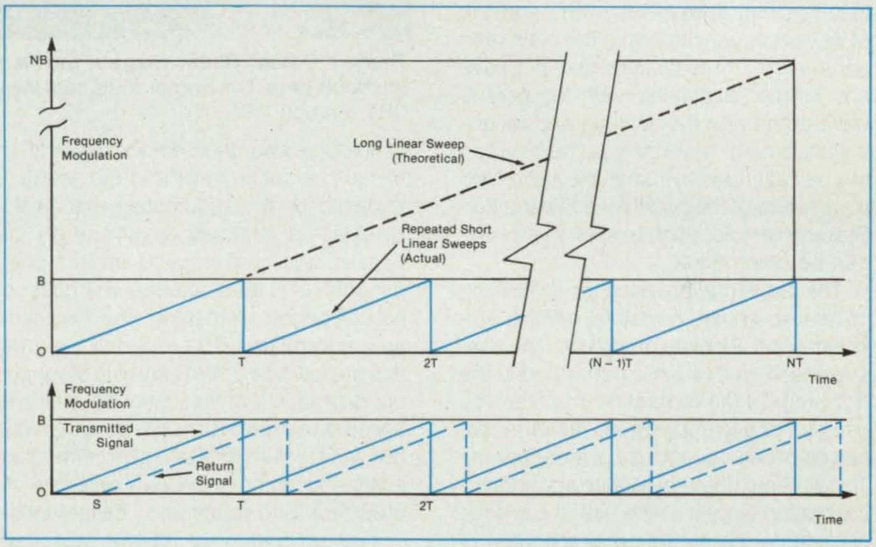

Figure 1. **Transmitted and Return Signals**, each containing *N* linear frequency sweeps of bandwidth *B* and duration *T*, would be processed in such a way as to synthesize the effect of a single linear frequency sweep of bandwidth *NB* and duration *NT*.

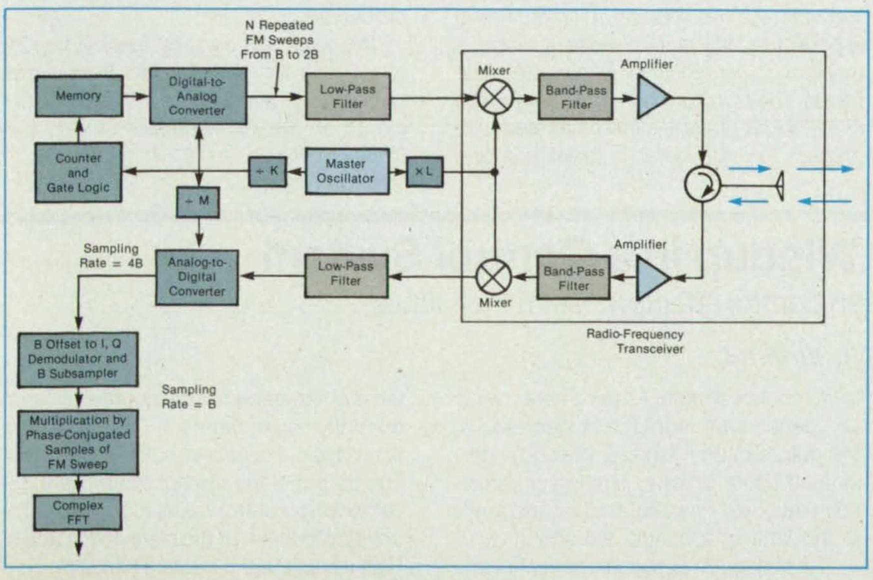

Figure 2. This **FM Radar System** would achieve a range resolution *N* times that of a conventional FM radar of the same bandwidth by implementing the bandwidth-synthesizing signal-processing scheme.

Another Technique for Calibration of Polarimetric Radar

The only artificial target(s) required is at least one trihedral corner reflector.

NASA's Jet Propulsion Laboratory, Pasadena, California

A technique for the calibration of a polarimetric radar system requires a minimum of only one artificial target in the scene, or if only the crosstalk of the system is to be calibrated, no artificial target is needed. This is the latest in a series of polarimetric-radar-calibration techniques developed by NASA's Jet Propulsion Laboratory and reported in *NASA Tech Briefs*. This is a relatively inexpensive technique that involves a four-stage procedure in which a different aspect of the radar system is calibrated at each stage.

The technique applies to polarimetric synthetic-aperture-radar data that have been preprocessed into a compressed form. As part of the preprocessing, the measured scattering matrix for each resolution element is symmetrized. This symmetrization is equivalent to an assumption that the transmitting and receiving subsystems are reciprocal. The assumption, in turn, is only approximately true, and one of its consequences is that the estimated parameters of the system may not have any simple relationship with the parameters of the real transmitting and receiving equipment. Nevertheless, the data can still be calibrated by use of the estimated parameters of the system, so that the true Stokes matrix for each resolution element can be determined.

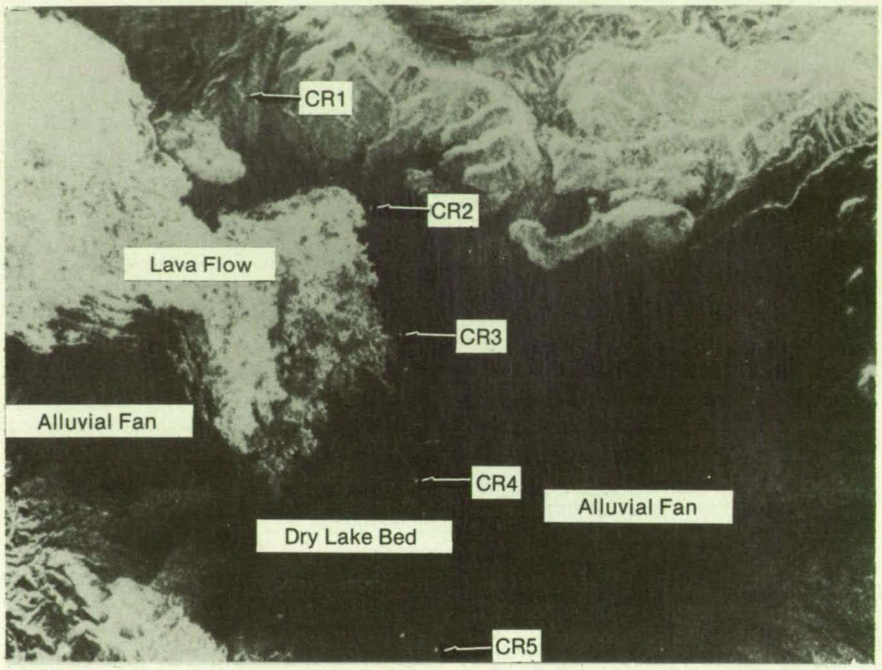

This is a **C-Band Radar Image of the Pisgah** lava flow in the Mojave Desert. To calibrate the radar data, five corner reflectors were placed in the scene at the locations marked CR1 through CR5.

The technique provides for calibration of relative phase, crosstalk, relative amplitude, and absolute amplitude. The relative-phase calibration is performed in the first stage of the calibration procedure by use of a phase-equalization scheme that has come into routine use in recent years. This scheme does not require any artificial calibration targets in the scene but does depend on the existence of a portion of the scene for which the difference between the phases in the two copolarization (horizontal/horizontal and vertical/vertical) backscattering channels are known.

The crosstalk calibration is performed in the second stage of the procedure. This calibration also does not require any artificial calibration targets in the scene. It is based on the assumption that (1) the crosstalk is relatively small and (2) the copolarization and cross-polarization components of the scattering matrices of natural targets distributed over the scene are uncorrelated. The crosstalk parameters are extracted from statistics of various cross products of (1) scattering matrices based on the preprocessed but otherwise raw radar-return data and (2) intermediate scattering matrices that lack only relative-amplitude and radiometric calibrations.

The calibration for relative amplitude (between the two copolarization channels) is performed in the third stage. It requires trihedral corner reflectors in the scene (see figure). The result is a radar image in which all the radar channels are calibrated with respect to each other in amplitude and phase. In the fourth stage, an overall absolute radiometric calibration is performed by comparison of the measured with the known radar cross section of trihedral corner reflectors in the scene. (Other artificial targets could be used, but trihedral corner reflectors are cheap and relatively insensitive to misalignments.)

One of the advantages of the four-step calibration procedure is that one does not have to perform the entire procedure if one does not need the full calibration. For example, if all that is needed is a calibration for crosstalk, it is not necessary to continue past the second stage of the procedure.

This work was done by Jakob J. van Zyl of Caltech for **NASA's Jet Propulsion Laboratory**. *For further information, Circle 12 on the TSP Request Card.*
NPO-18068

Preventing Integrator Windup in a Control System

Inputs to integrators are limited when control effectors reach their limits.

Langley Research Center, Hampton, Virginia

A design concept for a control system addresses the problem of how to (1) prevent control inputs to the plant (the system to be controlled) from exceeding the electrical limits imposed by the mechanical limits of the control actuators in the plant and (2) prevent windup in the integrators in the control system. As used here, "windup" denotes an increase or decrease in the output of an integrator beyond a designated upper or lower limiting or saturation value; e.g., a value that corresponds to the limit of a control actuator.

The concept is applicable to control systems of the general configuration illustrated at the top of Figure 1. (This configuration is typical of aircraft autopilot systems.) The output of the control system is **u**, the vector of *m* control inputs to the plant. The transfer function of the plant is denoted by *P*(*s*), where *s* is the Laplace-transform complex frequency. The sensor outputs (e.g., indications of speed and altitude) of the plant are represented by the feedback vector **y**, and the command input (e.g., the commanded values of speed and altitude) are represented by $\mathbf{y}_c$. The behavior of this control system is represented by

$$\mathbf{u} = \frac{G_I}{s}[y_c + H_1(s)y] + H_2(s)y$$

where G_I is an $m \times m$ matrix of integral gains, and $H_1(s)$ and $H_2(s)$ are stable matrix $m \times p$ transfer functions.

The new concept consists of two main parts. The first part is to rearrange the terms of the control equation (and correspondingly modify the block diagram of the control system) in such a way as to move the integrators into the output path of the control system, as shown in the lower part of Figure 1. This modification makes possible the second part of the concept, which involves limiting the inputs to the integrators when one of the control inputs of the plant reaches its limit.

Figure 2 illustrates the further modifications pursuant to the second part of the concept. The integral-gain matrix G_I is partitioned into m column vectors, $[G_1 \ldots G_m]$, each vector corresponding to an integrator input. A logic block is added to the output path of each G_i. To understand the operation of a logic block, suppose, for example, that the output of integrator 1 (control input 1) has reached its maximum or saturation value (e.g., a maximum throttle setting). At that point, logic block 1 sets the input to integrator 1 (δ_{o1}) at zero. The input to logic block 1 (δ_{i1}) is thereafter monitored for its sign. As long as δ_{i1} remains positive or zero, δ_{o1} is kept at zero to prevent the integrator output from exceeding its maximum or saturation value. When δ_{i1} becomes negative, δ_{o1} is then set equal to δ_{i1}, and the output of integrator 1 begins to fall below the saturation value. Similar considerations apply at the minimum saturation value, except that the arithmetic signs are reversed.

In designing a control system according to this concept, it is necessary to select the control input that is to be considered primary for each regulated variable in **y**. In the example of Figure 2, the selection has been made for each important issue

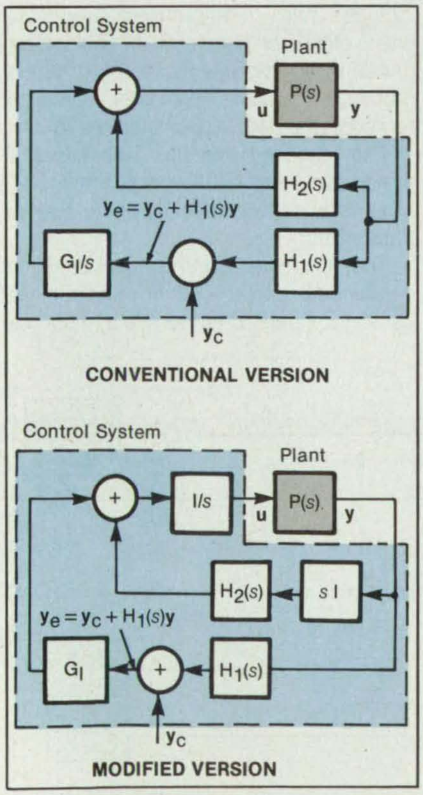

Figure 1. The **Positions of the Integrators Are Moved,** and differentiators are added to one branch to compensate for the move. These modifications make it possible to implement the new control concept illustrated in Figure 2.

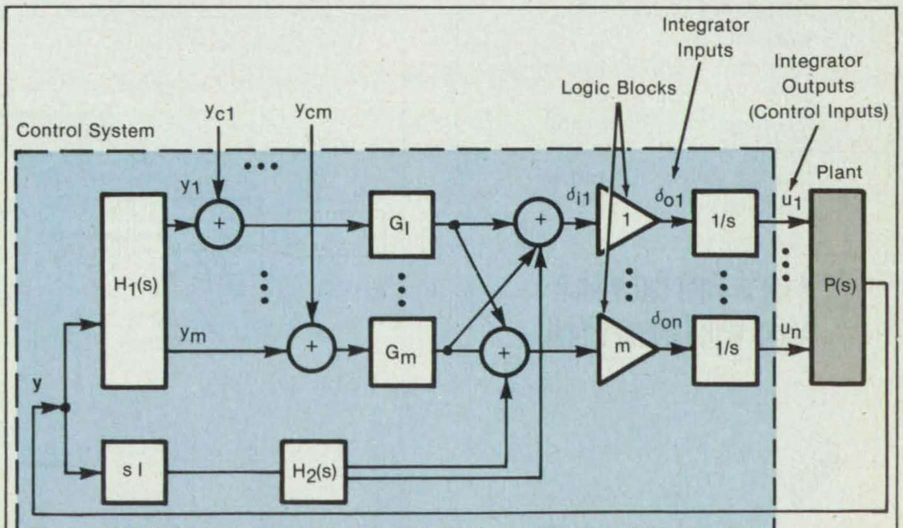

Figure 2. The **Gain Matrix Is Partitioned,** and logic blocks are added to implement the limitations on the control inputs.

that needs to be resolved early in the controller design process in which control input will be the primary control effector for each regulated variable. Assume the selection has been made for control input δ_{oi} to control the corresponding $\mathbf{y}_i$. This selection is reflected in the design of the limiting logic.

The gain vector G_1 has the following form:

$$G_1 = \begin{bmatrix} G_{11} \\ G_{12} \\ \vdots \\ G_{1m} \end{bmatrix}$$

Each gain G_{1i} (i = 1 to m) feeds y_{e1} to the corresponding control-input integrator. If, for example, control input 1 reaches a limit, gains $G_{12} \ldots G_{1m}$ must be set to zero. Otherwise, y_{e1} (which is non-zero while the control input 1 is on the limit) would bias the remaining active controls 2 . . . m and could destabilize the total system.

This work was done by Isaac Kaminer of Boeing Co. for **Langley Research Center**. *For further information, Circle 119 on the TSP Request Card.*

Inquiries concerning rights for the commercial use of this invention should be addressed to the Patent Counsel, Langley Research Center [see page 18]. Refer to LAR-14337.

Optical Phase-Locked Loop for Optical Communication

Phase-error variance of less than 0.05 mrad^2 is achieved with a relatively-narrow-band loop.

NASA's Jet Propulsion Laboratory, Pasadena, California

Tracking of the phase of a laser beam has been demonstrated with an experimental optical phase-locked loop of narrower bandwidth than has been used before. Potential applications for optical phase-locked loops include free-space and fiber-optic communications, navigation, and scientific instrumentation in which receivers may be required to track the phases of transmitted signals.

Heretofore, coherent optical communication systems have been based on diode lasers (as distinguished from diode-pumped solid-state lasers). Because of the broad spectra emitted by diode lasers, typical coherent phase-tracking loops that contain diode-laser oscillators must have bandwidths of several megahertz — too wide for use in deep-space communication or wherever else received signals may be weak. Recently developed diode-pumped solid-state lasers emit spectra of subkilohertz width, enabling the use of receiver phase-tracking loops that have bandwidths of only a few kilohertz.

The experimental apparatus (see figure) includes two diode-pumped solid-state lasers of the non-planar-ring-oscillator type, one of which represents the transmitting (tracked) oscillator, the other of which represents the local oscillator in a receiver (the tracking oscillator). The output of the transmitting oscillator is amplitude-modulated with a pulse-position-modulated data stream.

The transmitted signal is attenuated and combined in a beam splitter with the local-oscillator signal, and the two signals are

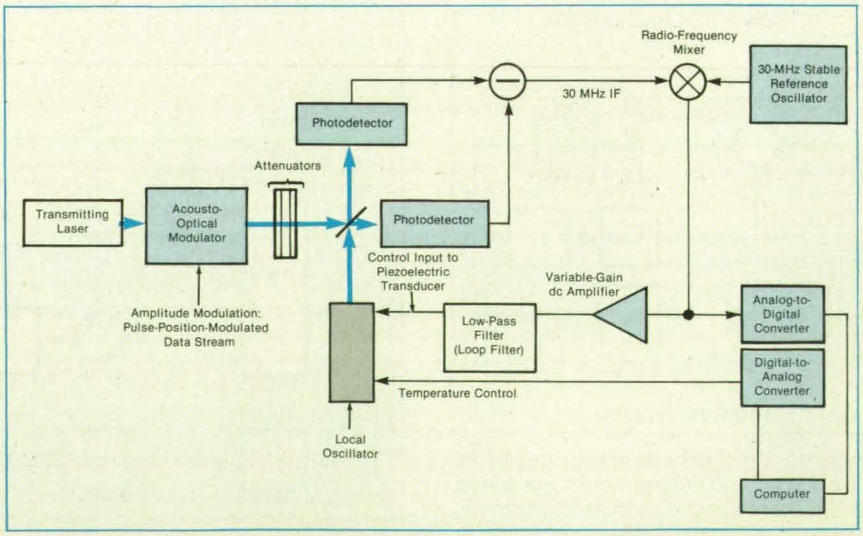

This Optical Phase-Locked Loop exhibits a phase-error variance of 5×10^{-5} rad^2 at a closed-loop bandwidth of 20 kHz.

detected using balance-detector configuration to an IF frequency of 30 MHz. The difference between the outputs of the photodetectors is mixed with the 30-MHz output of a stable reference oscillator to obtain a raw baseband signal. The raw baseband signal is processed through a variable-gain dc amplifier to obtain an error signal. The error signal is low-pass-filtered and fed to a piezoelectric transducer that adjusts the frequency of the local oscillator.

The piezoelectric transducer operates rapidly enough to track the instantaneous phase within a narrow range: its tuning range is not wide enough to enable it to compensate for large, slow drifts in lasing frequency. Consequently, a frequency-compensation loop must be included to maintain the piezoelectric transducer at the center of its dynamic range. This is accomplished by applying a small bias signal at the temperature controller of the local-oscillator laser. The bandwidth or the update rate of the temperature controller is usually limited to less than 10 Hz because temperature control is inherently slow.

When the loop is in lock, any difference between the frequencies or phases of the two laser oscillators results in a dc signal at the output of the radio-frequency mixer, which functions as a phase comparator. Temperature control is accomplished by sampling the output of the phase comparator and applying the proper compensating signal at the temperature-control input.

The results of the phase-locking experiment indicate that at a closed-loop bandwidth of 20 kHz, the phase-error variance is only 5×10^{-5} rad^2. At and above this closed-loop bandwidth, the laser spectrum resembles that of an oscillator that has a white frequency noise with an instantaneous spectral width of 0.2 Hz.

This work was done by Moe Z. Win, Chien C. Chen, James R. Lesh, William K. Marshall, and Marc D. Rayman of Caltech and Robert A. Scholtz of the University of Southern California for **NASA's Jet Propulsion Laboratory**. *For further information, Circle 92 on the TSP Request Card. NPO-18200*

Improvements in Processing and Aiming for Squint-Mode SAR

Techniques reduce Doppler drift and accommodate large range walk.

NASA's Jet Propulsion Laboratory, Pasadena, California

An improved technique for aiming the antenna of a synthetic-aperture radar (SAR) operating in the squint imaging mode (SIM) complements an improved algorithm for processing the raw SIM SAR data. These techniques were developed to reduce the deleterious effects of two unique characteristics of SIM SAR: large range walk and large variation of the Doppler centroid as a function of range.

Range walk is defined as the difference between the ranges (distances) to a point target when the target enters and when it leaves the illuminating radar beam. A large range walk is undesirable because it causes significant dispersion of the point-target response in range if the standard frequency-domain range-and-Doppler-processing algorithm is employed for the azimuth compression. A large variation of the Doppler centroid with range is undesirable because it necessitates an increase in the rate of updating the azimuth-reference function that is used in processing the raw SAR data.

The improved technique for aiming is based on the assumption that the yaw, pitch, and roll angles of the vehicle (a spacecraft in the original application, but presumably also an aircraft) carrying the SAR are known, that the yaw and pitch of the vehicle are controllable, and that the antenna is electronically steerable in tilt about the roll axis of the vehicle. The technique involves a specification of adjustments of the yaw, pitch, and tilt (see Figure 1) that orient the boresight of the antenna such that the Doppler centroid line (the

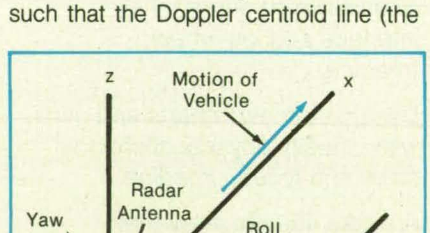

Figure 1. **Selected Aspects of the SAR Geometry** are illustrated to define terms used in the text.

CyberResearch April Product Showcase

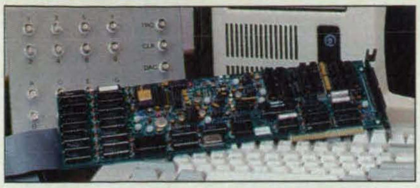

1 MHz 12-Bit ComputerScope Offers Unique Advantages

The ComputerScope High-Speed Data Acquisition System from **RC Electronics** includes a 1MHz A/D board, a BNC Terminal Panel, and Digital Oscilloscope Software. A specially-designed series of software modules provides tightly-integrated *real-time* performance. Call us for detailed information on the EGAA software system.

- Sixteen 12-bit Analog Input Channels.
- 64K-Sample Buffer for Maximum Performance.
- Supports Pretriggering Sample Mode.
- Comes complete with ComputerScope Software.

#INST 601 1MHz ComputerScope System.....**$2495**
#INST 605 EGAA Multi-Tasking Software.........**$795**
#INST 615 Electronic Chart Recorder & AutoDisk Data Logging Software Modules...**$1195**

Circle Reader Action No. 360

WorkBenchPC – The One to Choose

During the past year there have been several new "icon-based" software packages introduced. Of all these packages, **WorkBenchPC** is the easiest to use, yet at the same time it's the most powerful. It does the best job of imitating the "look-and-feel" of a Macintosh computer. Yet it uses this look-and-feel to bring new power to data acquisition, control and analysis.

WorkBenchPC provides seamless integration with your data acquisition hardware. It finds the boards installed in your system, checks their configurations, and presents you with only valid menu options. You choose between "normal mode" operation which supports real-time data logging and display, and "fast mode" which collects data at the maximum speed of your hardware. Find out for yourself how much this new software can make your life easier.

Call for your FREE WorkBenchPC Demo Disk Today!

#STS 050 WorkBenchPC Software......................**$995**

Circle Reader Action No. 361

NEW Snap-Master Software: Data Acquisition for Windows

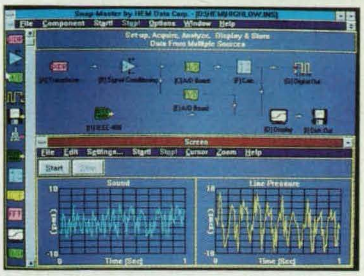

Discover Snap-Master — the only Windows-based data acquisition and analysis software to achieve high-speed, real-time data acquisition with multiple simultaneous A/D boards.

Snap-Master lets you define your own custom instruments using icons and easy-to-understand flow charts. A pre-defined database of sensors is integrated with the data acquisition system.

#HDS 200 Snap-Master Acquisition Module........**$995**
#HDS 210 Snap-Master Analysis Module............**$495**

Use modules as an integrated package or stand-alone

Circle Reader Action No. 362

EASYEST LX Software from Keithley/Metrabyte

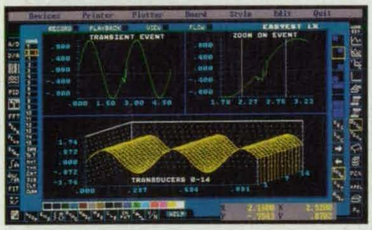

Easyest LX gives you an integrated set of tools for easy and effective implementation of a data acquisition and analysis system on any IBM-compatible PC. Each tool is represented by an icon, and the all-in-one screen puts everything in view for instant access. **No other package lets you do so much, so quickly, so easily.**

- Acquisition & analysis combined
- DMA acquisition at full speed of H/W
- All tools always displayed on screen
- Control A/D, D/A, Digital I/O, etc.
- Analyze time & frequency domains
- **Call for free Demo Disk.**

#ASY 200 EASYEST LX Software w/ 1 Free DAS Board Driver....................**$995***

*New, lower price NOW IN EFFECT. Save even *more* with CyberResearch!

Circle Reader Action No. 363

Two Instruments on a PC Card for just *$195!*

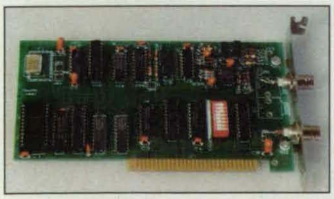

The new **SPC 100** Programmable Signal Generator and Frequency Counter from **StarPC** is a half-slot card for use in any IBM-compatible PC, with the astonishingly low price of just **$195**. Featuring 16-bit D/A resolution with .005% accuracy, it comes complete with software to control the board in either command line or menu mode. Additional drivers for are provided for Microsoft Basic, Pascal, & Fortan, QuickBASIC, TurboPascal, & assembly language to ease programming of custom systems.

- Programmable Level, Pulse Width, I/O Address, & Burst or Sweep Modes
- 1 Hz–25 KHz Analog, 5 Hz–1 MHz Pulse, & DC–10 MHz Frequency Counter
- Perfect for Automated Test Systems, Educational Uses, & Troubleshooting

#SPC 100 Programmable Signal Generator & Frequency Counter..................**$195**

Circle Reader Action No. 364

The Ultimate in High Speed/High Precision A/D

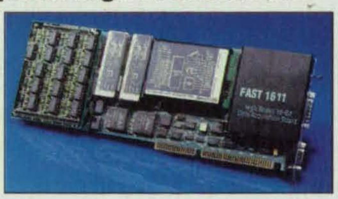

High speed and high resolution need no longer be mutually incompatible. The **FAST** series from **Analogic** offers 1 MHz A to D conversion speed combined with 14-bit or 16-bit resolution for ultra-high accuracy measurement. **You save thousands** by using a low-cost PC system in place of an expensive VME workstation.

- 4 available operating modes.
- Trigger and pacing signal controls let you customize acquisition process.
- On-board memory configured as circular buffer or single-sweep FIFO.
- Flexible channel-scan sequencing is easily programmed.

#FAST 1411 14-Bit, 1 MHz A/D Board w/ 1 Million-Sample Buffer..............**$3495**
#FAST 1611 16-Bit, 1 MHz A/D Board w/ 1 Million-Sample Buffer..............**$3895**

Additional models available with buffer memory for up to 8 million samples.

Circle Reader Action No. 365

FREE PC Systems Handbook for Scientists & Engineers

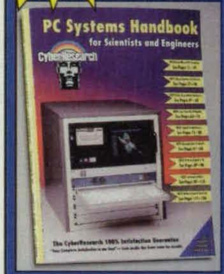

This Combination Tutorial/Catalog Includes Many Examples of PC-based Systems

The CyberResearch *PC Systems Handbook for Scientists & Engineers* describes over 1400 unique and hard to find items for PC-based engineering. Packed with useful technical information and easy-to-read diagrams, this invaluable reference should be part of every engineer's library.

Fax, Call, or Write for a complimentary copy.

Circle Reader Action No. 366

The CyberResearch Advantage:

- ☑ FREE Application Engineering
- ☑ Everyday Low Prices
- ☑ Broadest Product Selection
- ☑ 100% Satisfaction Guarantee

CyberResearch

Mailing Address:
P. O. Box 9565
New Haven, CT 06535

Worldwide
(203) 483-8815
Fax: (203) 483-9024

TOLL-FREE (800) 486-8800

Your One-Stop Source for Rack-Mount PC's

CyberResearch carries the broadest line of rack-mount and industrial computers. Now we've added new models with built-in VGA monitors. You get a compact unit with '386 or '486 power and a color display.

Optional Rack-Mount Keyboards Also Available

- Built-In 10" VGA Color Monitor & VGA Card
- 4 Megabytes of RAM (2MB for VRC 386-16S)
- Enhanced 101-Key Keyboard
- 1.2 MB Floppy Drive (or 1.44/3.5" if preferred)
- 2 Serial RS-232 Ports & 1 Parallel Port
- DOS 3.3 Software (or DOS 5.0, if preferred)

#VRC 386-16S VGA Rack-Mt. PC, 80386sx, 16MHz..............................**$2995**
#VRC 386-33 VGA Rack-Mt. PC, 80386, 33MHz..................................**$3695**
#VRC 486-33E VGA Rack-Mt. EISA, '486, 33MHz...............................**$5595**

Circle Reader Action No. 366

long axis of the area on the ground illuminated by the radar beam) is aligned with the iso-Doppler lines. This alignment reduces the variations in the Doppler centroid, thereby simplifying the processing of the raw SAR data.

The improved algorithm for processing the SAR data is a modified version of the standard frequency-domain range-and-Doppler-processing algorithm, which results in significant degradation of the point-target response at squint angles greater than 8°. The improved algorithm includes an additional step in which a secondary range-reference function used to process the raw SAR data in the range-and-Doppler domain is updated according to the change in the Doppler frequency across the azimuth spectrum; that is, a number of secondary range-reference functions based on different Doppler frequencies are generated.

In the improved algorithm (see Figure 2), the dispersed range impulse is compressed in the range-and-Doppler domain after the azimuth fast Fourier transform (FFT). The same range chirp rate is used in the range compression as is used in processing data in the broadside imaging mode. After the range-reference multiplication, the data are "corner-turned" to make them accessible in the azimuth direction. The azimuth FFT is applied for each azimuth line and is followed by a second corner turn so that the data can be again read in the range direction. Then the secondary range compression is applied. Secondary range-reference functions are generated for a number of frequencies in the azimuth spectrum. Each range line is multiplied with the corresponding secondary range-reference function (to compress the dispersed range impulse response), and then an inverse range FFT is applied. The data are then corner-turned for easy access in the azimuth dimension. The range-migration correction is made and is followed by azimuth-reference multiplication and inverse azimuth FFT. This completes the SAR image-formation process.

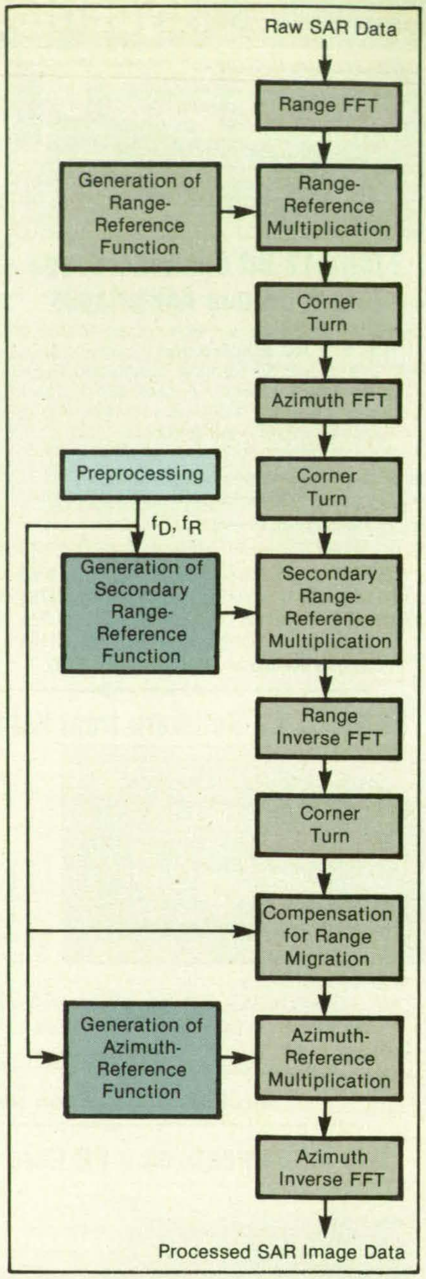

Figure 2. The **Squint-Imaging-Mode Processing Algorithm** includes a secondary range compression in the range-and-Doppler domain.

This work was done by Chi Y. Chang, Michael Y. Jin, and John C. Curlander of Caltech for **NASA's Jet Propulsion Laboratory**. *For further information, Circle 54 on the TSP Request Card.*
NPO-17908

Auxiliary Sensors for "Pushbroom" Imaging

Additional data on motion would enhance geometric fidelity.

NASA's Jet Propulsion Laboratory, Pasadena, California

A proposed subsystem of small auxiliary imaging sensors would yield additional data on the motion of a linear imaging sensor (e.g., in an airborne multispectral scanner) that is scanned across a scene nominally perpendicularly to its length ("pushbroom" scanning). A typical linear imaging sensor is one or a few picture elements wide and thousands of picture elements long, and the data from the strip subimages that it produces in sequence during a scan are processed, along with data on the scanning motion, into the full two-dimensional image of the scene. Consequently, accur-

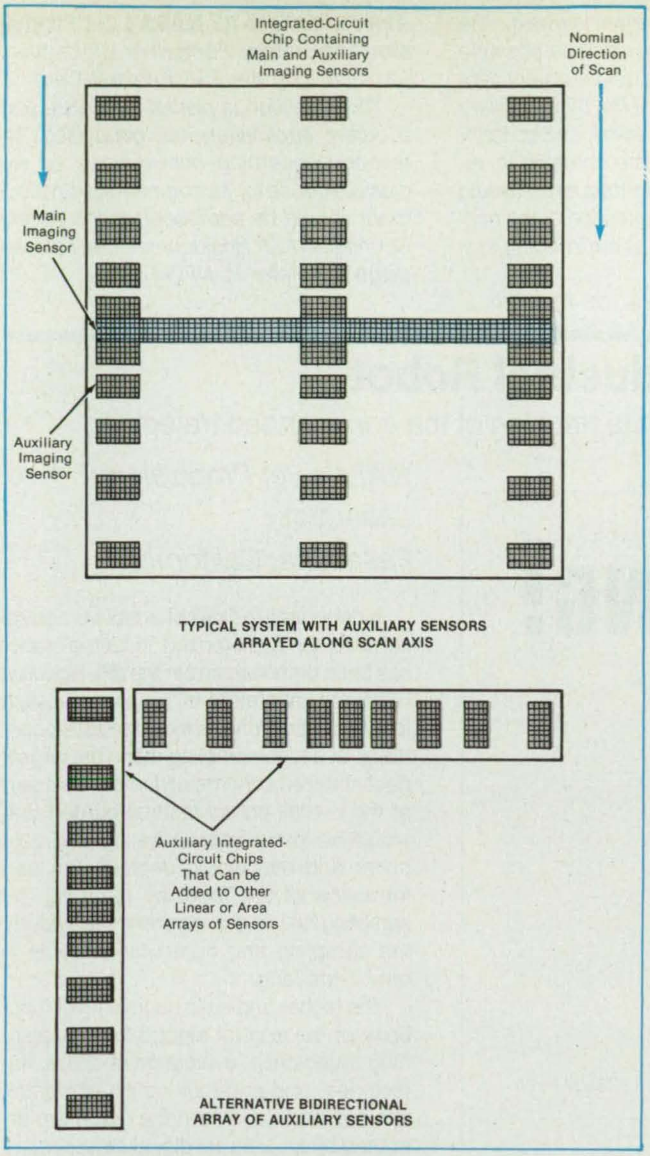

Auxiliary Imaging Sensors would be spaced at various intervals along the nominal scanning axis. Many alternative arrangements are possible; for example, auxiliary sensors could be arrayed bidirectionally.

ate data on the scanning motion are necessary for geometric fidelity of the image. The proposed auxiliary imaging sensors would yield data on components of motion to which the inertial, radar, and air-speed detectors of the aircraft or other platform are insensitive; these components would typically be vibrations of the aircraft and fluctuations in its velocity, both characterized by frequencies beyond the frequency responses of the aircraft motion sensors.

Each auxiliary sensor would typically resemble a small portion of the main sensor. Auxiliary sensors would be placed along (and possibly also across) the scan axis (see figure). Image data from each auxiliary sensor would be processed along with image data from the main sensor by standard digital image-correlation techniques to obtain the apparent motions of targets as they pass through the fields of view of different sensors at different times.

For example, data from a single target detected sequentially by two sensors would yield a linear approximation of velocity equal to the distance between these sensors divided by the time between the observations of the same target by these sensors. Similarly, data from a single target detected sequentially by three sensors would yield a linear approximation of velocity and acceleration. Data from a stream of targets detected sequentially by two or three sensors would give a time history of velocity (or velocity and acceleration) sampled at a frequency related to the distance between the auxiliary sensors.

In principle, an array of many auxiliary sensors at many different spatial intervals would be needed to sample motions over a wide range of frequencies. In practice, one would likely minimize the data requirements by spacing the auxiliary sensors according to a power law; e.g., the first auxiliary sensor as close as possible to the main sensor, the next auxiliary sensor α times as far away, the third auxiliary sensor α^2 times as far away, and so forth. Harmonic analysis of the changes in velocity at each sampling frequency would then give a good approximation of the nonlinear relative motions of the imaging system and the scene.

This work was done by Kenneth L. Jones of Caltech for **NASA's Jet Propulsion Laboratory**. *For further information, Circle 127 on the TSP Request Card.*

This invention is owned by NASA, and a patent application has been filed. Inquiries concerning nonexclusive or exclusive license for its commercial development should be addressed to the Patent Counsel, NASA Resident Office-JPL [see page 18]. Refer to NPO-17970.

Direct Adaptive Control of an Industrial Robot

Desirable features include fast sampling and accurate tracking of the commanded trajectory.

NASA's Jet Propulsion Laboratory, Pasadena, California

A decentralized direct adaptive control scheme for a six-jointed industrial robot has been demonstrated in the JPL Robotics Research Laboratory. In this scheme, each joint is controlled via a local feedback controller at a high sampling rate. This largely decentralized scheme eliminates that part of the overall computational burden that would be imposed by a centralized controller and that would degrade the performance of the robot by reducing the sampling rate. In the experimental system, the sampling and computation cycle is only 7 ms long.

The higher and intermediate-level functions of the control algorithm (e.g., planning trajectories, evaluation of actual trajectories, and communication of control information to and from the robot) are executed by an external digital control computer. Another computer that is part of the robotic equipment acts as an input/output device between the external computer and the joint motors; this computer includes (1) one microprocessor that serves as the local controller for each of the six joints and (2) a microcomputer that passes data and commands back and forth between this computer and the external control computer (see figure).

The adaptive feedback controller for each joint implements a proportional/integral/derivative position-control algorithm with position/velocity feedback and with gains updated in real time. The adaptive feature of the local control law implemented by each joint controller compensates for any static and dynamic cross-couplings between that joint and the other joints and contributes to accurate tracking of the commanded trajectory. When all joints move rapidly simultaneously, the interjoint couplings can sometimes cause instabilities under the decentralized control scheme. In such cases, the controller-adaptation laws are modified slightly to obtain stability in the presence of unmodeled cross-coupling effects.

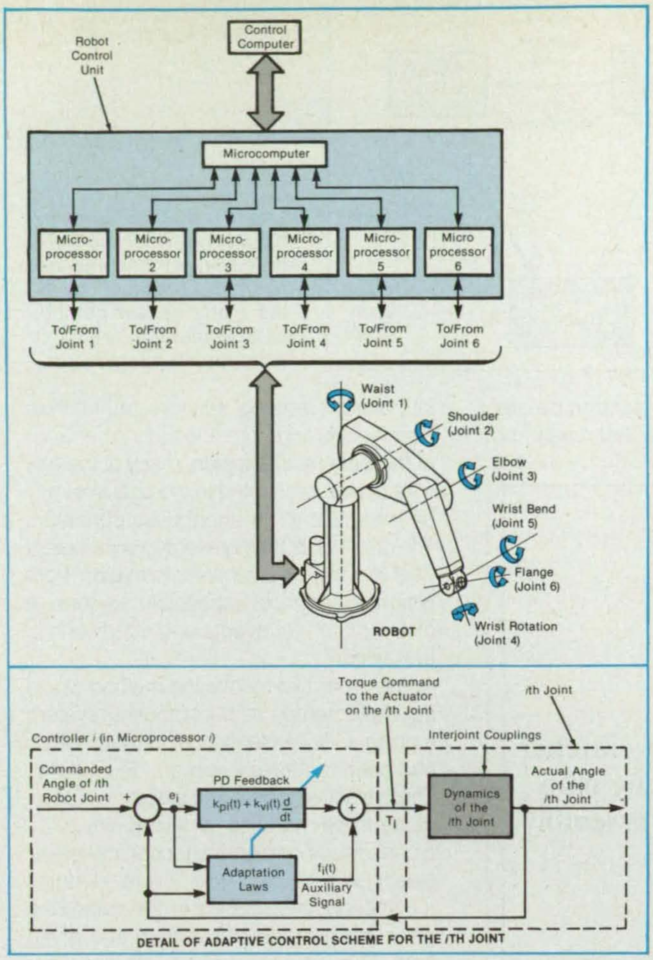

The **Decentralized Adaptive Controller** includes a separate feedback controller for each robot joint. The controller is robust in the face of unmodeled dynamics and provides accurate tracking of commanded trajectories, with a short sampling period.

The control and controller-adaptation laws are based entirely on the observed performance of the manipulator: there is no need to model the dynamics of the robot; nor is there any need to specify the inertial parameters of the payload. Thus, the adaptive controllers can cope with uncertainties and variations in the robot and the payload, including friction (which cannot be modelled accurately) and the mass of the payload (which can vary substantially).

This work was done by Homayoun Seraji and Thomas Lee of Caltech and Michel Delpech of the Centre National d'Etudes Spatiales for **NASA's Jet Propulsion Laboratory**. *For further information, Circle 13 on the TSP Request Card. NPO-17964*

Predictive Monitoring With Many Sensors

A few sensors would be selected according to the state of the monitored system.

NASA's Jet Propulsion Laboratory, Pasadena, California

A proposed method of predictive monitoring that would prevent a large number of sensor data from overwhelming a human operator or an electronic monitor is a subject of continuing research. The essence of the method is to select only a few of the many sensors in the system for monitoring at a given time and to set the alarm levels of the selected sensor outputs to reflect the limits of expected normal operation at the given time. The method is intended for use in a highly instrumented system that includes many interacting components and subsystems; e.g., an advanced aircraft, an environmental chamber, or a chemical-processing plant.

Several considerations motivate the research on this method. Typically, the timely detection of anomalous behavior of a system and the ability of the operator or electronic monitor to react quickly are necessary for the continuous safe operation of the system. In the absence of a sensor-planning method, an operator may be overwhelmed with alarm data that result from interactions among sensors rather than directly resulting from anomalous behavior of the system. In addition, many of the raw sensor data presented to the operator may be irrelevant to an anomalous condition. The operator is thus presented with a great deal of unfocused sensor information, from which it may be impossible to form a global picture of events and conditions in the system.

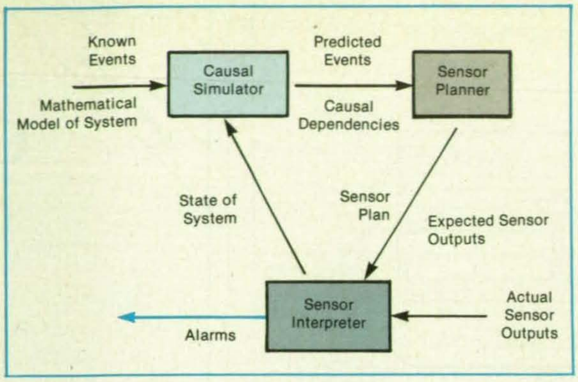

The **Predictive-Monitoring System** would concentrate limited monitoring resources on those few of the many sensor outputs of a system that are most important at the moment.

The predictive-monitoring method would be implemented in a computing system running artificial-intelligence software, which has been tentatively named "PREMON." The predictive-monitoring system would include three modules: a causal simulator, a sensor planner, and a sensor interpreter (see figure). As used here, "event" denotes a discontinuous change in the value of a given quantity (sensor output) at a given time. The inputs to the causal simulator would include a causal mathematical model of the system to be monitored, a set of events that describe the initial state of the system, and perhaps some future scheduled events. The outputs of the causal simulator would include a set of predicted events and a graph of causal dependencies among those events.

The sensor planner would use the causal-dependency graph generated by the causal simulator to determine which few of all of the predicted events are important enough that they should be verified. In many cases, the most important events would be taken to be those that either cause or are caused by the greatest number of other events. This notion of causal importance would serve as the basis for the selection of those sensors, the outputs of which could be used to verify the expected behavior of the system.

The sensor interpreter would compare the actual outputs of the selected sensors with the values of those outputs predicted by the causal simulator. Alarms would be raised where the discrepancies between predicted and actual values were significant.

This work was done by Richard J. Doyle of Caltech for **NASA's Jet Propulsion Laboratory**. *For further information, Circle 56 on the TSP Request Card.*
NPO-18013

Books and Reports

These reports, studies, handbooks are available from NASA as Technical Support Packages (TSP's) when a Request Card number is cited; otherwise they are available from the National Technical Information Service.

Responses of a DRAM to Energetic Heavy Ions

Results confirm methods used to analyze bit errors in this and other integrated circuits.

A report presents the results of experiments in which multiple-bit errors were induced in a 256-kbit commercial integrated-circuit dynamic random-access memory (DRAM) by a variety of normally incident heavy ions. DRAM's of the particular type have been used before in related experiments to investigate the transport of ion-induced electric charges.

A DRAM is uniquely suited for this purpose because it provides a bit-error map that is, in effect, a low-resolution image of the distribution of the charge produced by an impinging ion. The critical charge required to cause a bit error in a memory cell is given by $Q_C = C(V_{DD} - V_B)$, where C is the storage capacitance of the cell, V_{DD} is the supply voltage, and V_B is the input bias voltage of the sensing amplifier of the cell. The charge collected by each cell that registers an error caused by an ion hit must equal or exceed Q_C. Therefore, the charge collected in each cell at the edge of a multiple-bit-error cluster can be assumed to be equal to or slightly greater than Q_C.

The ions and energies in this experiment were selected to represent a variety of stopping powers and ranges in the silicon integrated-circuit substrate. The idea was to demonstrate the utility of the particular DRAM and the methods used to analyze the experimental data, with a view toward applying the methods and the data to other digital integrated circuits.

The following conclusions were drawn from the data:

- For most ions with Z up to 35 (Br) and for depths of penetration into silicon up to 35 μm, the amount of charge collected (as deduced from sizes of bit-error clusters) is approximately proportional to that portion of the kinetic energy of the ion that is deposited in the silicon.
- The amounts of charge collected in the cases of Cl ($Z = 17$) and Au($Z = 79$) are lower than indicated by the foregoing proportionality. However, these apparent anomalies are explainable in terms of currently available methods of analyses, including the PISCES computer program and applicable theories of the distribution and transfer of charges and energies.
- Consequently, the relatively simple DRAM used in these experiments can be used to evaluate (1) the properties of beams of energetic ions (e.g., with respect to stopping power and uniformity) and (2) the responses of such other, more-complicated integrated circuits as microprocessors to charges induced by such beams.

This work was done by John A. Zoutendyk, Lawrence S. Smith, and Larry D. Edmonds of Caltech for **NASA's Jet Propulsion Laboratory**. *To obtain a copy of the report, "Response of a DRAM to Single-Ion Tracks of Different Heavy-Ion Species and Stopping Powers," Circle 159 on the TSP Request Card. NPO-18351*

The TOPEX Ground Data System

Signals from orbiting sensors will be processed into data on sea-surface altitudes.

A report describes the architecture and functions of the ground-based data-processing system of the TOPEX/POSEIDON project, which is a joint American/French ocean-topography project. The purpose of the project is to acquire, process, and verify data on the height of the surface of the ocean and to distribute these data to the scientific community for use in mapping the geostrophic surface currents and tides of the oceans.

The TOPEX/POSEIDON satellite is scheduled for launch into orbit around the Earth in June 1992. Its ground track will repeat in a cycle of about 9.91 days. It will be used to determine the sea level along its ground track to within a standard deviation of 14 cm under typical conditions. For this purpose, it will carry six sensors: an array of laser retroreflectors, two radar altimeters, a radiometer for correction of the altimeter readings, and two radio positioning systems for use in determining the orbit with very high accuracy.

The TOPEX Ground Data System (TGS) is located at NASA's Jet Propulsion Laboratory. The TGS will normally communicate with the satellite via the Tracking Data Relay Satellite System (TDRSS) and associated ground communication facilities. An alternate communications path for certain mission phases or emergencies is provided via the JPL Deep Space Network. The TGS includes seven subsystems, each responsible for a specific set of functions necessary to the overall mission. The Telemetry, Command, and Communications Subsystem (TCCS) will capture incoming telemetry data, process these data into a form usable for monitoring the engineering health of the satellite, and create data sets that can be used by other subsystems of the TGS to produce scientific data. TCCS uses hardware assemblies, custom designed by Goddard Space Flight Center (GSFC), utilizing VLSI devices for performing telemetry frame synchronization and transmission of the NASCOM Blocks. The TCCS will also translate satellite-commanding information into a form compatible with that of the satellite, and will control the transmission of commands to the satellite.

The Satellite Sensor Performance Analysis Subsystem (SPAS) will monitor the health of the satellite. It will also control the activities of instruments aboard the satellite by (1) establishing an overall satellite-operations plan, then (2) analyzing telemetry data received from the satellite via the TCCS and location-related data received from the navigation subsystem described below, then (3) generating commands to be sent to the satellite to carry out the plan.

The Mission Planning, Sequencing, and Scheduling Subsystem (MPSSS) will coordinate the satellite-operations plan with the capabilities and constraints of the TGS. It will receive commands to be transmitted to the satellite from the SPAS and transform these commands into a set of command sequences that can be sent to the satellite when the TDRSS and ground communication services are available. It will also provide schedules of events for use by operations personnel.

The Navigation Subsystem (NAVS) will receive preprocessed tracking information from the Goddard Flight Dynamics Facility and use this information to provide satellite-location (i.e., ephemeris) information for the Science Data Subsystem. The Science Data Subsystem (SDS) will process altimetric and radiometric telemetry data along with ephemeris data into geophysical data records to be distributed to end users.

The Science Verification Subsystem (SVS) will also receive the interim and final versions of the geophysical data records and compare them with measurements collected at various test sites on the Earth. The purpose of this comparison is to validate and calibrate the satellite-instrument data and ground-data processes to ensure that the TGS is producing accurate data for scientific analysis.

The Precision Orbit Determination System (PODS) will also receive preprocessed tracking information from Flight Dynamics Facility at GSFC. By use of sophisticated techniques for mathematical modeling of orbits, it will produce the satellite ephemeris information of the required precision and accuracy for use by the SDS in producing final geophysical data records that satisfy the specifications of the TOPEX/POSEIDON project.

This work was done by Anil K. Agrawal and Alvin M. Willems of Caltech for **NASA's Jet Propulsion Laboratory**. *To obtain a copy of the report, "The TOPEX Ground Data System," Circle 132 on the TSP Request Card.* *NPO-18374*

Calculating Pressures in Electrochemical Cells

The initial pressure and void volume strongly affect the subsequent dependence of pressure on temperature.

NASA's Jet Propulsion Laboratory, Pasadena, California

A semiempirical method provides for the calculation of operating conditions in electrochemical storage cells equipped with pressure-relief vents. Conceived for use with $Li/SOCl_2$ cells, the method should also be applicable to other electrochemical cells in which the interdependence of pressure, temperature, and state of charge is a design issue.

The vent in an $Li/SOCl_2$ cell is intended to open before the pressure rises to a dangerously high value at the expected operating temperatures. The semiempirical method is used to design a cell to discharge both safely and completely, without reaching the designated venting pressure (which is below the maximum safe pressure).

According to the method, the total pressure in a cell is taken to be the sum of the vapor pressure of the electrolyte and the pressure of the inert gas (argon) that initially fills the void volume above the electrolyte. For this purpose the vapor pressure of the electrolyte as a function of temperature is measured in a cell in the fully charged and fully discharged states. An interpolation is performed for states of intermediate charge (see figure). The pressure of the inert gas as a function of temperature is determined from the initial and final temperatures and volumes of the inert gas, by use of the ideal-gas law. For this purpose, the final volume of the inert gas is estimated from the initial void volume, the decrease in void volume resulting from the thermal expansion of the electrolyte, the decrease in void volume resulting from the formation of end products, and the increase in void volume resulting from the consumption of starting materials.

Pressure-vs.-temperature-vs.-state-of-discharge calculations were performed in an application of this method to two commercial $Li/SOCl_2$ cells: a Honeywell 250-Ah cell and a Whittaker–Yardney 250-Ah cell. The following conclusions were drawn from these calculations:

- The cells exhibit a spread in temperatures that correspond to a given venting pressure.
- The spread in temperatures is diminished as the initial pressure of the inert gas increases.
- The temperature required to produce a given pressure increases with an increase in void volume.
- Suitable venting pressures for the Honeywell and Whittaker–Yardney cells with initial void volumes of 112 mL are in the ranges of 250 to 300 psi (1.7 to 2.1 MPa) and 200 to 500 psi (1.4 to 3.4 MPa), respectively, with initial inert-gas pressures of 15 to 40 psi (100 to 280 kPa) and 40 psi (280 kPa), respectively.

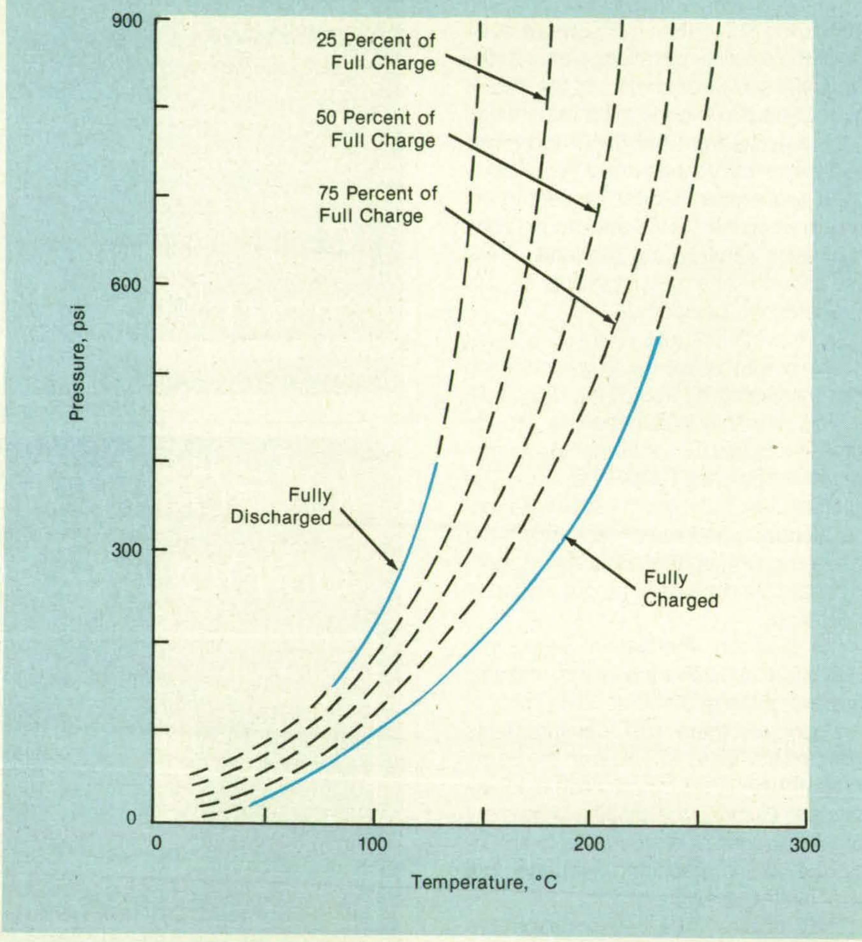

The **Electrolyte-Vapor Pressure** in a commercial $Li/SOCl_2$ cell was measured at various temperatures at full charge and full discharge. The full-discharge data were then extrapolated to unmeasured values. Finally, interpolations were made to states of 25, 50, and 75 percent of full charge. The solid portions of the curves indicate experimental data; the dashed portions represent extrapolations and interpolations.

This work was done by Ralph Lutwack, Harvey A. Frank, and Alan I. Attia of Caltech for **NASA's Jet Propulsion Laboratory.** *For further information, Circle 85 on the TSP Request Card.*
NPO-18078

Deformable Composite/Honeycomb Telescope Mirror

Piezoelectric actuators would help compensate for distortions.

NASA's Jet Propulsion Laboratory, Pasadena, California

Work continues to develop a lightweight, controllably deformable spherical astronomical-telescope mirror of about 1-m aperture. The reflecting surface of the mirror would be the polished front surface of a semirigid sheet; this sheet would be bonded to the front face sheet of a panel that would consist of graphite/epoxy face sheets bonded to aluminum honeycomb core. By use of piezoelectric transducers bonded to the rear face sheet of the panel (see Figure 1), strains would be introduced into the rear face sheet and the entire structure to correct long-wavelength, slowly-changing distortions of the reflecting surface; e.g., those caused by manufacturing tolerances, relaxations of residual manufacturing stresses, changes in temperature, and changes in orientation in the gravitational field.

The reflecting surface, panel, panel supports, and actuators would be designed as an integrated system. One of the problems in the development effort is to maintain the required accuracy of the reflecting surface (root-mean-square deviation of no more than a few microns) with as few piezoelectric transducers as possible. Thus far, the number and placement of transducers have not been optimized. In-

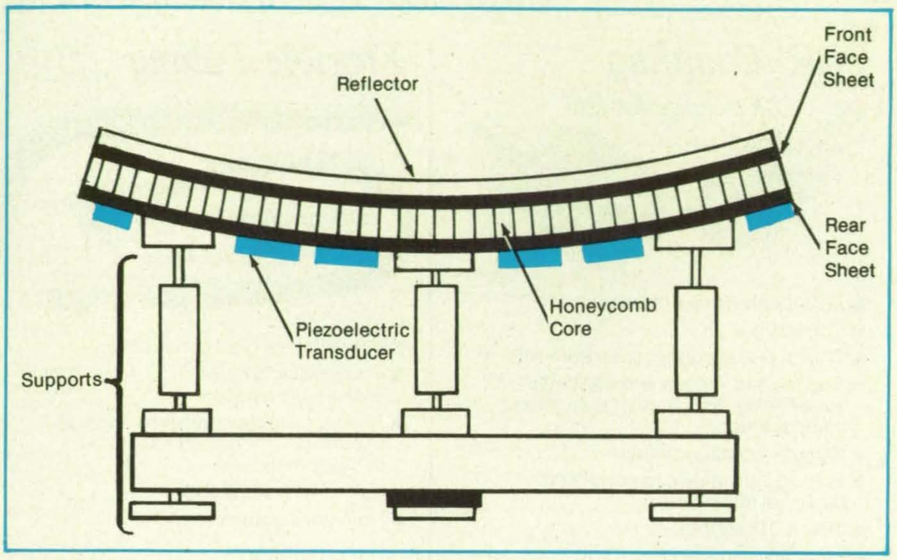

Figure 1. **Piezoelectric Transducers** would be bonded to the rear face sheet of a honeycomb panel that supports a spherical reflecting surface. Voltages would be applied to these transducers to compensate for distortions of the reflecting surface.

stead, for purposes of design and analysis, the distortions have been approximated by combinations of vibrational amplitudes of low order, and the coordinated control voltages applied to the various actuators have been selected to produce distortions equivalent to the opposites of these amplitudes.

The concept has been partly tested by computer simulations of the behavior of the curved mirror/honeycomb-core/transducer structure and by experiments on flat honeycomb panels. One panel to be tested soon is 0.792 m wide (flat-to-flat) and 2.54 cm thick with six radial strips of five actuators apiece (see Figure 2). Except that it is flat instead of spherical (the radius of curvature of the mirror would be 7.485 m), this panel resembles the one to be used in the mirror. The results of the experiments will be incorporated into the computer simulations in future efforts to improve the design.

This work was done by Chin-Po Kuo and Ben K. Wada of Caltech for **NASA's Jet Propulsion Laboratory**. *For further information, Circle 6 on the TSP Request Card.*
NPO-18128

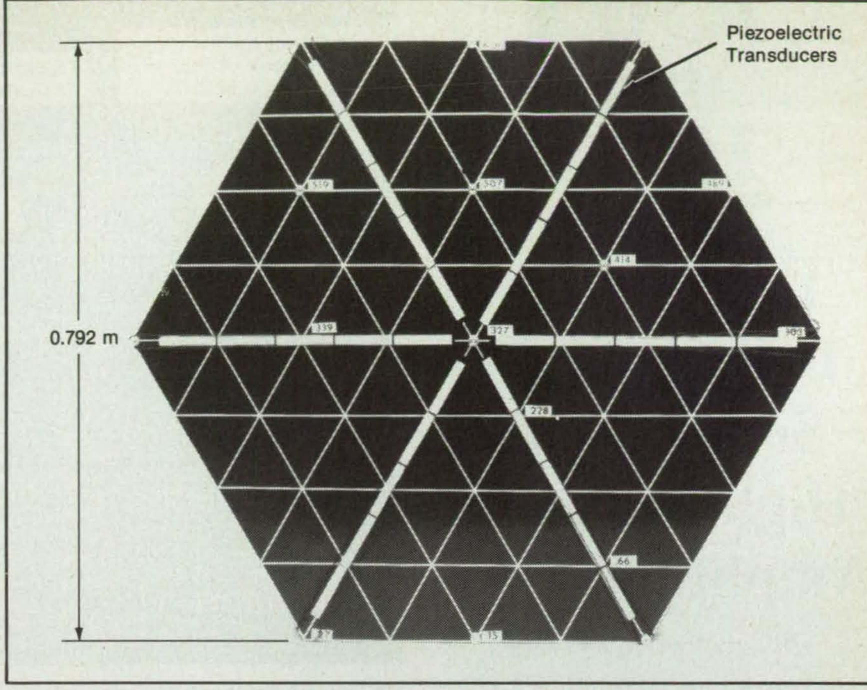

Figure 2. This **Experimental Flat Hexagonal Panel** is similar to the one that would be used in the mirror. Thirty transducers arranged symmetrically in radial strips are intended to compensate for those distortions that can be characterized as linear combinations of the first six vibrational modes.

AVIRIS Spectrometer Maps Total Water Vapor Column

Column abundances are mapped with good precision and spatial resolution.

NASA's Jet Propulsion Laboratory, Pasadena, California

Observations by NASA's Airborne Visible/Infrared Imaging Spectrometer (AVIRIS) have been processed into maps of vertical-column abundances of water vapor in the atmosphere. Such maps can provide valuable information for meteorology, climatology, and agriculture.

AVIRIS takes near-nadir measurements of spectral radiance in spectral sampling intervals 10 nanometers wide at wavelengths from 400 to 2,500 nm. Mounted in a U-2 airplane flying at an altitude of 20 km, AVIRIS scans a swath 11 km wide with an instantaneous field of view of 20 m by 20 m at the surface. In this case, spectral radiances are measured in two wavelength bands: a continuum band at 870 nm and a water band at 940 nm. According to a mathematical model developed for this purpose, the ratio between these two radiances is a function of the total column abundance of precipitable water as measured through (1) the path of downwelling solar radiation and (2) the path

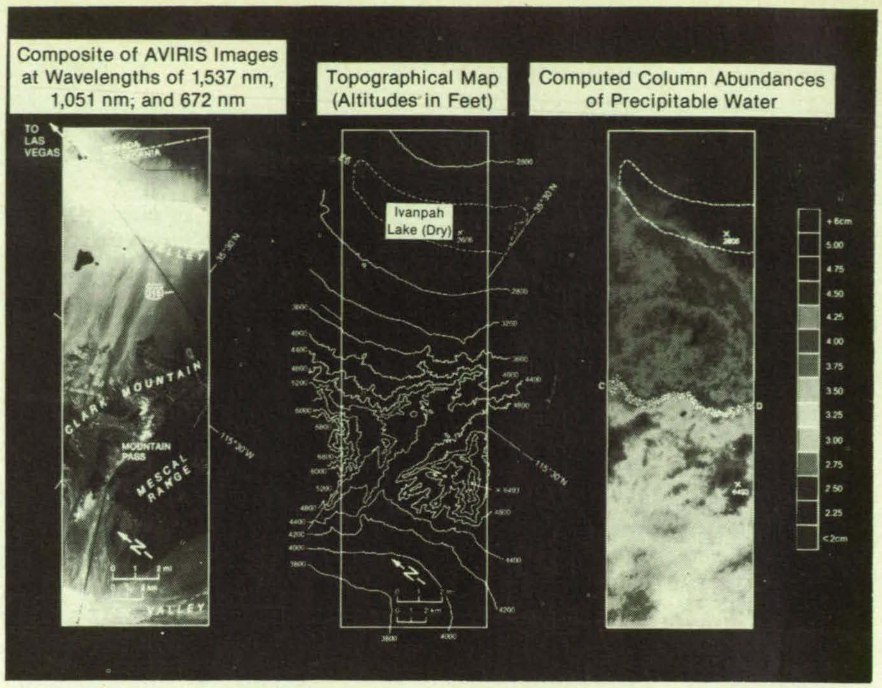

Column Abundances of Water Vapor estimated by the ratio method described in the text are compared with a composite three-wavelength image and a topographical map. The stippled region CD denotes a sharp change in column abundance that may represent the edge of the water-vapor boundary layer tapered against the topography. A denotes a location where optical depth was determined; B denotes a playa used as a calibration target.

of upwelling radiation reflected from the surface up along the observed path to the spectrometer.

The AVIRIS measurements are calibrated with the help of surface measurements of bidirectional reflectances of selected targets in the scene. Corrections for the altitude of the surface, the viewing angle, and flight conditions are made. The use of the ratio of radiances helps to compensate for variations in albedo (bright and dark areas) over the surface: this is because the two spectral bands are close and, consequently, the differences between the spectral reflectances in the two bands should be small.

The figure illustrates the results obtained by applying this method to a desert area in eastern California. An independent validation of the column abundance at one location derived from the AVIRIS data was supplied by a spectral hygrometer calibrated with respect to radiosonde observations. The column abundances of water vapor were found to conform to topography and to decrease with surface elevation. Overall, the ratio method was found to yield column abundances of good precision and high spatial resolution.

This work was done by James E. Conel, Robert O. Green, Veronique Carrere, Jack S. Margolis, Ronald E. Alley, Gregg A. Vane, Carol J. Bruegge, and Bruce L. Gary of Caltech for **NASA's Jet Propulsion Laboratory**. *For further information, Circle 118 on the TSP Request Card.*
NPO-18023

Books and Reports

These reports, studies, handbooks are available from NASA as Technical Support Packages (TSP's) when a Request Card number is cited; otherwise they are available from the National Technical Information Service.

Condensed Acids in Antarctic Stratospheric Clouds

Amounts of nitric, sulfuric, and hydrochloric acids are probably related to the depletion of ozone.

A report discusses measurements of the nitrate, sulfate, and chloride contents of stratospheric aerosols during the 1987 Airborne Antarctic Ozone Experiment. Data from these measurements are important in testing theories concerning the Antarctic "ozone hole." This study emphasizes data concerning the growth of $HNO_3 \cdot 3H_2O$ particles in polar stratospheric clouds, in the context of these theories.

Aerosols were sampled by an airplane flying between 57° and 72° south latitude at an altitude of 18 km. The aerosol particles were collected by impact on four 500-μm-diameter gold wires strung across aluminum rings. The wires were pretreated to give results specific to certain physical and chemical properties of the aerosols. One wire was coated with carbon and used for analyses, via scanning electron microscopy, of the sizes and concentrations of aerosol particles. One wire was coated with nitron [$CN_4(C_6H_5)_3CH$], which undergoes reactions that indicate the presence of nitrates. The other two wires were coated with barium chloride and silver nitrate to detect sulfuric and hydrochloric acids, respectively. Immediately after collection and while the flights continued, the acids were fixed as ammonium salts by exposing them to ammonia.

The results show that condensed nitric acid is found at temperatures below a threshold of 193.6 ± 3.0 K, generally encountered at south latitudes above 64° at the 18-km altitude. Consistent with theories of the condensation of $HNO_3 \cdot 3H_2O$, particles of nitric acid were not detected at temperatures above 200 K. Below the threshold temperature, the concentrations of nitric acid particles and of ozone were negatively correlated with each other, with a correlation coefficient of –0.7. This is consistent with theories in which the freezing-out of nitrates is a prerequisite for reactions of gaseous chlorine compounds with ozone.

The collected sulfates indicated the presence of liquid sulfuric acid aerosol particles in concentrations that ranged from 0.06 to 0.11 $\mu g/m^3$. Such concentrations are comparable to those found in northern midlatitude aerosols in the absence of volcanic activity. Hydrochloric acid was found to be present, but in only a few cases was the concentration great enough to be measurable by energy-dispersive x-ray analysis. From the limited available data, it was estimated that the mass of HCl in the specimens was about 4 percent of the mass of H_2SO_4.

This work was done by R. F. Pueschel, K. G. Snetsinger, O. B. Toon, G. V. Ferry, W. L. Starr, V. R. Oberbeck, and K. R. Chan of **Ames Research Center**, *J. K. Goodman of San Jose State University, J. M. Livingston of SRI International, S. Verma of TMA/Norcal, and W. Fong of Information Management, Inc. To obtain a copy of the report, "Condensed Nitrate, Sulfate, and Chloride in Antarctic Stratospheric Aerosols," Circle 87 on the TSP Request Card. ARC-12618*

N_2O as a Tracer of Antarctic Atmospheric Flows

Experimental data are relevant to studies of the depletion of ozone.

A report discusses the use of natural N_2O as a tracer gas in the effort to determine large-scale lower stratospheric air flows during the 1987 Airborne Antarctic Ozone Experiment. Data on such flows are essential to understanding the vertical motions and the horizontal transport of air into and out of the southern polar vortex and the "ozone hole," and as such can be used to test theories on the depletion of ozone. N_2O was chosen as a tracer because (1) it has purely tropospheric sources, (2) it has a tropospheric lifetime > 20 years and is therefore well mixed (with a geographic variation of less than 1 percent) throughout the troposphere, and (3) it has a long chemical lifetime in the lower stratosphere (altitudes of 12 to 20 km), where the Antarctic ozone is being lost.

Concentrations of N_2O were measured by an airborne second-harmonic absorption spectrometer containing a $Pb_{1-x}Sn_xTe$ tunable diode laser that operated near the ~1,300 cm^{-1} absorption line of N_2O. These measurements have a temporal resolution of 1 s, which, at the speed of the ER-2 airplane, yields a spatial resolution of ~200 m. Pressures, temperatures, and latitudes were also recorded by a meteorological measurement system.

Data were taken on 12 flights into the Antarctic vortex (which is bounded approximately by the circle at 60° south latitude) and on 5 flights outside the vortex during

August and September of 1987. Vertical distributions of N_2O were obtained within the vortex on most of these flights, and outside the vortex on some of them. Altogether, the measurements yielded an extensive new set of data on the concentration of N_2O in the lower stratosphere at latitudes from 41° S to 72° S during the late Antarctic winter and early Antarctic spring.

Instead of altitude, the "natural" vertical coordinate used to present the data on N_2O is the potential temperature, θ, which is based on an isentropic model of the variation of pressure, temperature, and density with altitude. For a given parcel of air moving in the lower stratosphere, θ tends to be conserved for several days, N_2O and θ are transported together by atmospheric motions, and mixing tends to equalize the concentrations of N_2O on surfaces of constant θ.

The data from flights into the vortex show that the concentration of N_2O decreased from 53° to 72° south latitude on surfaces of constant θ in the lower stratosphere. The data lead to two important conclusions: (1) The lower stratosphere at that time was occupied by "old" air, which had subsided several kilometers during the Antarctic winter; and (2) the distribution of N_2O in the vortex was approximately in a steady state at that time, indicating that the spring upwelling of air, suggested by several theories, did not occur.

This work was done by M. Loewenstein, J. R. Podolske, and K. R. Chan of **Ames Research Center** *and S. E. Strahan of the National Research Council. To obtain a copy of the report, "Nitrous Oxide as a Dynamical Tracer in the 1987 Airborne Antarctic Ozone Experiment," Circle 47 on the TSP Request Card.*
ARC-12453

Monitoring Global Temperatures From Satellites

Microwave radiometers measure temperatures with useful precision.

A report published in the 30 March 1990 issue of *Science* provides evidence that passive microwave radiometry from satellites provides more-precise information on atmospheric temperatures than does the relatively sparse distribution of thermometers over the surface of the Earth. Accurate estimates of global atmospheric temperatures are needed for detection of possible "greenhouse" warming, for evaluation of computer models of change in climate, and for understanding important factors in the climate system.

The authors examined data from microwave sounding units (MSU's) carried aboard the TIROS-N series satellites of the National Oceanic and Atmospheric Administration (NOAA). The MSU's are Dicke-type radiometers designed to measure the thermal emission of radiation by atmospheric O_2 at four frequencies near 60 GHz. The authors examined, in particular, data from MSU channel 2 (53.74 GHz), which measures the temperature of the middle troposphere.

Each MSU is calibrated externally by measurement of the cosmic background radiation, which is assumed constant at a temperature of 2.7 K. It is also calibrated internally by a warm target, the temperature of which is monitored by redundant platinum resistance thermometers. This calibration procedure cancels the effects of changes in the components of the MSU. Each Earth-viewing measurement is then calculated as a "brightness temperature" (T_b) by interpolation between the two calibration temperatures. Because the tropospheric O_2 closely approximates a blackbody in MSU channel 2, its thermometric temperature (the temperature that would be indicated by a thermometer in contact) is closely approximated by T_b.

Comparison of T_b data from channel 2 (averaged at 2-day intervals over both the Northern and Southern Hemispheres) from two satellites operating simultaneously during the period from 29 June 1981 to 16

April 1983 in Sun-synchronous, near-polar orbits revealed the following:

- The standard deviation of the sums of the data from the two satellites is much larger than the standard deviation of the differences between the data. This means that both satellites were measuring nearly the same variations in temperature and implies that hemispheric temperature anomalies can be measured with relatively little error from a single satellite. The 2-day average difference between temperatures measured by the two satellites was about 0.05 °C; the monthly average difference was about 0.011 °C. The authors estimate that the precision of monthly satellite measurements is about ±0.01 °C for the globe.
- The sums of the two sets of data reveal that dramatic globally averaged warming and cooling events of greater than 0.5 °C can occur in less than 2 weeks. The warmings are possibly associated with stormy periods, when large amounts of latent heat were released in precipitation of moisture previously evaporated from the Sun-warmed ocean. The coolings might be associated with the formation of widespread low-level cloudiness, which reflects significant amounts of incoming solar radiation.
- The long-term drift of one MSU relative to the other is so small (<0.01 °C in 2 years) that it is virtually unmeasurable.

To demonstrate that MSU measurements are closely related to thermometric temperature, the authors compared monthly temperature anomalies from thermometers over the contiguous United States for the period 1979 through 1987 to the monthly midtropospheric temperature anomalies measured from the satellites. (The distribution of thermometers over the United States is widely accepted as good enough for climate work.) The resulting anomaly time series were similar, as verified by a scatter plot and a correlation coefficient of 0.89. This correlation agrees with those between radiosonde near-surface and upper-air measurements.

Satellite data for the years 1979 to 1988 reveal large fluctuations in the hemispheric and global temperatures. The slower, interannual trends in the Northern and Southern Hemispheres follow each other, but on monthly-to-seasonal time scales; the trends in the two hemispheres often oppose each other. The warmest years during the experiment, in decreasing order of temperature, were 1988, 1987, 1983, and 1980; the years 1984, 1985, and 1986 were the coolest. There is no obvious long-term trend, and anomalies during the first 5 years nearly balance those during the last 5 years. The 10-year time series exhibits bifurcation in that there are 9 cool or warm years and only 1 year (1981) that could be considered "average." This pattern makes the definition of "normal" for global temperatures uncertain.

This work was done by Roy W. Spencer and John R. Christy of **Marshall Space Flight Center**. *To obtain a copy of the report, "Precise Monitoring of Global Temperature Trends From Satellites," Circle 37 on the TSP Request Card.*

Inquiries concerning rights for the commercial use of this invention should be addressed to the Patent Counsel, Marshall Space Flight Center [see page 18]. Refer to MFS-27248.

Dispersion of Evaporating Drops in a Vortex

Dynamic and thermodynamic interactions are described.

A report presents a theoretical study of the behavior of a cluster of evaporating liquid drops entrained in an annular cross section of a long, coherent gas vortex. This is one in a continuing series of studies that are contributing to our understanding of the evaporation and combustion of sprayed liquid fuels. The annular-cross-section/vortex configuration was chosen for study because it approximates configurations that have been observed in experiments. Experiments also show that the larger coherent vortexes at the edge of a spray control the entrainment of air into the spray and determine the distribution of number densities and sizes of drops in the mixing region between the spray and the surrounding air.

The mathematical model of the vortex and cluster is formulated in cylindrical coordinates and incorporates a number of simplifying assumptions, including that (1) both the vortex structure and the distribution of drops have infinite axial length and are uniform along the axial and azimuthal directions, (2) there are no body forces, (3) the ambient pressure is atmospheric, and (4) the far-field flow conditions are specified. In the model, the cluster of drops has two boundary surfaces, which lie, respectively, at the inner and outer radii of the annulus. The inner boundary develops with time as a result of the centrifugal force of vortical motion. Thus, three regions are considered: the inner region, which contains only gas with a line vortex on the axis; the cluster, which contains both gas and liquid drops; and the region outside the cluster where, again, only gas is present. The radial and azimuthal velocity profiles of both drops and gas are continuations of free vortex and solid body motions.

The annular cluster of drops is assumed to be spatially homogeneous in thermodynamic quantities. Each drop is considered to be surrounded by a sphere of influence, centered at the drop center, of diameter equal to the distance between the centers of two adjacent drops. The temperature of a drop and of the gas in its sphere of influence are assumed to vary with time and with the radius from the center of the drop.

The dynamic coupling between the liquid and gas phases is represented as a drag resulting from a slip velocity between the two phases. The net force of interaction between the drops and the gas that contains them is attributed to thrust from evaporation plus drag on each drop. The drag coefficient accounts for blowing from the surfaces of the drops. Thermodynamic coupling between the liquid and gas phases is accounted for through a model of heating and evaporation of the drops. The limitations imposed by the proximity of the drops upon the dynamic and thermodynamic coupling are taken into account; consequently, the overall mathematical model applies to both dense and dilute clusters of drops.

Computations were performed with this model for drops of n-decane in a vortex, under various initial and boundary conditions. The numerical results are presented as plots that show the dependencies of the evaporation time, the ratio between the final and initial volumes, and the ratio be-

NOVAMET
CONDUCTIVE PIGMENTS

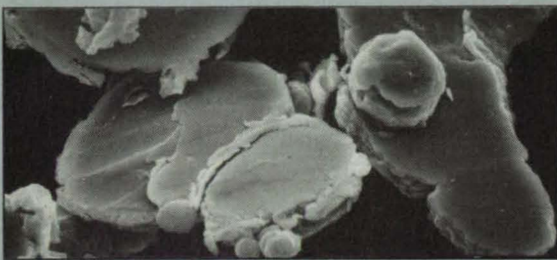

Conductive Silver Coated Nickel Flakes

Conductive Nickel Flakes

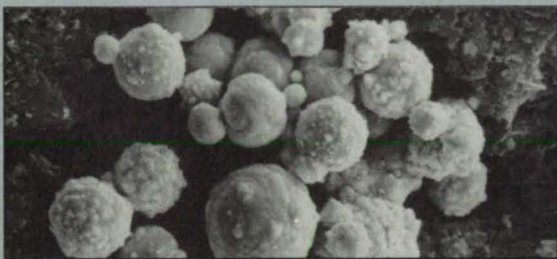

Conductive Silver Coated Nickel Spheres

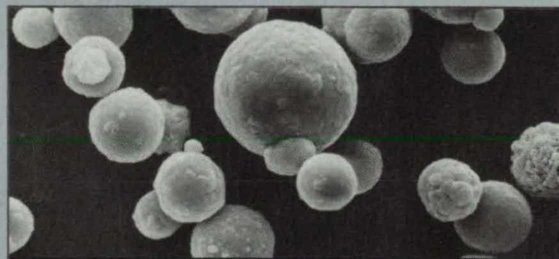

Conductive Nickel Spheres

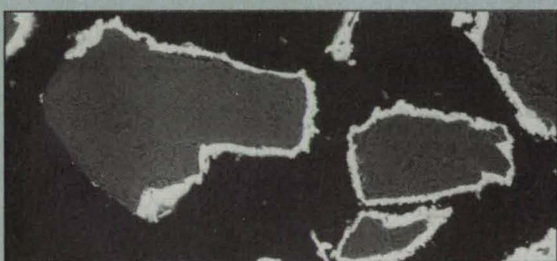

Conductive Nickel Coated Alumina

Nickel Coated Graphite

Also:

Conductive Nickel Coated Glass Frit
Conductive Nickel Coated Aluminum
Conductive Nickel Pigment 525
Conductive Silver (0.5%) Stabilized Nickel Flakes

And

Custom Nickel Coating
Custom Micron Separation of Nickel Powders
Custom Screening of all Novamet Pigments

NOVAMET

Novamet Specialty Products Corporation, An INCO Company
10 Lawlins Park, Wyckoff, New Jersey 07481, (201) 891-7976

Circle Reader Action No. 635

tween the final and initial thickness of the annulus upon (1) the initial ratio between the masses of air and fuel for several initial tangential velocities, (2) the initial Stokes number, (3) the initial radius of the drops, and (4) the initial inner and outer radii of the annulus. Differences between the behaviors and the parameters that most strongly affect the behaviors of dense and dilute clusters are indicated. It is found that for a dense cluster, the ratio between the final and initial volume, and the final and initial thickness of the annulus scale with the initial Stokes number.

This work was done by Josette Bellan and Kenneth G. Harstad of Caltech for **NASA's Jet Propulsion Laboratory**. *To obtain a copy of the report, "Some Aspects of Liquid Dispersion and Evaporation in Swirling Flows," Circle 133 on the TSP Request Card.*
NPO-18107

Phase Calibration of Polarimetric Radar Images

Causes of various types of errors are discussed.

A report addresses the problem of calibration of the differences between the phases, relative to the transmitted signals, of the signals received in the two polarization channels of a polarimetric imaging radar system. Such calibration is necessary to extract important polarization and phase information from a radar image. By making fuller use of this information, one can deduce more information about the target area — e.g., type of terrain, presence of vegetation, land/water boundaries, and the like.

The causes of various types of phase errors are discussed. These include differences between the lengths of signal paths in the equipment, differences between receiver gains, coupling between polarization channels, and noise. In addition, differences between the lengths of signal paths outside the equipment can cause spatial variations of phase errors if the phase centers of the vertically and horizontally polarized antennas are at different locations; a simple mathematical model is developed to explain this effect. The dependence of coupling between polarization channels upon angles of incidence can give rise to still more spatially varying phase errors, which can manifest themselves as spatially varying phase shifts in measured clutter statistics.

Phase calibration by use of both point targets that have known scattering properties (e.g., trihedral corner reflectors) and distributed targets (ocean waves or roughness of natural terrain, which give rise to clutter) is discussed. It is shown that a method for calibrating phase by use of distributed targets gives results equivalent to those obtained by use of calibrating reflectors, provided that (1) the scattering is reciprocal, (2) the two copolarized components of the scattering matrix are statistically correlated, and (3) the like- and cross-polarized components of the scattering matrix are statistically uncorrelated. These assumptions are valid for some limited types of clutter; for example, it has been verified in synthetic-aperture-radar scattering in the X-band from a tree canopy and in the C- and L-bands from a dry lakebed.

These assumptions would not apply to L-band scattering from cornstalks or other predominantly two-bounce scattering. It would be difficult to apply the method to scatter from ocean scenes because the cross-polarized scatter in them is too low relative to leakage of signals between channels in the equipment. Further, experimental data indicate that nadir regions in radar images may not be usable.

This work was done by Anthony Freeman of Caltech and Dan R. Sheen and Erik S. Kasischke of the Environmental Research Institute of Michigan for **NASA's Jet Propulsion Laboratory**. *To obtain a copy of the report "Phase Calibration of Polarimetric Radar Images," Circle 49 on the TSP Request Card.*
NPO-17921

Materials

Hardware, Techniques, and Processes

Electrochemical System Would Supply O_2, H_2O, N_2, and H_2

Atmospheric gases would be stored in propellant rather than compressed.

Lyndon B. Johnson Space Center, Houston, Texas

A proposed electrochemical system would generate O_2, H_2O, N_2, electrical energy, and (optionally) H_2 from hydrazine (N_2H_4), nitrogen peroxide (N_2O_4), and their derivatives, which are normally used as propellants in rocket engines. While intended primarily to supply atmospheric gases for the inhabited portion of a spacecraft, the concept of the system may be applicable to some terrestrial enclosed environments, laboratories, chemical processing plants, or portable medical facilities.

The electrochemical process (see figure) is based on the reactions $N_2O_4 \rightarrow N_2 + 2O_2$, $N_2O_4 + 2N_2H_4 \rightarrow 3N_2 + 4H_2O$, and (optionally) $N_2H_4 \rightarrow N_2 + 2H_2$. The reactions would take place in fuel cells and would consume heat in the comfortable range of room temperatures. Thus, the system could also be used to cool the enclosed environment. The electrical energy generated by the fuel cells could be supplied to other systems, and the byproduct water could be purified for consumption. The purified gases could be fed to the environmental system or stored in a conventional cryogenic system.

The system is expected to generate more oxygen or nitrogen per unit overall weight than can be stored conventionally as compressed gas or refrigerated liquid. According to a preliminary estimate, the weight of the electrochemical cells and associated equipment would be less than 100 lb (45.4 kg).

This work was done by Richard T. Walter of **Johnson Space Center** *and Paul D. Van Buskirk of Lockheed Engineering and Sciences Co., Inc. For further information, Circle 106 on the TSP Request Card.*
MSC-21404

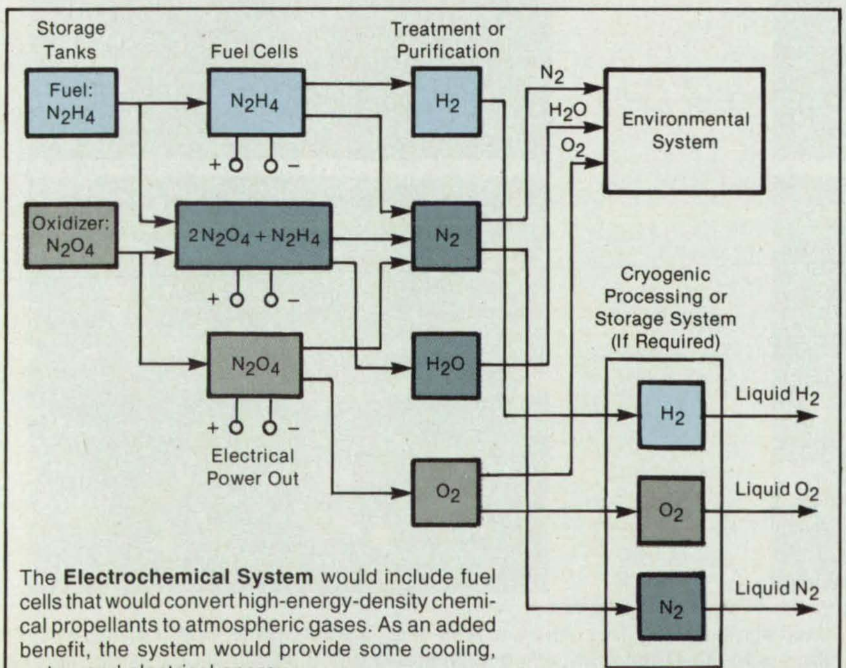

The **Electrochemical System** would include fuel cells that would convert high-energy-density chemical propellants to atmospheric gases. As an added benefit, the system would provide some cooling, water, and electrical energy.

Sol-Gel Synthesis of Aluminoborosilicate Powders

The sol-gel process gives some control over the properties of the powders.

Ames Research Center, Moffett Field, California

The application of the sol-gel process to the synthesis of aluminoborosilicate powders with the molar ratio 3:1:2 (Al_2O_3:B_2O_3:SiO_2) has shown the potential for control of the microstructures of these materials. The development of materials in the Al_2O_3:B_2O_3:SiO_2 system that have enhanced processing characteristics should prove advantageous in extending the high-temperature endurance of fibrous refractory composite insulation made from ceramic fibers in this system.

In the beginning of a demonstration of one method of synthesis, an ethanol solution of tetraethyl orthosilicate (TEOS) was partially hydrolyzed, and an ethanol solution of trimethyl borate (TMB) was added while stirring. The resulting borosiloxane sol was added to a slurry of aluminum isopropoxide (AIP) [and, in an alternative version, to aluminum secbutoxide (ASB)]. This mixture was hydrolyzed by the dropwise addition of a solution of ethanol and water, with additional stirring. A second method of synthesis was similar, except that the alumina precursor was added before the boria precursor, and an ethanolic solution of TMB was then added to the corresponding aluminosiloxane sol.

The resulting sol-gels were dried to powders in an air-circulated oven at 80 °C for 24 to 48 h. Each powder was ground with a porcelain mortar and pestle and heated again at 600 °C for 2 h in flowing air. These precalcined powders were sifted through an 80-mesh (177-μm) sieve. Agglomerates that could not pass through the sieve were ground until they passed freely through the sieve; two passes were all that were necessary. Powder compacts were made from the resultant material by cold pressing at variable loads in a carbon-steel die that had been lubricated with sprayed zinc stearate.

The mean diameters of particles of powders synthesized from AIP were 5 μm less than those of particles of powders synthesized from ASB. Powders synthesized from AIP included regularly shaped agglomerates composed of what appear to be rod-shaped crystallites; those based on ASB included shardlike glassy agglomerates (see figure). However, all powders were amorphous after precalcination, with the metal oxides comprising 87 percent of the weight, and uncombusted organics the remainder.

The compaction behaviors of the powders reflected the characteristics of the particles. Compacts of greater density at lower compaction pressures were achieved with AIP-based powders. Differential thermal analysis revealed a transition from gel to glass at a temperature of about 835 °C and an exotherm, which was attributed to a crystalline transformation, at approximately 900 °C. An increase in the loss of weight above 1,100 °C could have been due to the vaporization of boria. The temperature range and magnitude of the increase varied according to the method of synthesis.

ASB-base powders contained less of trace impurities than did AIP-base powders; this was attributed to the chemical

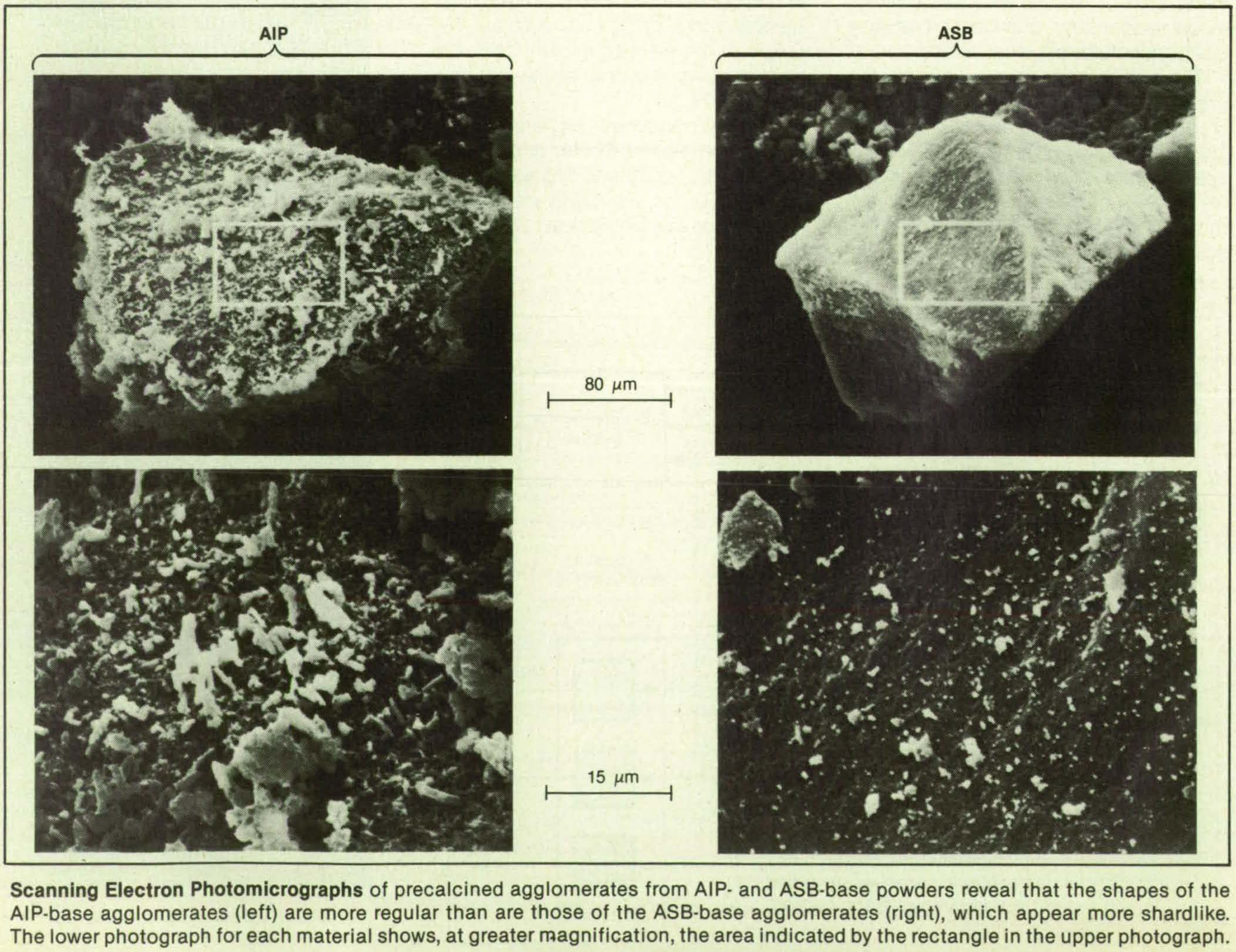

Scanning Electron Photomicrographs of precalcined agglomerates from AIP- and ASB-base powders reveal that the shapes of the AIP-base agglomerates (left) are more regular than are those of the ASB-base agglomerates (right), which appear more shardlike. The lower photograph for each material shows, at greater magnification, the area indicated by the rectangle in the upper photograph.

purity of the alumina precursor. No correlation between these contaminants and the characterized powders was evident.

This work was done by Jeffrey Bull and Daniel Leiser of **Ames Research Center** *and Guna Selvaduray of San Jose State University. For further information, Circle 64 on the TSP Request Card.*
ARC-12764

Colorimetric Detection of Substances in Liquids and Gases

The colors of solvatochromic dyes dispersed in thin films change upon exposure.

Marshall Space Flight Center, Alabama

Thin polymer films containing solvatochromic dyes are used as sensing elements in a new method for the colorimetric detection of substances dissolved in liquids and gases. Solvatochromic dyes have been known for years as dyes that do not react chemically with liquids in which they are dissolved but do respond to changes in the chemical compositions of the liquids by changing in color.

In the new method, a dye that responds to the substance(s) that one seeks to detect is incorporated in a film of polymer that is pervious to the substance(s). The film is exposed to the gas or liquid that contains the substance(s), and its color changes rapidly. The concentration of the substance(s) in the liquid or gas is determined either visually by comparison of the color of the film with a predetermined standard color chart or spectrophotometrically; e.g., by measurement of the wavelength of maximum absorbance.

The method admits of useful variations. For example, another film that is pervious to only certain specified substances can be placed on the sensing film so that only those substances are allowed to reach the dye and produce detectable changes in color. One could also combine this approach with measurement of the change of the absorption spectrum with time to determine the permeability of the covering film to the specified substances.

Experimental sensing films to measure humidity were made of three polymers containing the solvatochromic dye 2,6-diphenyl-4-(2,4,6-triphenyl-N-pyridinio)phenolate, which is sensitive to water molecules. The wavelength of maximum absorption in the ultraviolet and visible spectrum of these films was found to decrease with relative humidity. The best results (in the sense of the steepest and most nearly linear dependence on humidity) were obtained with poly(vinyl acetate) (see figure). The time required to attain the equilibrium value of the wavelength of maximum absorption depends on the thickness of the film and the rate of flow of air across the film; poly(vinyl acetate) films 10 μm thick were found to give equilibrium values within 10 to 15 s.

This work was done by J. Milton Harris, R. Andrew McGill, and Mark S. Paley of the University of Alabama in Huntsville for **Marshall Space Flight Center**. *For further information, Circle 135 on the TSP Request Card.*

Inquiries concerning rights for the commercial use of this invention should be addressed to the Patent Counsel, Marshall Space Flight Center [see page 18]. Refer to MFS-26128.

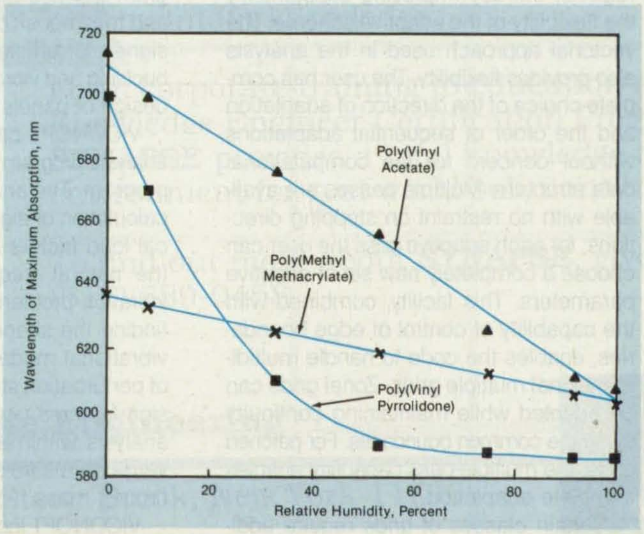

The **Wavelength of Maximum Absorption of Light** in three polymer films that contained a solvato-chromic dye was measured as a function of relative humidity.

Computer Programs

COSMIC: Transferring NASA Software

COSMIC, NASA's Computer Software Management and Information Center, distributes software developed with NASA funding to industry, other government agencies and academia.

COSMIC's inventory is updated regularly; new programs are reported in *Tech Briefs*. For additional information on any of the programs described here, circle the appropriate TSP number.

If you don't find a program in this issue that meets your needs, call COSMIC directly for a free review of programs in your area of interest. You can also purchase the annual *COSMIC Software Catalog*, containing descriptions and ordering information for available software.

COSMIC is part of NASA's Technology Utilization Network.

COSMIC® *John A. Gibson, Director,*
Phone (404) 542-3265 ; FAX (404) 542-4807
The University of Georgia, 382 East Broad Street, Athens, Georgia 30602

Computer Programs

These programs may be obtained at a very reasonable cost from COSMIC, a facility sponsored by NASA to make computer programs available to the public. For information on program price, size, and availability, circle the reference number on the TSP and COSMIC Request Card in this issue.

Mechanics

Adapting Grids for Computing Two-Dimensional Flows

Grids are modified according to initial computed flows to enable recomputation at greater accuracy.

SAGE2D is a two-dimensional implementation of the Self Adaptive Grid Evolution computer program. Solution-adaptive grid programs are useful software tools for efficient and accurate predictions of flows. In supersonic and hypersonic flows, grid points in such strong gradient regions as shocks, contact discontinuities, shear layers, and the like must be distributed carefully to minimize grid errors and enable the computation of accurate flow structures. SAGE2D makes it possible to obtain a more accurate solution by intelligently redistributing (i.e., adapting) the initial grid points on the basis of an initial flow-field solution obtained on the initial grid. The user then computes a new solution by use of the adapted grid.

In adaptive-grid methodology, the problem is posed in an algebraic, unidirectional manner for multidimensional adaptations. The procedure is analogous to applying fictitious tension and torsion spring forces proportional to the local gradient of flow at every grid point and finding the equilibrium position of the resulting system of grid points. The multidimensional problem of grid adaptation is split into a series of one-dimensional problems along the computational coordinate lines. A tridiagonal solver algorithm must then be used to solve the reduced one-dimensional problem to find the locations of grid points along a coordinate line. Multidirectional adaptation is achieved by the sequential application of the method in each coordinate direction.

The fictitious tension force directs the redistribution of points to the strong-gradient region. To maintain smoothness and a measure of orthogonality of grid lines, fictitious torsional forces are introduced to relate information between the family of lines adjacent to one another. The smoothness and orthogonality constraints are direction-dependent, inasmuch as they relate only the coordinate lines that are being adapted to the neighboring lines that have already been adapted. Therefore, the solutions are nonunique and depend on the order and direction of adaptation. Nonuniqueness of the adapted grid is acceptable because it makes possible an overall reduction of local error through redistribution of the grid.

SAGE2D provides the capability to modify the adaptation techniques in boundary regions, thereby improving substantially the flexibility of the adaptive scheme. The vectorial approach used in the analysis also provides flexibility. The user has complete choice of the direction of adaptation and the order of sequential adaptations without concern for the computational data structure. Multiple passes are available with no restraint on stepping directions; for each adaptive pass the user can choose a completely new set of adaptive parameters. This facility, combined with the capability of control of edge boundaries, enables the code to handle multidimensional multiple grids. Zonal grids can be adapted while maintaining continuity along the common boundaries. For patched grids, the multiple-pass capability enables complete adaptation.

Certain classes of grids require additional inputs from the user. By use of approaches described in the documentation, SAGE2D can handle grids with a cyclical or "O"-type structure (e.g., "O"- type grid around a sphere) as well as the specialized grid structure associated with compressor and turbine flows and airfoil flows (e.g., H- and C-type grids that require periodic or matching boundaries).

SAGE2D is written in FORTRAN 77 and is intended to be machine-independent. It has been successfully implemented on Sun, SGI IRIS, DEC MicroVAX, and Cray YMP computers. Source code is provided, but no sample input and output files are provided. The code reads two data files, one that contains the coordinates of the grid (x, y) and the other that contains corresponding flow-field variables. It is assumed that these sets of data are formatted as defined in the plotting software package PLOT3D. Versions of PLOT3D suitable for use on several different computers are available from COSMIC. About 2.5 Mb of main memory is required for execution. SAGE2D is available on a 0.25-in. (6.35-mm) streaming-magnetic-tape cartridge in UNIX tar format (standard distribution medium) or on a 9-track 1,600-bit/in. (630-bit/cm) ASCII CARD IMAGE format magnetic tape. SAGE2D was developed in 1989 and first released in 1991.

This program was written by Carol B. Davies of Sterling Software and Ethiraj Venkatapathy of Eloret Institute for **Ames Research Center**. *For further information, Circle 157 on the TSP Request Card.*
ARC-12757

Designing Assemblies of Plates

VICONOPT facilitates design and analysis with respect to buckling and vibrations.

VICONOPT is a computer program that calculates vibrations and instabilities of assemblies of prismatic plates. The program provides capabilities for optimization and the imposition of constraints. It is designed for efficient, accurate analysis of buckling and vibration and for the optimum design of panels of composite materials.

VICONOPT can be used either as an analysis program or as an optimum-design program. The analysis features cover the calculation of eigenvalues — i.e., the critical load factors in buckling problems or the natural frequencies in undamped-vibration problems — with the option of finding the shapes of the corresponding vibrational modes and associated levels of perturbation stresses. The optimum-design features use the results of buckling analysis within a sizing strategy to converge on a safe design of low (nearly optimum) mass.

VICONOPT includes two major compo-

nents: VIPASA — Vibration and Instability of Plate Assemblies Including Shear and Anisotropy; and VICON — VIPASA With Constraints. Optimization is accomplished by use of CONMIN — CONstrained function MINimization, (ARC-10836) in a manner similar to that used by PASCO — Panel Analysis and Sizing COde (LAR-13164). Improvements in the sizing strategy have greatly reduced the time required for optimization.

VIPASA implements the stiffness-matrix method based on the exact theory of flat plates. It also incorporates a theoretically derived algorithm that guarantees convergence on all required eigenvalues. This enables the user to employ multilevel substructuring very concisely and flexibly to reduce solution times, data-preparation times, and memory usage. VIPASA is based in part on the assumption of modes with sinusoidal longitudinal variation of half-wavelength λ, whereas VICON modes are sums of such modes. In VICONOPT, Lagrangian multipliers are introduced to constrain the response to be compatible with rigid or elastic supports, including transverse beams attached at arbitrary locations. If no constraints are present so that VIPASA may be used, the results are exact. While an infinite number of λ's are theoretically necessary to make VICONOPT exact, only a few are usually required to achieve engineering accuracy.

The VICONOPT sizing strategy involves three types of resizing steps: the initial stabilization step, the CONMIN optimization step, and the final stabilization step. The initial stabilization step brings unstable or overstable initial designs to a "just" stable configuration by altering design variable thicknesses to converge on a configuration such that the most critical eigenvalue for the set of buckling modes specified by the user becomes unity. The CONMIN optimization step entails linear programming techniques that alter design variables so that the mass of the assembly of plates is reduced without violating the buckling and configurational constraints. The final stabilization step returns the optimized configuration to a "just" stable condition. This step is necessary because the linearizing assumptions made during optimization are likely to require correction.

VICONOPT was written in FORTRAN 77 for implementation on DEC VAX-series computers. The main memory requirement is approximately 2 Mb. The program is available on a 9-track, 1,600-bit/in. (630-bit/cm) magnetic tape in VAX BACKUP format (standard medium) or a TK50 tape cartridge. The program should be readily adaptable to any workstation or to mainframe-class computers with a few modifications, which are outlined in the documentation. Graphical output can be obtained easily on most computers, inasmuch as the only graphical routines required are those to move, draw, and write text. VICONOPT was developed in 1990.

DEC VAX and VMS are trademarks of Digital Equipment Corp.

This program was written by F. W. Williams, D. Kennedy, R. Butler, and G. Aston of University of Wales College of Cardiff and M. S. Anderson of Old Dominion University for **Langley Research Center**. *For further information, Circle 90 on the TSP Request Card.*
LAR-14523

Solving Large Sparse Symmetric Eigenproblems

The LANZ program is based on the Lanczos algorithm.

The LANZ computer program implements a sophisticated algorithm based on the simple Lanczos method for solving the generalized eigenvalue problem. LANZ uses a technique called dynamic shifting to improve the efficiency and reliability of the basic Lanczos algorithm. The program has been successfully used to solve such problems as (1) finding the vibration frequencies and mode-shape vectors of a structure and (2) finding the smallest load at which a structure will buckle.

There are several methods for solving the large symmetric generalized eigenvalue problem. LANZ offers an alternative to the popular subspace iteration approach. The program includes a new algorithm for solving the tridiagonal matrices that arise when using the Lanczos method. Procedurally, LANZ starts with the user's initial shift, then executes the Lanczos algorithm until (1) the desired number of eigenvalues are found, (2) no storage space is left, or (3) LANZ determines that a new shift is needed. When a new shift is needed, the program selects it on the basis of accumulated information. At each iteration, LANZ examines the converged and unconverged eigenvalues along with the inertia counts to ensure that no eigenvalues have been missed.

LANZ is written in FORTRAN 77 and C language. It was originally designed to run on computers that are like the Cray Y-MP in that they support vector processing and is therefore optimized for vector computers. Makefiles are included for the Sun3, Sun4, Cray Y-MP, and CONVEX 220 computers. When implemented on a Sun4 computer, LANZ required 670K of main memory. The program is available on a 0.25-in. (6.35-mm) streaming magnetic cartridge tape in UNIX tar format. LANZ was developed in 1989.

Sun3 and Sun4 are trademarks of Sun Microsystems, Inc. Cray Y-MP is a trademark of Cray Research, Inc. CONVEX 220 is a trademark of Convex Computer Corp.

This program was written by Mark T. Jones of ICASE: Universities Space Research Association and Merrell L. Patrick of Duke University for **Langley Research Center**. *For further information, Circle 111 on the TSP Request Card.*
LAR-14506

Program Analyzes Crack-Growth Data

This program processes data from cyclic crack-growth tests.

The Crack Growth Rate Data Analysis computer program is used for cyclic crack-growth testing of compact tension specimens. The program facilitates the digitization of data on crack-opening displacement vs. load and the reduction of these data into data on crack-growth rate vs. stress-intensity excursion.

Key features of the program include (1) the extraction of data on crack-growth rates by use of the elastic-compliance method and (2) least-squares regression analysis of the data to determine constants for Collipriest, Paris, and modified Forman growth-rate equations. Data may be entered into the program from a keyboard or from a magnetic storage medium. Output is fed to a printer, plotter, and/or magnetic storage medium. The program also expedites editing of the crack-growth data and the combination of multiple data files.

The Crack Growth Rate Data Analysis computer program was developed in 1987 for use on the Space Shuttle program. The program is written in HP BASIC and runs on a HP9000 microcomputer. It also utilizes a Hewlett–Packard digitizer and plotter. This program is available only on 5-1/4 in. (13.3 cm) HP9000 SDF-format diskettes. Hewlett–Packard, HP BASIC, and HP9000 are trademarks of Hewlett–Packard, Inc.

This program was written by Charles M. Demonet and James E. Collipriest of Rockwell International Corp. for **Johnson Space Center**. *For further information, Circle 123 on the TSP Request Card.*
MSC-21643

Finite-Element Program for Analysis of Cracked Bodies

ZIP3D analyzes elastic, plastic, and fracture behavior.

ZIP3D is an advanced finite-element computer program developed for the analysis of cracks in three-dimensional elastic or elastic/plastic bodies. The program calculates mixed-mode fracture-mechanics parameters in cracked solids. However, bodies without cracks can also be analyzed to obtain stresses, strains, and displacement fields.

ZIP3D uses eight-node isoparametric elements and small-strain deformation theory. A special reduced-shear integration scheme is provided for bending-dominant problems. The elastic/plastic analysis is based on the incremental plasticity theory using the von Mises' yield criterion, isotropic hardening, and Drucker's flow rule. The initial-stress algorithm is used in this analysis. Three types of material stress/strain curves can be modeled: elastic/perfectly plastic, Ramberg–Osgood, and multilinear representations.

Some unique features of ZIP3D are: (1) the computation of mixed-mode strain-energy-release rates for elastic solids using a three-dimensional virtual-crack-closure technique, (2) the calculation of the J-integral for elastic and elastic/plastic materials by use of the equivalent-domain-integral method, (3) the capability to extend the crack under monotonic or cyclic loading, and (4) the capability to close or open the crack faces during cyclic loading.

ZIP3D is written in FORTRAN V for batch or interactive execution on the CRAY-2, CRAY X-MP and CRAY Y-MP series computers running a UNICOS operating system. Analysis of large models can require as much as 16M words of memory. ZIP3D is distributed on a 5.25-in. (13.34-cm) 360K MS-DOS format diskette in PKZIP format with the PKUNZIP program. A personal computer is required to extract the files before moving the program to the CRAY computer. ZIP3D was developed in 1990.

CRAY-2, CRAY X-MP and CRAY Y-MP are trademarks of Cray Research, Inc. UNICOS is a registered trademark of Cray Research, Inc. PKZIP and PKUNZIP are trademarks of PKWARE, Inc.

This program was written by James C. Newman, Jr., of **Langley Research Center** *and Kunigal N. Shivakumar of Analytical Services and Materials, Inc. For further information, Circle 97 on the TSP Request Card.*
LAR-14611

HOLEGAGE 1.0 — Strain-Gauge Drilling Analysis Program

Interior stresses are inferred from changes in surface strains as a hole is drilled.

There is no simple and perfect way to measure residual stresses in metal parts that have been welded or deformed to make such complex structures as pressure vessels and aircraft, yet these locked-in stresses can contribute to structural failure by fatigue and fracture. One proven and tested technique for determining the internal stress of a metal part involves drilling a test hole while measuring the relieved strains around the hole, as in the hole-drilling strain-gauge method described in

Circle Reader Action No. 321

ASTM E 837. The program HOLEGAGE processes strain-gauge data and provides additional calculations of variations of internal stresses that are not provided by standard E 837 methods of analysis.

In the typical application of the technique, one uses a three-gauge rosette with a special hole-drilling fixture for drilling a hole through the center of the rosette to produce a hole with very small eccentricity error in the gauge pattern. Another device is used to control the drilling and halt the drill at controlled depth steps. At each step, strains from all three strain gauges are recorded.

The influence coefficients used by HOLEGAGE to compute stresses from relieved hole strains were developed by published finite-element-method studies of thick plates with holes of various sizes and depths. The program uses a parabolic fit and an interpolating scheme, as recommended in the reference, to project the coefficients to holes of other sizes and depths. In addition, other published experimental data are used to extend the coefficients to relatively thin plates. These influence coefficients are used to compute the stresses in the original part from the strain data.

HOLEGAGE computes interior planar stresses by use of strain data from each drilled-hole depth layer. Planar stresses can be computed in any or all of three ways, including (1) a least-squares fit for a linear variation with depth, (2) an integral method to give incremental stress data for each layer, and/or (3) a linear fit to the integral data (with some surface data points omitted) to estimate the surface stresses that existed before the sanding done in preparation for the installation of the strain gauges introduced additional residual stresses. Options are included for estimating the effect of eccentricity of the hole on calculations, smoothing noise from the strain data, and putting the data into the program either interactively or from a data file.

HOLEGAGE was written in FORTRAN 77 for DEC VAX computers under VMS and is transportable except for system-unique TIME and DATE system calls. The program requires 54K of main memory and was developed in 1990. The program is available on a 9-track 1,600-bpi (630 b/cm) VAX backup-format magnetic tape (standard medium) or a TK50 tape cartridge. The documentation is included on the tape.

DEC VAX and VMS are trademarks of Digital Equipment Corp.

This program was written by Roy W. Hampton of **Ames Research Center**. *For further information, Circle 2 on the TSP Request Card.*
ARC-12807

Mathematics and Information Sciences

Programs Handle PostScript Files

Four programs interpret and format files in the PostScript language.

PSTOOLS is a package of four computer programs that operate on files written in the page-description language, PostScript. The programs include a PostScript previewer for the IRIS workstation, a PostScript driver for the Matrix QCRZ film recorder, a PostScript driver for the Tektronix 4693D printer, and a PostScript code beautifier that formats PostScript files to be more legible.

The three programs PSIRIS, PSMATRIX, and PSTEK are similar in that they all interpret the PostScript language and send out the graphical results to a device. They share common code, which is included as a library of routines. PSPRETTY formats a PostScript file by appropriately indenting procedures and code delimited by "saves" and "restores." PSTOOLS does not use Adobe fonts.

PSTOOLS is written in C language for implementation on SGI IRIS 4D-series workstations running IRIX 3.2 or later. A README file and UNIX manual pages provide information regarding the installation and use of the PSTOOLS programs. A six-page manual that provides slightly more detailed information may be purchased separately. The package of programs is available on a 0.25-in. (6.35-mm) streaming-tape cartridge in UNIX tar format. PSIRIS (the largest program) requires 800K of main memory. PSMATRIX requires the general-purpose interface bus (gpib) circuit board (IEE 488) and the "libgpib.a" library of software, which is available from Silicon Graphics, Inc. The programs with graphical interfaces require that the IRIS have at least 24 bit planes. This package was developed in 1990 and updated in 1991.

SGI, IRIS 4D, and IRIX are trademarks of Silicon Graphics, Inc. Matrix QCRZ is a registered trademark of the AGFA Group. Tektronix 4693D is a trademark of Tektronix, Inc. Adobe is a trademark of Adobe Systems Inc. PostScript is a registered trademark of Adobe Systems Inc. UNIX is a registered trademark of AT&T.

This program was written by Diana Choi and David Yip of **Ames Research Center**. *For further information, Circle 3 on the TSP Request Card.*
ARC-12839

Mechanics

Tool Changer for Robot

A mechanism stores a tool and helps a robot extract it.

Goddard Space Flight Center, Greenbelt, Maryland

A mechanism enables a robot to change tools on the end of its arm. The mechanism is actuated by the motion of the robot: it requires no additional electrical or pneumatic energy to make or break the connection between the tool and the wrist at the end of the arm.

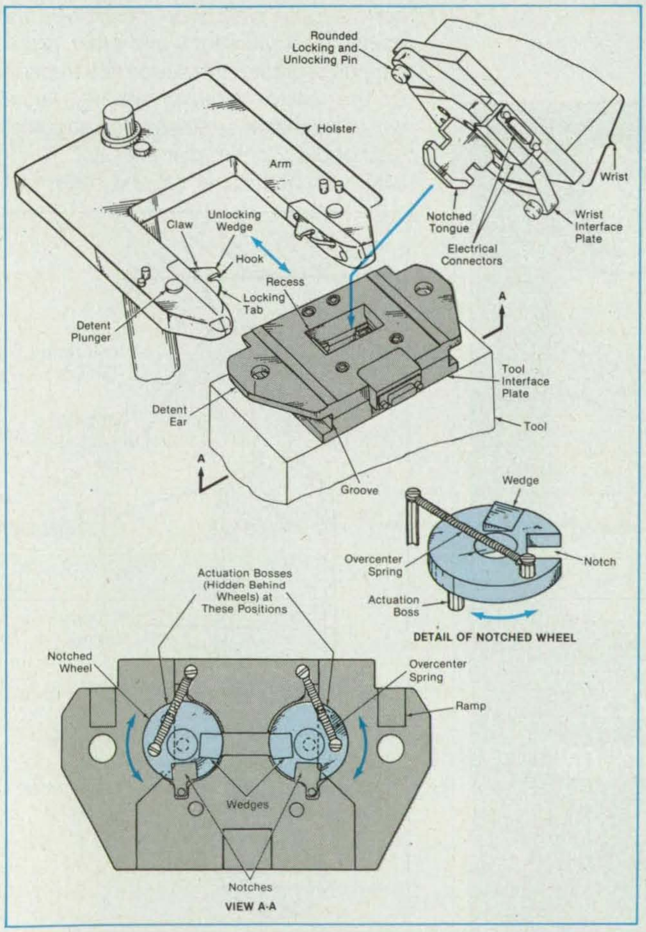

The **Arms of the Holster Engage Slots** on the sides of the tool interface plate when a tool is stored. The robot arm engages the notched tongue on the wrist interface plate with a recess in the tool interface plate to remove a tool for use. Wheels inside the tool interface plate secure the tongue in the recess while the tool is in use.

The mechanism includes three basic subassemblies (see figure): a wrist interface plate attached to the robot arm at the wrist, a tool interface plate attached to the tool, and a holster. A separate tool interface plate and holster are provided for each tool the robot uses. When a tool is not in use, it rests in its holster, held securely in place by a pair of spring-loaded detent plungers.

When the robot needs a tool, it places its toolless wrist and wrist interface plate over the holster, so that a notched tongue is directly above a chamfered recess in the tool interface plate and rounded locking pins are directly over holes in detent ears. The robot then lowers the tongue into the recess. The chamfered edges on both the recess and the tongue guide the wrist interface plate into the tool interface plate. The rounded locking pins push the spring-loaded detent plungers down into the holster so that the detent ears are released. At the same time, electrical connectors on the two interface plates mate, and the tongue slides through aligned notches in notched wheels within the tool interface plate (view A–A).

The robot can then slide the tool off the holster. As the robot does so, actuation bosses on the notched wheels are forced against locking tabs on the claws in the holster. This rotates the notched wheels, causing the solid portions of the wheels to enter the notches in the tongue. Overcenter springs continue to rotate the wheels as the tool interface plate is slid from the holster until wedges on the wheels are firmly driven into the notches in the tongue. Thereafter, the springs continue to exert force on the wedges. The wheels thus hold the tongue securely while the tool is being used.

If either wheel cannot be rotated into a tongue notch — perhaps because of misalignment — a claw restrains the affected actuation boss. This prevents the tool from being removed unless it is safely attached to the robot.

When the robot puts the tool back into the holster after using it, the procedure is reversed. The robot slides the tool onto the arms of the holster. As it does so, a pair of ramps on the forward undersurface of the detent ears compresses the detent plunger and its springs. The hooks of the claws make contact with the actuation bosses and rotate the notched wheels in the direction opposite that of the tool-removal phase; the notches in the wheels are thereby realigned, and the tongue can be moved up and away from the tool interface plate. As the tongue moves away, the detent plungers reenter the detent ear-holes. The tool interface plate and its tool are once again locked in the holster.

This work was done by George M. Voellmer of **Goddard Space Flight Center**. *For further information, Circle 152 on the TSP Request Card.*

This invention is owned by NASA, and a patent application has been filed. Inquiries concerning nonexclusive or exclusive license for its commercial development should be addressed to the Patent Counsel, Goddard Space Flight Center [see page 18]. Refer to GSC-13239.

Passive Accelerometer

Motion of a ball in a liquid would indicate acceleration.

Marshall Space Flight Center, Alabama

The passive accelerometer has been proposed to measure quasi-steady spacecraft accelerations of the order of $10^{-6} \times$ normal Earth gravitation, possibly in the presence of vibrations and other disturbances of greater amplitude and frequency. The passive accelerometer (see figure) would consist of a transparent graduated tube about 2 cm in diameter and 10 cm long, with hemispherical end caps, con-

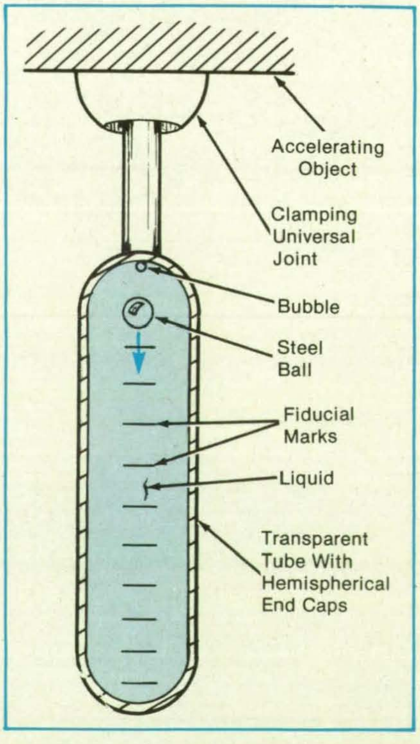

The **Passive Accelerometer** would measure small accelerations along its cylindrical axis. The principale of operation would be based on Stokes' law.

taining a steel ball about 0.4 cm in diameter, and filled (except for a small bubble) with water or other liquid of known viscosity. Modified versions, possibly containing different liquids or balls of different materials, might find use on Earth in measurements of small tilts or horizontal accelerations or as educational laboratory devices.

This accelerometer is called "passive" because it would put out no signal and would have to be aligned and observed by a technician. The tube would be attached to the accelerating vehicle or object by a universal joint, which would also be used to align the tube along the acceleration. To perform alignment, the technician would adjust the orientation until the ball and bubble reached their equilibrium positions at the apices of the opposing hemispherical end caps. Then the technician would pull the ball to the bubble end by use of a magnet. Next, the magnet would be removed, allowing the ball to fall back to its equilibrium position.

The technician would measure the time of release and the times when the ball passed the fiducial marks on the tube. From these times and the known distances between the marks, one can compute the velocity of the ball. Then by use of the Stokes equation for a rigid sphere falling through a viscous liquid, one can use the velocity and the known viscosity of the liquid to compute the component of acceleration along the tube.

Despite its simplicity and low cost, the passive accelerometer is expected to provide accurate measurements of small quasi-steady accelerations. As an additional advantage, the passive accelerometer would automatically integrate out the unwanted higher-frequency components of acceleration because the integration time would be the observation interval, which would typically be of the order of minutes to tens of minutes.

This work was done by Robert J. Naumann, Charles Baugher, and Iwan Alexander of **Marshall Space Flight Center**. *For further information, Circle 18 on the TSP Request Card.*

Inquiries concerning rights for the commercial use of this invention should be addressed to the Patent Counsel, Marshall Space Flight Center [see page 18]. Refer to MFS-28546.

Panel-Method Computer Code for Potential Flow

Low-order panel method is used to reduce computation time.

Ames Research Center, Moffett Field, California

The panel code PMARC (Panel Method Ames Research Center) can numerically simulate the flow field around or through complex three-dimensional bodies such as complete aircraft models or a wind tunnel. PMARC is based on potential-flow theory. The code is written in standard Fortran 77, with the exception of the namelist extension used for input. The structure of PMARC facilitates the addition of new features to the code and the tailoring of the code to specific problems and computer-hardware constraints.

In a panel method, the surface of the body over which the flow field is to be computed is represented by a set of panels. Singularities are distributed on the panels to perturb the flow field around the body surfaces. PMARC uses source and doublet singularities distributed uniformly over each panel. Since the singularity strength

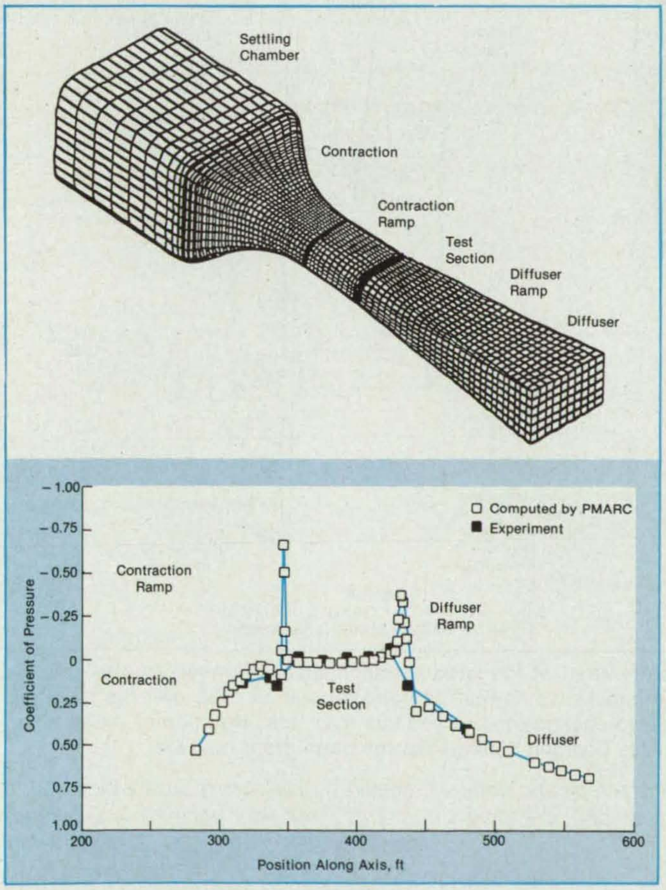

Shown is a **PMARC Panel Representation** of a wind tunnel consisting of a contraction, test section, and diffuser. Pressure coefficients computed by PMARC are compared with experimental data.

is constant on each panel, the method is labeled a low-order panel method. Higher order panel methods allow the singularity strength to vary linearly or quadratically across each panel. Experience has shown that low-order panel methods can provide nearly the same accuracy as higher-order methods over a wide range of cases with significantly reduced computation times; hence, the low-order formulation was adopted for PMARC.

To avoid unnecessary duplication of previous work, existing software was utilized whenever possible to reduce the development time of PMARC. The basic potential-flow computational methods and techniques were patterned after the 1,000-panel version of VSAERO (developed by Analytical Methods Inc.), which is currently available through COSMIC.

The management of the data within the PMARC code is highly optimized. All of the arrays within the code are adjustable arrays; thus, the size of the code (i.e., the number of panels that it can handle) can be changed very quickly. This allows PMARC to be sized to run on anything from a personal computer like a Macintosh to a supercomputer like the Cray Y-MP. The output and plot files from PMARC have been organized to maximize the amount of information they contain while minimizing their size. A geometry preprocessor and a geometry/aerodynamic data post-processor have been written for creating and inspecting geometry paneling and for analyzing the results of PMARC.

The present version of PMARC includes several advanced features. The first is an internal-flow-modeling capability, which allows the analysis of closed ducts, wind tunnels, and similar internal-flow problems. The second is a simple jet model, which allows the modeling of the gross effects of a jet in crossflow. The third is a time-stepping wake model, which gives PMARC the ability to model both steady and unsteady flow problems.

In a test case, PMARC was used to compute the flow field in a wind tunnel consisting of a contraction, a test section, and a diffuser. The tunnel was modeled using more than 5,000 panels (upper part of figure). The pressure coefficients on the tunnel walls were computed by PMARC and then plotted as a function of position along the longitudinal axis. The results agree well with experimental data, as shown in the lower part of the figure.

This work was done by Dale L. Ashby and Michael R. Dudley of **Ames Research Center** *and Steven K. Iguchi of Sterling Federal Systems. The PMARC computer code is currently available through COSMIC. Further information may be found in NASA TM-101024 [N89-12554], "Development and Validation of an Advanced Low-Order Panel Method."*

Copies may be purchased [prepayment required] from the National Technical Information Service, Springfield, Virginia 22161, Telephone No. (703) 487-4650. Rush orders may be placed for an extra fee by calling (800) 336-4700.
ARC-12385

Latches for Equipment Drawers

A mechanism makes rack hardware interchangeable, regardless of drawer height.

Lyndon B. Johnson Space Center, Houston, Texas

A pair of panel-handle latches provides quick connection and disconnection of an equipment drawer in a rack.The latches enable the interchange of drawers of different heights without alteration of the fittings on the front of the rack. They provide load-carrying capacity in three orthogonal directions, press the front panel of the drawer flush against the rack, and establish electrical grounding paths between the panel and the rack.

A rotating latch is built into each of the two handles on the front panel of a drawer. When a user pushes the drawer into a rack, a hook on a pivoting lever on each latch becomes positioned over a pin in an adjustable striker assembly (see figure). At the same time, a shear pin at the top of the handle engages a mounting bracket on a slide guide in the rack. The user rotates the lever so that the hook engages the striker pin and pulls the front panel of the drawer flush with the front surface of the front post of the rack. The user continues to rotate the lever into the handle frame, where it is latched and closed by a spring-loaded retainer in the handle. The user then secures the drawer by rotating a lock into its closed position.

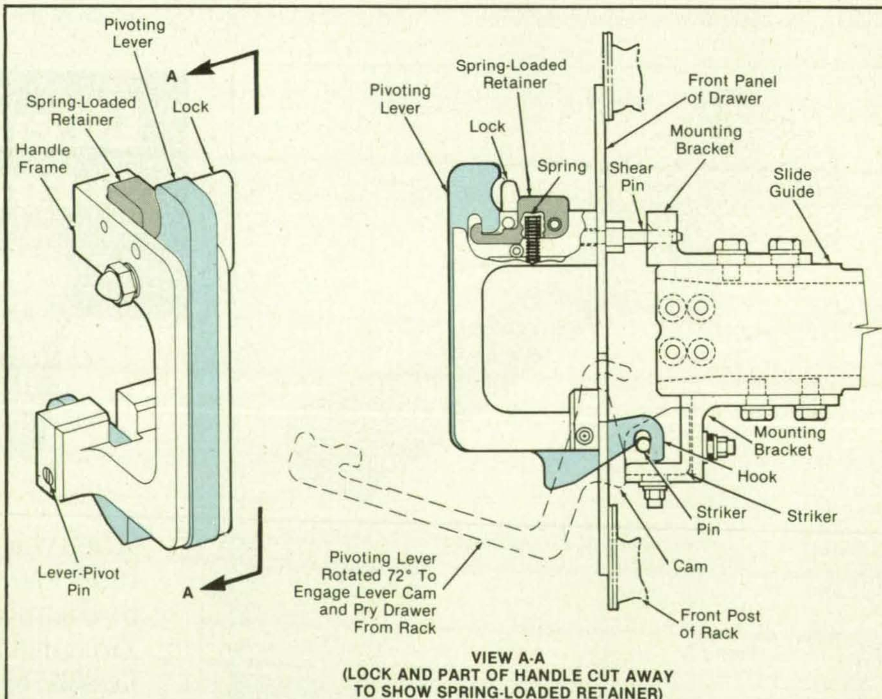

The **Pivoting Lever** is the heart of the latching mechanism. At insertion, the lever is rotated slightly counterclockwise so that its bottom hook can slip over the pin; it is then rotated clockwise to engage the pin and the lever lock. Rotation of the lever to the full counterclockwise position disengages the panel from the rack.

To remove the drawer, the user rotates the lock into its open position, presses the locking retainer down, and rotates the pivoting lever downward until its cam hits the striker assembly. Additional downward force on the lever causes the cam to pry the drawer loose from the rack and from any mating mechanical and electrical connectors.

The latch requires little or no maintenance. All parts that rotate are equipped with bushings on fixed pins, so that wear should be low and reliability high.

This work was done by T. C. Martin of General Electric Co. for **Johnson Space Center**. *For further information, Circle 53 on the TSP Request Card.*
MSC-21756

Improved Stacking of Vent Lines of a Parachute

Adverse concentrations of loads in the vent band would be reduced.

Marshall Space Flight Center, Alabama

A proposed new way of stacking the vent lines of a parachute would reduce adverse concentrations of loads in the vent band. The new stacking arrangement would replace the previous arrangement, in which adverse concentrations of loads occurred at the points of the vent band where the first and last vent lines are adjacent. The new arrangement would provide a more nearly uniform distribution of load among the vent lines and the points of attachment of vent lines to the vent band.

In the old method, vent lines are stacked in a clockwise or counterclockwise sequence (see figure). The resulting stack is quite high, and the first and last lines are separated by the full height of the stack even though in a plan view they appear adjacent to each other. The angle between them (as measured in a meridional plane) at the vent band gives rise to a high concentration of crosswise tension (tending to twist the band at that point).

In the new method, the first line would be placed across the vent, and the second line would be placed on the first and adjacent to it (see figure). The third vent line would be placed on the second, but adjacent to the first on the side opposite that of the second. The fourth line would be placed on the third, but adjacent to the second. The fifth line would be placed ad-

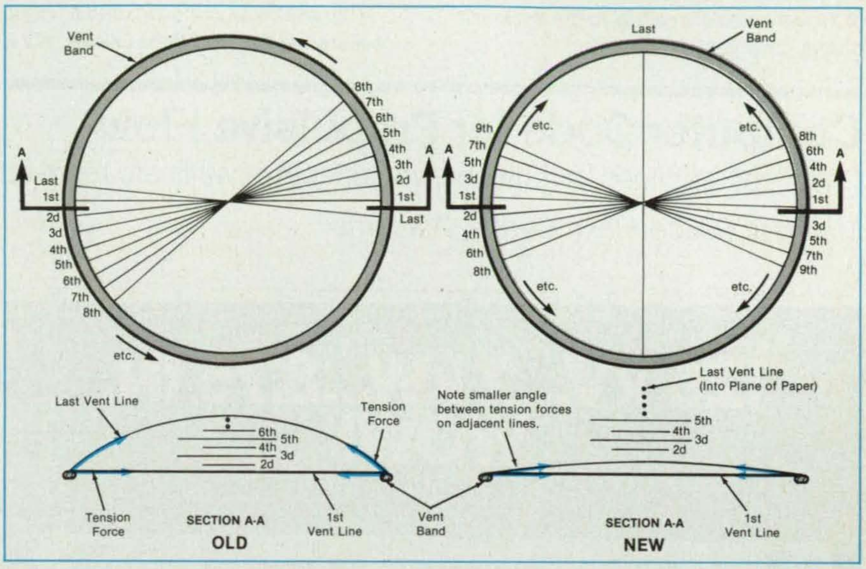

The **Old and New Stacking Arrangements** differ in the sequences in which the vent lines are laid across the vent.

jacent to the third, and so forth, one on the other, even-numbered lines on one side of the first line, odd-numbered lines on the other side, until the last vent line is in place. The angle between any two adjacent vent lines at the vent band would be small, and the separation between them at the center of the vent would be equal to the thickness of only one vent line.

The new method would eliminate the large stack height between the first and last lines and, just as important, maintain a constant stack height between any two adjacent vent lines around the entire vent. This would distribute the loads at the vent band more nearly evenly among the lines.

This work was done by John E. Hengel of **Marshall Space Flight Center**. *For further information, Circle 29 on the TSP Request Card.*

Inquiries concerning rights for the commercial use of this invention should be addressed to the Patent Counsel, Marshall Space Flight Center [see page 18]. Refer to MFS-28508.

Computer Code for Propulsive Flow

Chemical reactions, turbulence, and effects of walls are represented.

Marshall Space Flight Center, Alabama

The Finite Difference Navier–Stokes (FDNS) computer code has been enhanced for use in recent studies of propulsive flows in and near rocket nozzles. As a result, FDNS is now applicable to complicated geometries and chemically reacting flows that may include turbulence and thermal interactions with walls. In FDNS, the solutions of the equations for the subsonic, supersonic, and boundary-layer regions of the flow field are combined into a single reliable, accurate (see figure) software tool of computational fluid dynamics.

The current, advanced version of FDNS can be used to solve the two-dimensional planar, two-dimensional axisymmetric, or three-dimensional Navier–Stokes equations of flow along with the associated equations for generation, consumption, and transport of heat and of chemical species. These are nonlinear, coupled differential equations that are formulated as transport equations in the primitive variables. The exact differential equations are approximated by finite-difference equations on a computational grid based on general curvilinear coordinates.

The finite-difference equations are solved numerically. A second-order central-differencing scheme and fourth-order dissipation terms are used to model convection. Second-order central-differencing schemes are used to model viscosity and the source

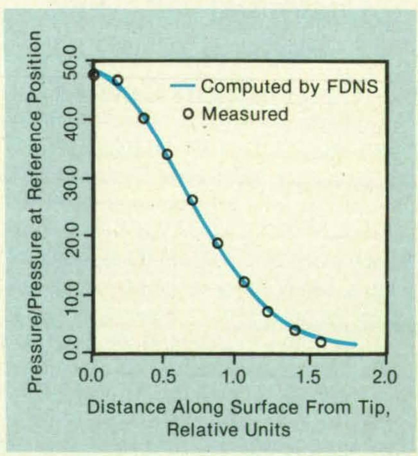

The **Accuracy of FDNS** is illustrated by this comparison of the computed and measured distribution of pressure along the surface of a cylinder with a spherical top in a flow of mach 6.05.

terms in the differential equations. A first-order upwind scheme is used for all equations for the transport of scalar quantities, including the equations of a mathematical model of turbulence.

A time-centered Crank–Nicholson time-marching scheme is used for the temporal discretization in time-accurate solutions. For steady-state solutions, an implicit Euler time-marching scheme is recommended. The selection of the time-marching scheme can be controlled via input data. Whether the flow is compressible or incompressible and whether it is laminar or turbulent, a pressure-based predictor/multicorrector procedure is used to ensure coupling between the pressure and velocity fields and to obtain a solution with a divergence-free flow field at the end of each time-marching step.

FDNS includes the two-equation standard and extended k–ϵ mathematical models of turbulence with standard wall-function boundary conditions. The applicable turbulence models can be selected via input data. With regard to chemistry, FDNS can treat an ideal gas, a real gas, a mixture of gases at chemical equilibrium, and a mixture of gases reacting chemically at a finite rate. The mathematical models of chemistry in FDNS include an equilibrium H_2/O_2 system with an equilibrium-constant method and an efficient finite-rate chemistry method with reaction-rate information controlled via input data.

This work was done by Y. S. Chen, R. S. Farmer, and J. A. Freeman of SECA, Inc., for **Marshall Space Flight Center**. *For further information, Circle 48 on the TSP Request Card.*

Inquiries concerning rights for the commercial use of this invention should be addressed to the Patent Counsel, Marshall Space Flight Center [see page 18]. Refer to MFS-26125.

Axial-Loading Circumferential Dovetail Turbine-Blade Mount

Blades are less likely to be shaken loose during operation.

Marshall Space Flight Center, Alabama

A new circumferential dovetail configuration for mounting blades in the rotor disk of a turbomachine provides for the insertion of the blades in an axial direction. Previously, blades were inserted into a typical dovetail slot in the radial direction through slots in the edge of the disk. The slot geometry limited the circumferential length of each dovetail joint to half the circumferential blade pitch; this small dovetail length limited the load-carrying capacity of the dovetail joint. The new loading configuration allows circumferentially longer and, therefore, stronger dovetail joints.

With the new configuration, the base of a blade is inserted into a dovetail slot through an axial channel at the periphery of the disk (see figure). When all blades have been loaded, a retaining ring is placed on the disk so that it secures all blades in their slots. Protuberances on the ring are shaped to dovetail with recesses

The **Retaining Ring** holds the base of each blade in the circumferential dovetail slot. The blades are first inserted axially via loading slots into the circumferential dovetail slot. The ring is then placed over the loading slots and fastened with a split ring held by an arm of the disk. Previously, blades were inserted radially into loading slots, moved circumferentially into locking slots, then fastened with setscrews.

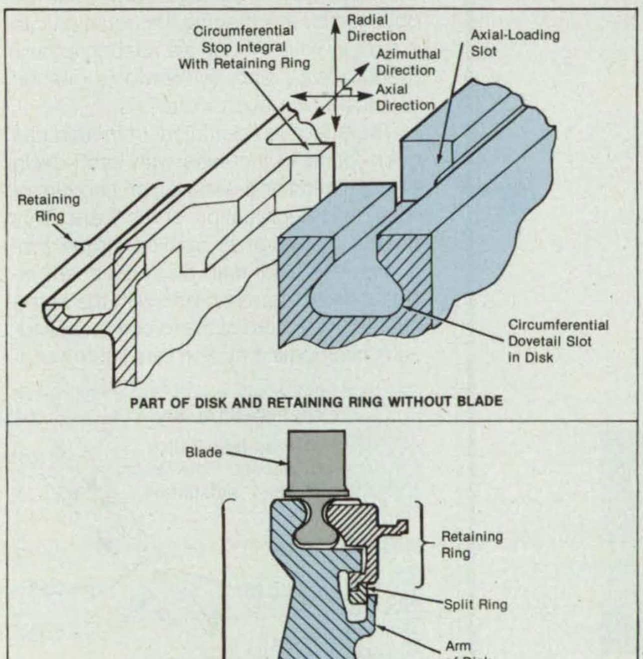

on the side of the base of the blade that faces the ring. The ring is held radially by a disk rabbet and axially by a split ring that is, in turn, held by an arm of the disk. The retaining ring holds the blades without setscrews, which are used in the radial-loading configuration and which are prone to loosening in operation.

This work was done by Martin J. Pierce, Steven D. Ward, and Ronald R. Eskridge of General Electric Co. for **Marshall Space Flight Center**. *For further information, Circle 11 on the TSP Request Card.*

Inquiries concerning rights for the commercial use of this invention should be addressed to the Patent Counsel, Marshall Space Flight Center [see page 18]. Refer to MFS-28544.

Torque, Tension, and Friction in Bolts

Tension at a given torque depends strongly on friction.

Lyndon B. Johnson Space Center, Houston, Texas

Improved equations predict fairly accurately the relationships among the tension in a bolt, the torque applied to the bolt during installation, the effective coefficient of friction, and the number of times the bolt has been installed. The equations were derived from a study of experimental data and include parameters that must be determined empirically for each type of bolt and nut in a given application. Once these parameters are determined, the improved equations can be used to design bolted joints in which the bolts are torqued closer to their yield points than they are in current design practice, which requires large safety margins because it is based on less-accurate equations. Thus, in bolted joints designed according to the new equations, one could use fewer and/or smaller bolts to carry the same loads, thereby reducing weights.

The first equation is

$$P = \frac{a}{(\mu d)^{0.3}} T^{[b(\mu d)^{-0.096}]}$$

where P is the axial load in the stem of the bolt, T is the torque applied to the bolt, d is the maximum pitch diameter specified for the class to which the bolt belongs, μ is the effective coefficient of friction, and a and b are constants. Although μ is generally not known in advance and appears only implicitly in the equation, it can be obtained by rearranging the equation into a form in which it can be fitted to experimental P-vs.-T data by Newton's method of successive approximations.

The effective coefficient of friction has been found to increase with each cycle of installation and removal, on account of wear and degradation of lubricant. This means that a given applied torque produces less axial load on subsequent installation of the same bolt with the same nut because more of the torque is expended in overcoming friction (see figure); con-

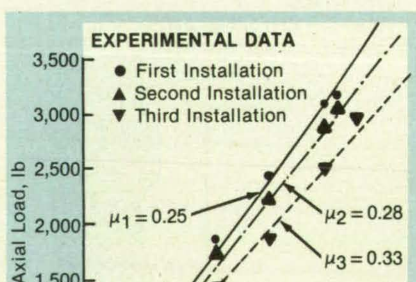

The **Axial Load on a Bolt** and the torque applied to the bolt were measured in three installation/removal cycles. The dashed lines represent fits of the first equation to the experimental data, using the indicated coefficients of friction.

versely, one must apply greater torque to obtain the same axial load as before. The effect can be approximated by

$$\mu_N = \mu_0(1+\Delta)^N$$

where μ_N = the effective coefficient of friction after the Nth installation, μ_0 = the coefficient of friction before the first installation, and Δ is a constant that is typically of the order of 1/8.

This work was done by Julian Morawski of Rockwell International Corp. for **Johnson Space Center**. *For further information, Circle 23 on the TSP Request Card. MSC-21786*

Expandable Compartmental Storage

Readily-accessible, removable compartments hold large and small articles.

Lyndon B. Johnson Space Center, Houston, Texas

A storage cabinet is equipped with racks that hold articles in net compartments. The elastic net expands and contracts to accommodate articles of various sizes and quantities. The stored articles are clearly visible and accessible. They can be loaded in the rack quickly and can be easily moved as a group to another location.

The cabinet is 41.5 in. (105.4 cm) wide, 40 in. (101.6 cm) deep, and 80 in. (203.2 cm) tall. It contains four forward doors, color-coded so that their contents can be identified before the doors are opened. Each door is opened by pulling a recessed handle at its top and pivots forward and downward 90° (see figure). The doors can be removed by unlatching the pivot mechanisms at their bases.

Each door contains four net storage compartments. Each compartment is covered by a smaller door that consists of two overlapping nets on a frame. Each such compartment door can be swung open to load or unload bulky articles. Small articles can be inserted or removed by reaching a hand between the overlapping nets.

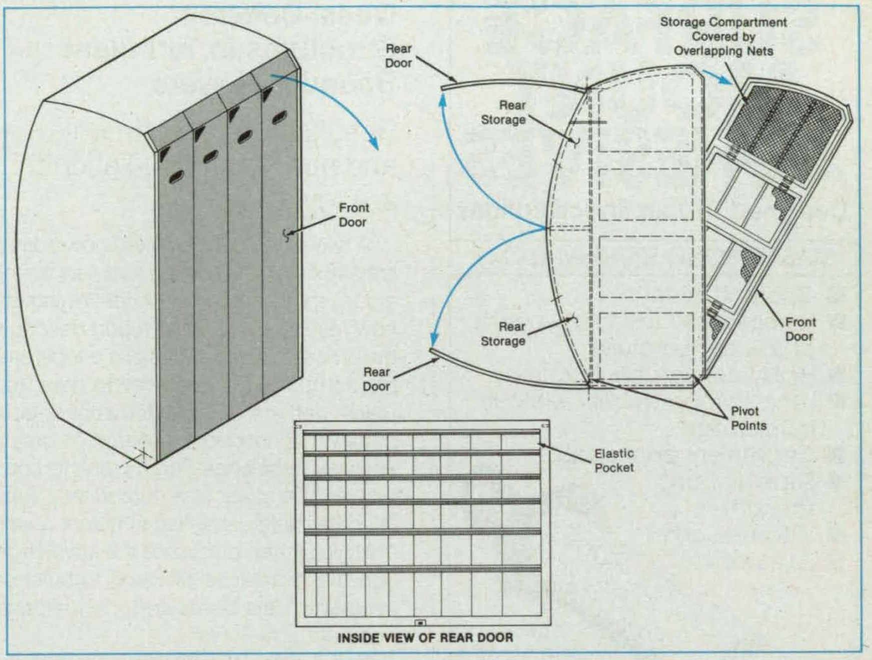

Netted Compartments in Doors hold articles securely while allowing quick and easy access. Pockets on the inside of the rear doors offer convenient storage of small objects.

The cabinet also contains a pair of rear doors that can be reached by tilting the entire rack forward 90°. These doors can be unlatched and pivoted to expose two large rear storage compartments. Again, net frames on the rear compartments can be opened to insert or remove large articles, or a hand can be extended between overlapping nets to reach small articles.

A special feature of the rear doors is their lining. They are covered on the inside with elastic pockets in various sizes. The pockets are convenient for storing small items — tools, charts, and various personal articles, for example. Like the forward doors, the rear doors can be removed.

This work was done by Elray P. Thomas of Johnson Engineering Corp. for **Johnson Space Center**. *For further information, Circle 7 on the TSP Request Card. MSC-21339*

Books and Reports

These reports, studies, handbooks are available from NASA as Technical Support Packages (TSP's) when a Request Card number is cited; otherwise they are available from the National Technical Information Service.

Study of Disturbances in Rotating Plane Poisseuille Flow

Instability and transition to turbulence are simulated numerically.

A report describes a computer-simulation study of instability and transition to turbulence in plane Poisseuille flow in a rotating channel. More specifically, the flow is along a channel of rectangular cross section that is much wider in one dimension (called the "spanwise" dimension) than in the other dimension (called the "normal" dimension) and is initially laminar with small random disturbances. The initial flow is then perturbed by suddenly making the channel rotate about the spanwise centerline.

The resulting motions of the fluid are governed by the Navier-Stokes equations of incompressible flow, using periodic boundary conditions in the streamwise (along the channel) and spanwise directions. The principal parameters that affect the flow are the Reynolds and rotation numbers (the rotation number is defined as the frequency of rotation multiplied by half the width of the channel in the normal dimension divided by the mass-averaged mean velocity. Four different combinations of these parameters, selected to match those of a series of experiments reported in 1989, are used in the Navier-Stokes equations.

The equations are solved numerically in a computational domain of sufficient streamwise length and spanwise width to contain the vortices that evolve from the initial small disturbances. This domain allows the solution algorithm to make a relatively unbiased selection of the dominant spanwise wavelength of the streamwise vortices and of the streamwise wavelengths of the dominant secondary modes that develop subsequently in the presence of the streamwise vortices. The computation is continued until the simulated flow attains a statistically steady state.

The evolutions of the vortices for the four different combinations of parameters are studied in detail. In all cases examined, two-dimensional streamwise vortices with spanwise wave numbers consistent with the linear (small-disturbance) theory develop in the linear (early) stage. Then spanwise wave selection takes place, leading to a dominant spanwise wave number. In the statistically stationary (late) stage, depending upon the Reynolds and rotation numbers, three different cases are observed: wavy modes with streamwise wavelengths an order of magnitude longer than spanwise wavelengths, twisting modes with short streamwise wavelengths comparable to the spanwise wavelengths, and the simultaneous presence of both modes.

It is also shown that these modes are nondispersive traveling waves. These results agree well with those of the experiments.

This work was done by John Kim of **Ames Research Center** *and Kyung-Soo Yang of Stanford University. To obtain a copy of the report, "Numerical investigation of instability and transition in rotating plane Poisseuille flow," Circle 25 on the TSP Request Card.*
ARC-12862

Quasi-Coherent Structures in Turbulent Boundary Layers

Results from experiments and numerical simulations are reviewed.

A two-part report reviews knowledge of coherent structures in the turbulent boundary layers, including both confirming and new results. Part I of the report describes the processes and status of a cooperative project to summarize existing data from many workers in the international community that conducts research on boundary-layer turbulence. Part II presents some results of a study of a numerically simulated flat-plate canonical turbulent boundary layer. It also discusses the advantages and disadvantages of using turbulence-simulation data bases in studies of quasi-coherent structures.

Part I lists four distinctions that one must make to clarify the nature of the various experimental results and observations; for example, the need to distinguish between reliable experimental data and inferences or hypotheses that go beyond the data. It then describes the eight known classes of quasi-coherent boundary-layer structures and summarizes some of the knowledge about each class. These classes are (1) low-speed streaks near a wall, (2) ejections of low-speed fluid outward from the wall, (3) sweeps of high-speed fluid inward toward the wall, (4) vortical structures of several proposed forms, (5) strong internal shear layers near the wall, (6) near-wall "pockets" (seen as regions swept clean of marked fluids in experiments), (7) large-scale discontinuities in streamwise velocity, and (8) large-scale motions capped by bulges in the interface between the turbulent boundary layer and the outer potential flow.

In discussing the eight types of quasi-coherent structures and what is known in the community as the "inner/outer controversy" (current uncertainties in establishing causal connections between phenomena observed in inner and outer fluid layers), the report notes three difficulties that reduce the information available from the experimental data. These are (1) the necessity to take ensemble averages of probe outputs, with consequent losses of phase information, (2) the inability to see more than one or two of the various types of structures simultaneously, and (3) the resulting inability to see the spatial relations between the various quasi-coherent structures. Nevertheless, the following conclusions can be drawn: (1) The inner layers are capable of maintaining turbulent flow without any fluctuations from the outer layers. (2) The level of fluctuations and the production of turbulence in the inner layers can be significantly affected by fluctuations in the outer layers of the boundary layer or by disturbances in the free stream. (3) In the canonical flat-plate layer, roughly 70 percent or more of the turbulence produced in the inner layers maintains itself; that is, this turbulence is apparently triggered by events that occur within the inner layer. (4) The inner and outer layers interact, but only weakly.

Part II describes the continuing investigation of the quasi-coherent structures in a numerically simulated boundary layer, which has produced the following preliminary results: (1) All eight known classes of boundary-layer structures have been identified in the simulated boundary layer. (2) High-speed regions in the sublayer are less elongated than are the low-speed regions. (3) Low-pressure regions tend to be elongated, and this phenomenon could be used to detect instantaneous vortex cores. (4) Archlike vortical structures of a broad range of sizes are common in the boundary layer, while quasi-streamwise vortexes with significant streamwise extent are relatively rare. (5) High-pressure regions are spheroidal and often occur just upstream and below the heads of vortical arches. (6) There is a strong instantaneous spatial association between vortical structures and both ejections and sweeps. (7) Both ejections and sweeps occur along quasi-streamwise vortexes, but ejections are most common in frozen computational fields just upstream and behind vortical arches. Sweeps occur most often on the outboard sides of the "necks" of vortical arches. (8) Some near-wall shear layers have been observed to roll up into transverse vortexes, which are in turn associated with significant local contributions to Reynolds shear stresses through ejection motions. (9) "Backs" of outer-region, large-scale motions have been identified in the simulation data. In at least some cases, the backs are interfaces between low-speed fluid trailing a solitary large-scale vortical structure and the following high-speed fluid.

This work was done by S. K. Robinson of Langley Research Center, S. J. Kline of Stanford University and P. R. Spalart of Boeing Co. for **Ames Research Center**. *To obtain copies of the reports, "Quasi-Coherent Structures in the Turbulent Boundary Layer," Circle 16 on the TSP Request Card.* *ARC-12629*

Recursive Algorithms for Dynamics of Geared Robots

Inertias of motors and gears are taken into account.

NASA's Jet Propulsion Laboratory, Pasadena, California

Improved recursive algorithms compute the dynamics of a robotic manipulator driven through gears by motors located away from the joints. These algorithms are intended to replace prior algorithms that implement direct-drive mathematical models, in which drive motors are considered to be located at the joints and to behave as ideal actuators.

The direct-drive models are inadequate to address the more-complicated dynamics of gear-driven manipulators, in which the rotational inertias of the motors are amplified by the gear ratios and can sometimes even dominate the dynamics. Reliance on a direct-drive model can lead to significant errors in the design of the control system of a manipulator, with consequent degradation of the stability and performance of the robotic system.

The development of the improved algorithms began with the Newton–Euler equations of motion of a manipulator, specialized to the case in which each joint has one degree of rotational freedom and the motor and gears that drive each joint are mounted on the inboard link of the two links connected by that joint (see figure). These equations were used to obtain a mass matrix and Coriolis terms. The mass matrix is more complex than it would be in the corresponding direct-drive model; it includes additional diagonal and off-diagonal terms that represent the additional cross-coupling between joints that is attributable to the inertias of the motors.

A recursive algorithm that computes the mass matrix and that involves a number of arithmetic operations approximately proportional to n^2 (where n is the number of links) was derived by use of the spatial-operator algebra discussed in a previous article in *NASA Tech Briefs*. New operator factorizations of the mass matrix and expressions for its inverse were obtained. Building on the foregoing, a recursive forward-dynamics algorithm that requires a number of arithmetic operations approximately proportional to n was derived.

Despite the additional complexity of the dynamical models of the geared manipulator, the mass-matrix and forward-dynamics algorithms for geared manipulators closely resemble the corresponding algorithms for direct-drive manipulators and require a relatively small amount of additional computation. Consequently, present direct-drive algorithms can be extended easily to gear-drive cases.

This work was done by Abhinandan Jain and Guillermo Rodriguez of Caltech for **NASA's Jet Propulsion Laboratory**. *For further information, Circle 9 on the TSP Request Card.* NPO-18230

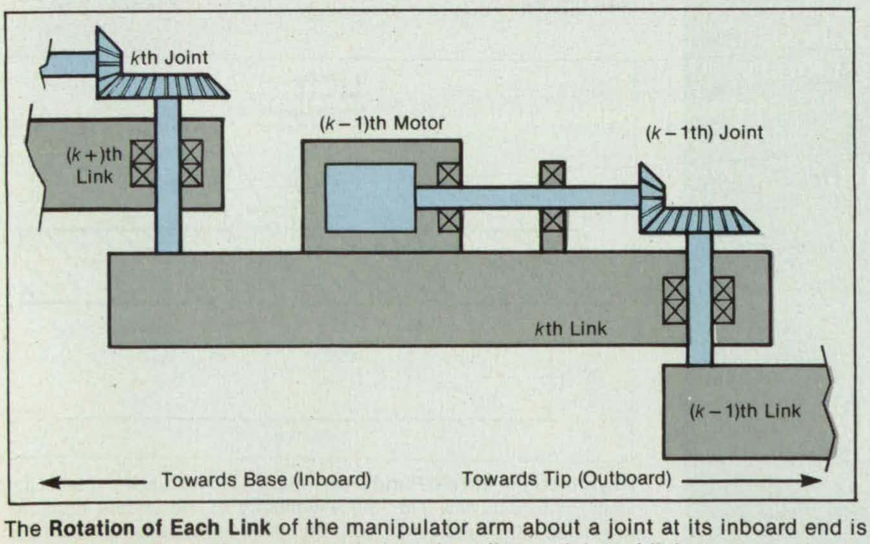

The **Rotation of Each Link** of the manipulator arm about a joint at its inboard end is driven by a motor and gears mounted on the adjacent inboard link.

Fabrication Technology

Hardware, Techniques, and Processes

Determining Asymmetry of a Weld Puddle

The shape of the puddle would be inferred from the surface-temperature distribution.

Marshall Space Flight Center, Alabama

A proposed sensing-and-data-processing subsystem would provide information on the asymmetry of a weld puddle with respect to the original (prior to welding) midplane of a butt joint. The subsystem is needed because the subsurface portion of the weld puddle is invisible, and asymmetry often leads to lack-of-fusion defects, in which the abutting faces to be joined are not fully consumed by the moving puddle. The subsystem would be part of a welding-control system, enabling the system to correct for such asymmetry.

Asymmetry of a weld puddle is caused by differences between the flows of heat away from the puddle on the two sides of the joint. These differences can be caused by differences between the compositions, sizes, shapes, and/or thicknesses of the two pieces to be joined, and/or by large heat sinks close to the weld. The side of the puddle from which more heat flows to the adjacent metal slopes less steeply; that is, the bottom of the puddle is displaced more toward the other side (ses figure).

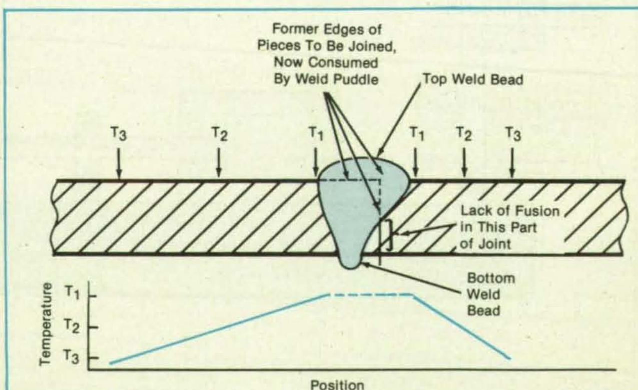

Asymmetry in a Weld Puddle can result in lack of fusion in part of the weld joint. One can infer the asymmetry of the puddle from the asymmetrical distribution of temperature on the surfaces of the pieces to be joined.

Although the flow of heat within the workpieces and the consequent shape of the puddle cannot be observed directly, they can be inferred approximately from the distribution of temperature on the surfaces of the pieces to be joined. Accordingly, the proposed subsystem would include an infrared camera aimed at the weld and the surrounding area. Temperatures and gradients of temperature would be computed from the infrared imagery and fed as input along with other relevant data to a mathematical model of the weld pool that takes account of thermal conduction and possibly such other effects as convection and surface tension.

Mathematical models of various degrees of sophistication that have already been developed for welding-control systems are capable of predicting the cross-sectional shape of the weld; a suitable model would have to be modified to accept the infrared-image data as input. The minimal outputs required of the model for the purpose of control would be the cross-sectional shape and the width and position of the bottom weld bead.

This work was done by David A. Gutow of Rockwell International Corp. for **Marshall Space Flight Center**. *For further information, Circle 51 on the TSP Request Card.*
MFS-29785

Preelectroplating Treatment of Titanium Honeycomb Core

A new technique eliminates excess copper filler.

Langley Research Center, Hampton, Virginia

It is necessary to develop new materials that have improved specific properties at high temperatures and to use highly efficient structural concepts to meet the stringent structural-weight requirements of the National Aerospace Plane. The titanium aluminide (Ti_xAl) composites are among the materials that offer improved properties. The honeycomb-core sandwich offers high structural efficiency. As a result, a study was initiated at NASA Langley Research Center to develop joining and fabrication processes to facilitate the efficient incorporation of Ti_xAl into lightweight, high-temperature honeycomb sandwich structures.

The enhanced-diffusion-bonding (EDB) process using electroplated copper as filler material has been demonstrated to produce joints in Ti/14Al/21Nb alloy that have load-carrying capability at elevated temperatures. However, prior plating techniques for applying the copper exhibited several deficiencies, including lack of precise repeatability and the deposition of excess copper on and in the honeycomb structure. This led to the development of a process in which a maskant on the honeycomb core permits the electroplating of a controlled amount of filler metal on the edge of the honeycomb core only.

The new technique is used to treat titanium honeycomb core electrochemically by applying a conversion coat to keep the honeycomb active and receptive to electroplating with a solution of sodium bichromate and hydrofluoric acid. The solution is used at room temperature on reverse current (dc) with 300-series stainless steel screen or graphite cathodes. The new technique incorporates an improvement over an older technique that involves the use of these chemicals; in the older technique excessive copper is applied because a lacquer maskant used to prevent selectively the deposition of copper peels off in the etching solution.

In a test of the new technique, the concentration of the sodium bichromate was decreased from 290 to 252 g/L, the concentration of the hydrofluoric acid was increased from 55 to 56 mL/L, and the processing temperature was decreased from the range of 180 to 212 °F (82 to 100 °C) to room temperature. By applying reverse current at 6 V with stainless-steel screen or graphite as cathodes at room temperature, it was possible to accomplish the application of lacquer maskant, treatment, and electroplating within 1 h. Also, with the addition of the reverse current, alkaline copper, nickel/cobalt, and silver preplates could be used along with the acid copper, nickel, and nickel/tungsten.

As a result of applying the filler metal only where it is needed, less than 5 percent of the face-sheet area is affected by the metallurgical reactions associated with bonding. With this treatment, the EDB process has been used to fabricate sandwich panels of Ti/14Al/21Nb face sheet and Ti/3Al/2.5V honeycomb core for coupon and structural-element tests at room and high temperatures. Panels as light as 0.5 lb/ft^2 (2.4 kg/m^2) have been fabricated.

This work was done by Michael L. Kelly and James S. Harvey of **Langley Research Center**. *For further information, Circle 144 on the TSP Request Card.*
LAR-14256

Fastener for Hot, Oxidizing Environments

It can be assembled and disassembled quickly from the outside.

Lyndon B. Johnson Space Center, Houston, Texas

A threaded fastener is designed for service at extremely high temperatures in oxidizing atmospheres. The fastener consists of four parts (see figure). The body—a head with a tapering shank—is made of a high-temperature-resistant composite material and has a ceramic coat to protect it from oxidation. A collar, composed of two halves with continuous external threads, is made of a strong refractory metal alloy. The two halves are fitted onto the shank and secured to the shank by a lockring.

The fastener is inserted in a hole in the panel to be fastened until the conical surface of the head makes contact with a similar conical surface countersunk in the hole. The threaded halves are then secured on the shank. A screwdriver, spanner wrench, or other suitable tool is inserted in a slot or slots in the head to turn the fastener in a threaded receptacle behind the panel. When the fastener is fully tightened, the top of its head is flush with the surface of the panel.

Note that the cross section of the shank is not circular but square. This geometry enables the body to grip and turn the threaded collar instead of merely sliding within it.

The ceramic coat that gives the body of the fastener its resistance to oxidation is brittle; if subjected to tension or shear, it would crack and the fastener would quickly oxidize and fail. The taper on the shank transforms the shear and tension from the threads in the collar into a combination of radial compression and axial tension in the shank (which the shank can withstand readily). In turn, the conical taper in the head assures that the ceramic coat is stressed mainly in compression, which it can withstand readily.

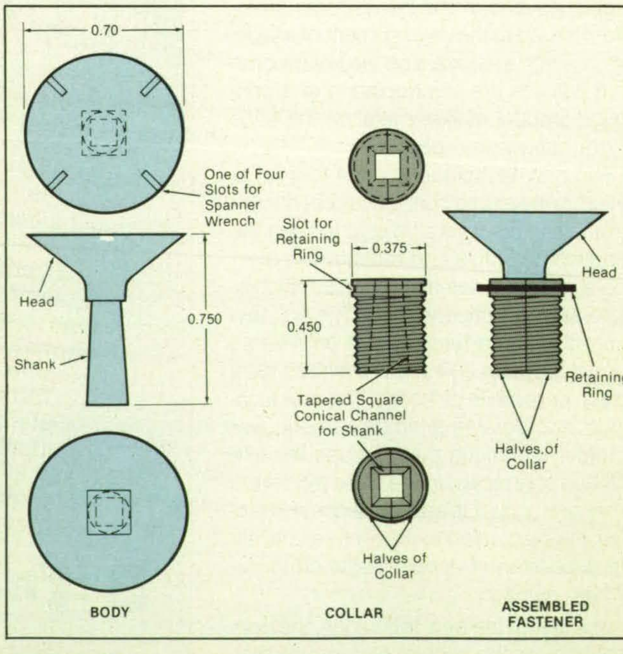

Threaded Halves of the metallic collar fit around the tapered shank of the body of the fastener. A retaining ring holds the collar on the body. Dimensions are in inches.

This work was done by Thomas J. Dunn of **Johnson Space Center**. *For further information, Circle 5 on the TSP Request Card.*

This invention is owned by NASA, and a patent application has been filed. Inquiries concerning nonexclusive or exclusive license for its commercial development should be addressed to the Patent Counsel, Johnson Space Center [see page 18]. Refer to MSC-21580.

Stiffened Carbon/Carbon Compression Panels

Panels with integral stiffeners were made with woven fabric in two-dimensional, cross-ply layups.

Langley Research Center, Hampton, Virginia

Carbon/carbon composite materials are being considered for structural applications in which their light weights and their strengths at high temperatures are attractive. Potential high-temperature structural applications on advanced aircraft and spacecraft include leading edges, fairings, and control surfaces. Understanding how to design and fabricate subcomponent panels that can support either tensile or compressive loads is basic for the use of carbon/carbon materials for lightweight structural components. Therefore, an experimental and analytical program was conducted to develop the technology required to design, fabricate, and predict the performances of stiffened carbon/carbon compression panels.

The design study resulted in designs for lightweight compression panels. A single-panel design was selected, and both coated and uncoated carbon/carbon test specimens were fabricated, tested, and analyzed. Fabrication procedures were developed and demonstrated by the construction of blade-stiffened carbon/carbon compression panels containing woven fabric in a two-dimensional, cross-ply layup (see figure).

Compression buckling and failure tests were conducted on three uncoated single-stiffener specimens, four uncoated blade-stiffened panels, and one coated blade-stiffened panel. Some test specimens incorporated stitching to reinforce the attachment of the stiffeners to the panel skins. Each test configuration was analyzed, and the results of the analysis were compared with the results of the experiments.

The results of these fabrication trials and experiments showed that carbon/carbon compression panels with integral stiffeners can be successfully fabricated by use of woven fabric in a two-dimensional, cross-ply layup configuration. The results of the experiments on both coated and uncoated panels showed that local skin buckling did not cause collapse of the panels and that ultimate failure occurred at loads 10 to 20 percent above the buckling loads.

The results showed further that for carbon/carbon panels subjected to in-plane loading, separation of the stiffeners from the panel skins was not a problem. Thus, stitching along the base of a stiffener to strengthen the attachment to the skin of a panel is not necessary and does not produce a significant improvement in the buckling strength or ultimate failure strength of the panel. Comparisons between the experimental and analytical results for the configurations investigated showed that conventional finite-element analysis procedures adequately predict the onset of skin buckling in both coated and uncoated blade-stiffened compression panels.

This work was done by James W. Sawyer of **Langley Research Center**. *No further documentation is available.*
LAR-14367

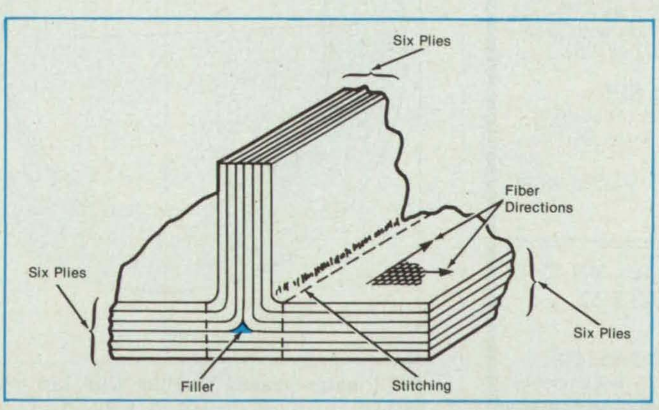

Stiffened Panel specimens were made in this layup configuration. Some included stitching.

Leak Stopper for Metal-to-Metal Tube Fittings

A plastic-coated steel device is both conformal and strong.

Lyndon B. Johnson Space Center, Houston, Texas

A washerlike seal stops leakage at Dynatube™ joints between metal tubes. The seal is made of materials that resist attack by corrosive and oxidizing fluids. In addition, the seal aligns itself in the joint for maximum effectiveness.

The seal is a thin stainless-steel washer that includes an inner lip and that is partly coated with polytetrafluoroethylene (see figure). The inside diameter of the washer is about the same as that of the Dynatube fitting, and there is a slight interference fit between the lip and the inner diameter of the Dynatube fitting. The seal is therefore press-fit or snapped in place in fitting and stays there, regardless of the orientation of the fitting.

The polytetrafluoroethylene coat adheres well to the surface of the stainless-steel core. The core provides strength, while the polytetrafluoroethylene coat provides the soft material to flow into scratches on the fitting and forms the seal. Seals for 1/2-in. (12.7-mm) fittings have been fabricated. Seals for 1/4-in. (6.35-mm), 5/8-in. (15.88-mm), and 3/4-in. (19.05-mm) fittings have been designed. The stainless-steel core is nominally 0.005 in. (0.127 mm) thick. Polytetrafluoroethylene coats 0.002 in. (0.05 mm) and 0.005 in. (0.13 mm) thick have been manufactured and tested. Other thicknesses of polytetrafluoroethylene may be used, depending on the size of the leak in the fitting. The lip is offset 0.020 in. (0.51 mm).

This work was done by Joseph R. Trevathan of **Johnson Space Center**. *For further information, Circle 110 on the TSP Request Card. MSC-21800*

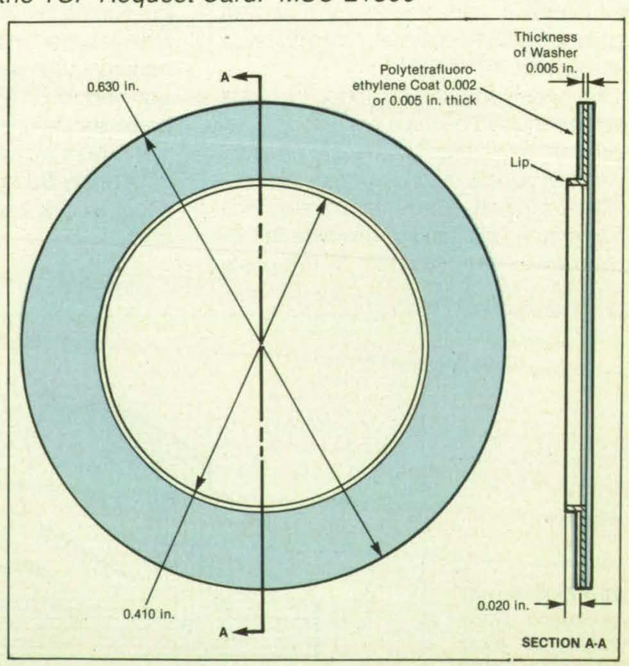

The **Plastic-Coated Washer With Lip** fits securely in a leaky fitting. Typical dimensions for a 0.5-in. (13-mm) seal are shown.

Easy Attachment of Panels to a Truss

Panels would be guided into precise position and locked in easily.

Langley Research Center, Hampton, Virginia

A conceptual antenna dish, solar collector, or similar lightweight structure would consist of hexagonal panels supported by a truss. The truss would be erected in the field, and the panels would be attached to the truss by specially designed quick-capture and locking mechanisms (see Figure 1) that would be easy to operate.

The workers would first build only enough of the truss structure to support a single panel. They would attach the first panel to the truss, then add just enough truss structure to support a second panel adjacent to the first. Then they would attach the second panel, build more of the truss, and so forth (see Figure 2). By constructing the truss in increments, they would maintain access to the panel-attachment nodes on the truss; that is, the attachment nodes would not be obstructed by the supporting structure.

The workers would carry a panel to the truss so that it would approach at a tilt of 5° to 15° from its final intended orientation. They would attach the panel to the truss at the two outermost attachment nodes more or less simultaneously, then rotate the panel about the axis between these two nodes so that the panel would become connected to the structure at the remaining node.

Each attachment node on the panel would include recesses that would mate with studs on the truss, as shown in Figure 2 and described more fully in the following article, "Probe and Drogue for Quick Attachment and Detachment" (LAR-14479). The recesses would be shaped to guide the studs to final nesting positions; the workers would need only to align the truss and panel nodes coarsely.

Initially, capturing studs at each node on the truss would be made to protrude slightly from the surrounding truss structure to make attachment easy. Once three adjacent panel nodes had been attached to the three capturing studs at a truss node, the workers would retract the capturing studs with the help of an interior worm gear, drawing the three panels inward and spring-loading them onto mounting studs on flexible posts.

The edges of each panel would be undercut by a 30° chamfer. This would pre-

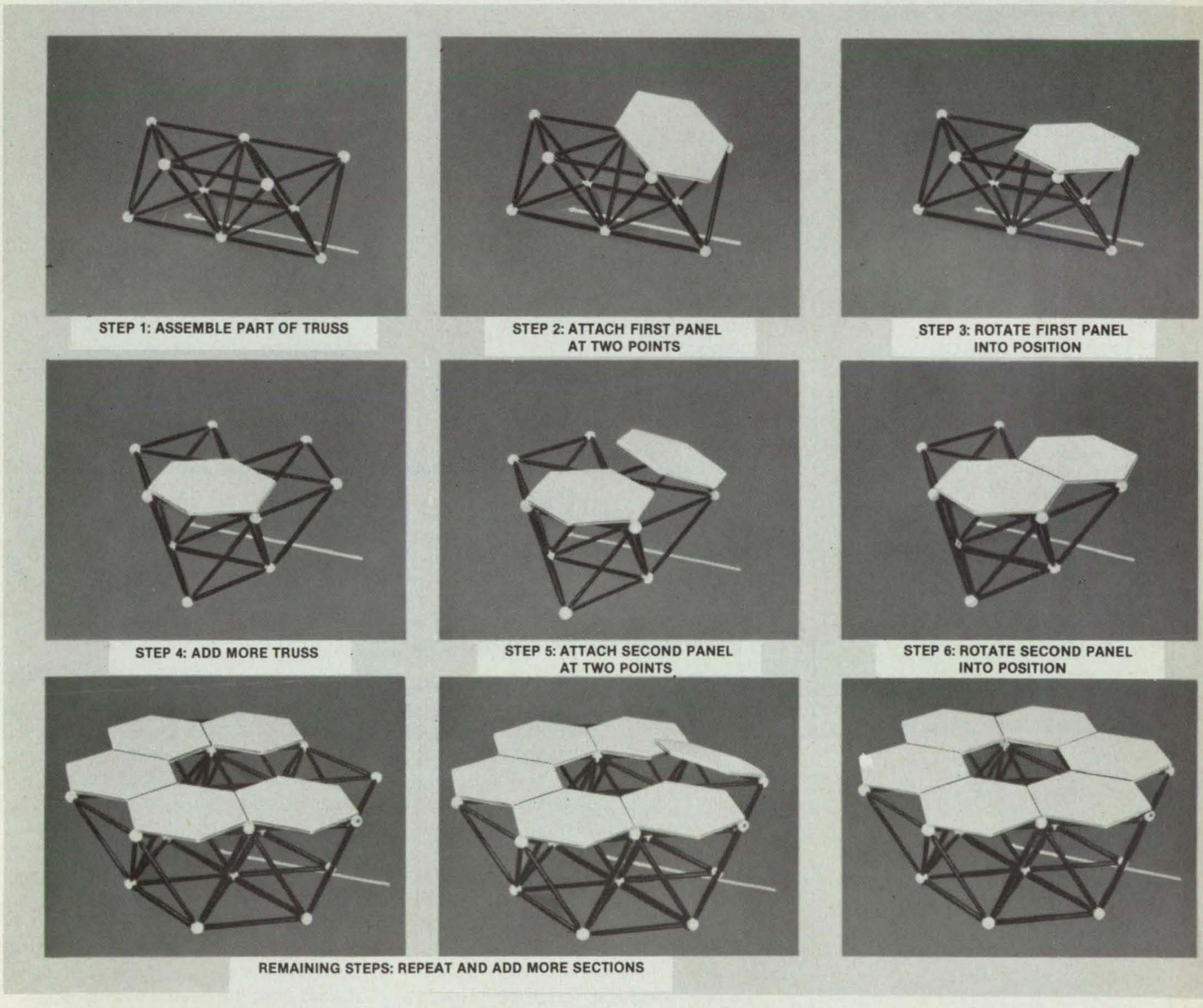

Figure 1. The **Truss Would Be Built in Increments** along with attachment of panels. Each panel would be brought toward the truss at an angle and attached to two nodes on the truss. Then the panel would be rotated into attachment at a third node.

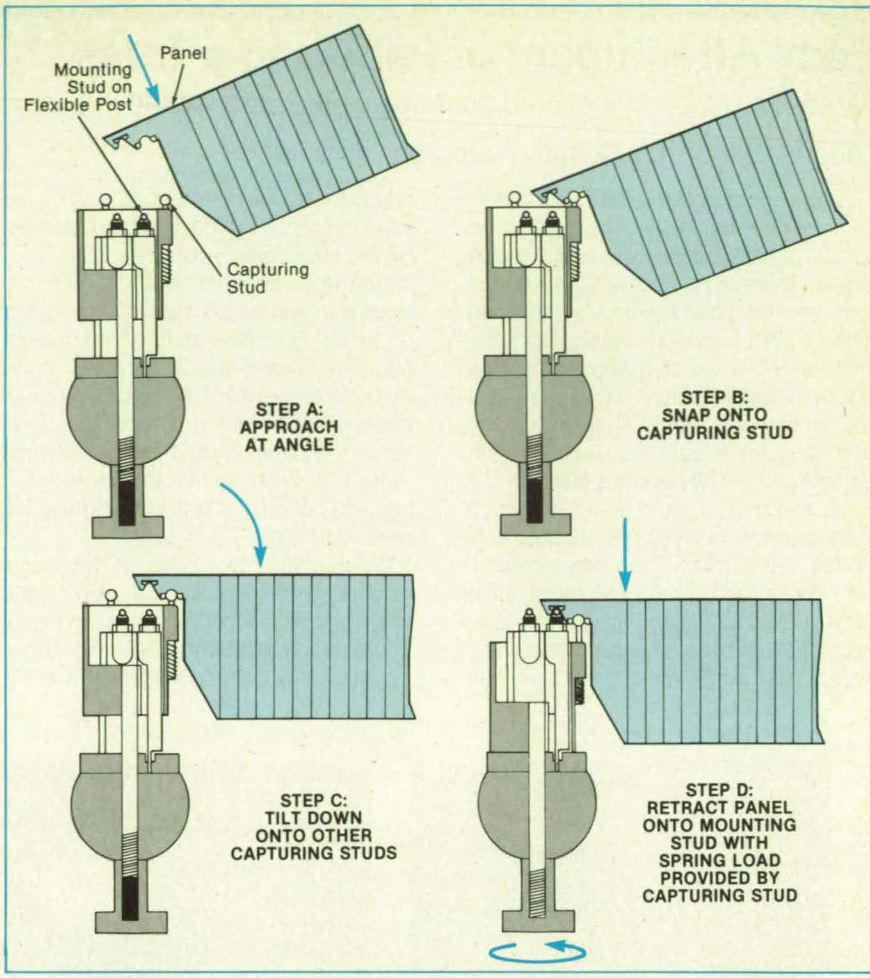

Figure 2. The **Attachment of a Panel to a Truss Node** would involve this sequence of simple motions.

vent mutual interference by the edges of two adjacent panels when one or both of them were tilted.

This work was done by Mark Thomson and Mark Gralewski of Astro Aerospace Corp. for **Langley Research Center**. *For further information, Circle 45 on the TSP Request Card.*

Inquiries concerning rights for the commercial use of this invention should be addressed to the Patent Counsel, Langley Research Center [see page 18]. Refer to LAR-14478.

Probe and Drogue for Quick Attachment and Detachment

A capturing stud locks positively and accepts misalignment.

Langley Research Center, Hampton, Virginia

A prototype probe-and-drogue attachment mechanism connects and disconnects parts quickly and locks them together positively. It accommodates a large alignment error when the parts are brought together. The probe portion of the mechanism is intended to be the capturing stud, and the drogue is the mating recess in a panel to be captured, as described in the preceding article, "Easy Attachment of Panels to a Truss" (LAR-14478).

The probelike stud (see figure) mates with a similarly, approximately conically shaped receptacle. The probe includes a beveled piston that is held away from the small end of the outer shell by a spring. The bevel on the piston transforms the spring load into an outward bias on a set of detent locking balls. When the probe is pushed into the drogue, the protruding parts of the balls snap into detent seats in the drogue. Thereafter, any attempt to pull the probe out of the drogue acts, via the bevel on the piston, to wedge the balls into the seats even more firmly: the probe cannot then be removed from the drogue unless a cable is pulled to compress the spring and draw the piston away from the balls, thereby releasing the balls radially inward from the seats in the drogue.

It is not necessary to pull the cable when inserting the probe in the drogue because insertion compresses the piston spring and loosens the balls so that they can slide into the seats in the drogue. The probe can be inserted into the drogue at any angle within a 30° cone; a spherical bearing in the piston accommodates angular misalignments within this cone. The approximately conical shapes of the probe and drogue help to correct initial lateral misalignments as well as angular ones.

This work was done by Mark Thomson, Mark Gralewski, and Grant Young of Astro Aerospace Corp. for **Langley Research Center**. *For further information, Circle 20 on the TSP Request Card.*

Inquiries concerning rights for the commercial use of this invention should be addressed to the Patent Counsel, Langley Research Center [see page 18]. Refer to LAR-14479.

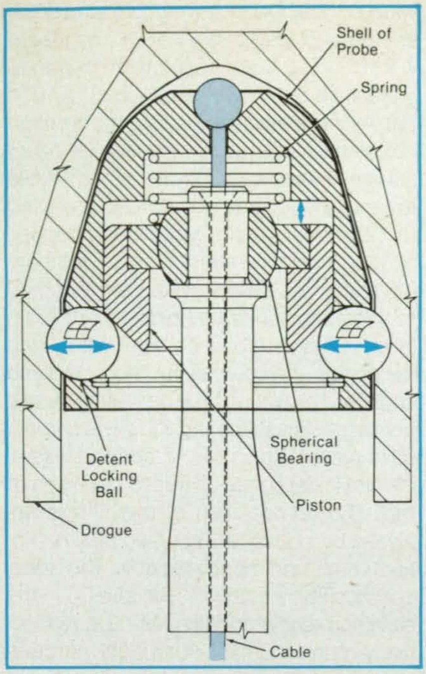

The **Probe Nests** in a similarly contoured drogue. Three balls at the wide end of the probe engage seats in the drogue. The cable is used to release the probe from the drogue.

Laboratory Produces $YBa_2Cu_3O_{7-x}$ Superconductive Films

A vacuum deposition system was modified at relatively low cost.

Goddard Space Flight Center, Greenbelt, Maryland

NASA's Goddard Space Flight Center has assembled laboratory equipment to produce superconducting thin films of $YBa_2Cu_3O_{7-x}$ in sufficient quantities for the development of new detector devices. The principal apparatus is a vacuum evaporative-deposition system that was modified to obtain the desired results without incurring the cost of a completely new system.

The vacuum chamber of the unmodified deposition system contained a single electron-beam evaporation source. The modification included the installation of two additional electrical-resistance-heated sources. In preparation for deposition, the

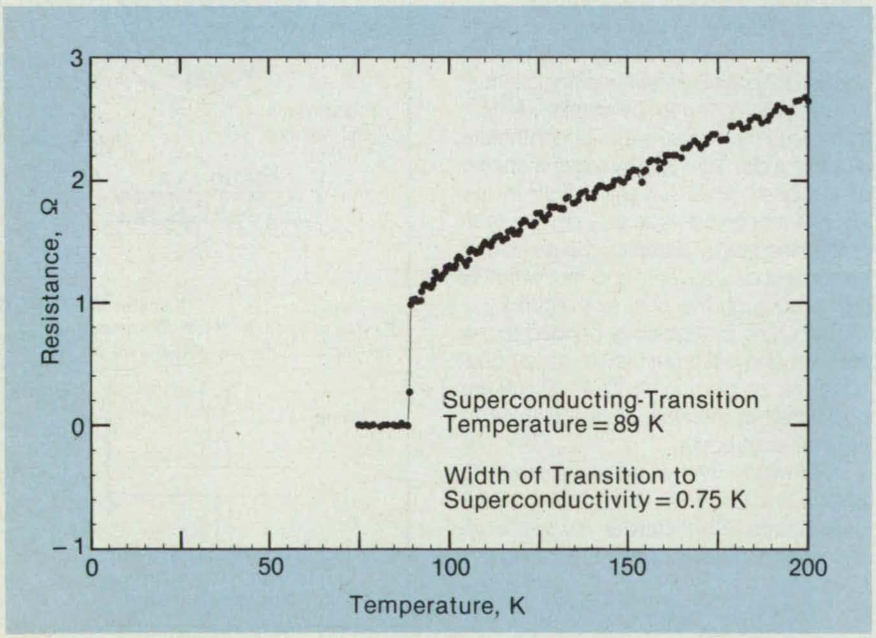

The **Electrical Resistance** of a thin film of barium copper oxide deposited on a lanthanum aluminate substrate in the deposition system was measured as a function of temperature.

vacuum chamber is first cryopumped down to a base pressure of 5×10^{-7} torr (about 7×10^{-5} Pa), then refilled with oxygen to a pressure of 5×10^{-6} torr (about 7×10^{-4} Pa). All three evaporation sources are then operated simultaneously: the electron-beam source is used to evaporate yttrium, while the electrically heated sources are used to evaporate barium fluoride and copper.

The deposition substrates are lanthanum aluminate wafers, which are attached to a rotating substrate holder about 10 in. (about 25 cm) above the sources. During deposition, the sources are monitored and controlled by use of three oscillating-quartz-crystal thickness monitors that are shrouded to prevent crosstalk. An additional sample film is deposited on silicon during each run. The composition of this film is analyzed by inductively coupled plasma optical emission spectroscopy. The ideal composition includes Y, Ba, and Cu in the stoichiometric proportions of 1:2:3, respectively, corresponding to weight percentages of 16.0, 49.6, and 34.4, respectively.

After deposition, the films are annealed in flowing oxygen in a tube furnace to turn them into superconducting oxides. Initially, the furnace is heated from room temperature to 500 °C, at which point water vapor is introduced into the flowing oxygen to remove fluorine (that originated in the barium fluoride source) from the deposited films. The heating continues until the temperature reaches 900 °C. This temperature is maintained 30 minutes, and then the furnace is allowed to cool to room temperature. The flow of water vapor is turned off during the cooling process.

The resistivities of the completed films are determined by use of the four-wire resistance-measuring technique. Films produced in this system have exhibited zero electrical resistance at temperatures as high as 89 K, with transitions to superconductivity narrower than 1 K (see figure). Films thus produced are being processed to make sensing elements of infrared-transition-edge bolometers and superconducting-quantum-interference-device (SQUID) junctions for SQUID magnetometer sensors.

This work was done by Christine A. Allen and Michael J. Viens of **Goddard Space Flight Center**. *No further documentation is available.*
GSC-13440

"Easy-on, Easy-off" Blanket Fastener

A disk and post fit snugly and release quickly.

Goddard Space Flight Center, Greenbelt, Maryland

A set of simple fasteners hold a flexible blanket of protective padding or thermal insulation on a set of posts on a supporting structure. The fasteners can be detached quickly and easily by pulling them away from the posts. The fasteners can be reused several times. No tools are needed for installation or removal.

Each fastener consists of a disk of silicone rubber cast on a disk of Mylar (or equivalent) polyethylene terephthalate that, in turn, is fastened to the blanket. A central hole in the polyethylene terephthalate disk has a diameter slightly larger than that of the post, while a central hole in the silicone-rubber disk is slightly smaller than that of the post. Therefore, the disks can be press-fit over the post and nest securely in a groove on the post (see figure).

Each disk is adhesively bonded to the blanket, and each post is similarly bonded to the supporting structure. Disks are positioned at intervals on the blanket to register with posts.

This work was done by Ronald E. Kolecki and Carroll H. Clatterbuck of **Goddard Space Flight Center**. *For further information, Circle 143 on the TSP Request Card.*
GSC-13373

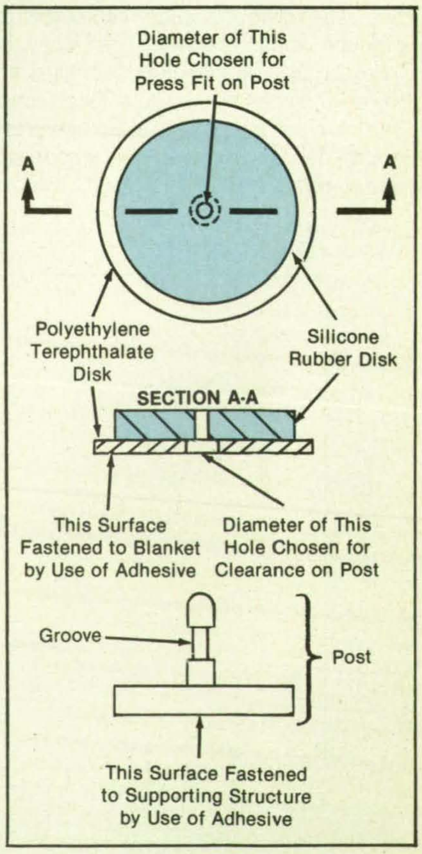

The **Silicone-Rubber Disk and Post** join securely but can be easily separated by pulling along the axis of the post.

Mathematics and Information Sciences

Robust Method for Robotic Mapping

A robot constructs a map from its experience.

Lyndon B. Johnson Space Center, Houston, Texas

A robust qualitative method enables a robot to explore an unknown environment and construct a map. The new method was inspired by the study of the cognitive maps used by humans. In contrast with traditional methods in which the environment is described mainly by metrical information, the new method incorporates procedural knowledge for movement and a topological model of the environment in addition to the metrical information. Potential applications include robotic sentries for warehouses, robotic delivery trucks for factory floors, robotic floor cleaners, robotic lawnmowers, and the like.

The topological model consists of nodes and arcs corresponding to *distinctive places* and *local travel edges* linking nearby distinctive places (see figure). An accurate topological model is created by linking places and edges, and enables the accumulation of metrical information with reduced vulnerability to metrical errors. A *distinctive place* is defined as the local maximum of some measure of distinctiveness (e.g., height) appropriate to its immediate neighborhood, and is found by a *hill-climbing search*. Local travel edges are defined in terms of *local control strategies* required for travel. The knowledge of how to find distinctive places and follow edges is the *procedural knowledge,* which the robot learns dynamically during exploration and which guides the robot during the navigation.

The use of the topological description of the environment intermediate between the sensorimotor interaction with the world and a metrically accurate model constitutes a major innovation. The topological description confers the following advantages:

- Because it includes discrete places and edges, travel from one topologically defined place to another does not suffer from cumulative metrical errors.
- A topological model can support a class of effective strategies for traveling from one place to another even without a metrical model of the environment. This decouples the critical short-term need for effective travel strategies from the longer-term process of analyzing metrical observa-

tions to produce a metrical model of the environment.

The use of zero-dimensional ("hill-climbing") and one-dimensional ("path-following") control strategies to define the places and edges that make up the discrete topological model of the continuous environment constitutes a second major innovation. Within a given neighborhood, the robot uses locally observable features to select a control strategy that will enable it to "hill-climb" to a maximally distinctive place within that local neighborhood. Upon return to that neighborhood, the hill-climbing control strategy will enable it to return to the distinctive place, thus eliminating any cumulative error. When moving away from a distinctive place, the robot selects a path-following control strategy that will enable it to follow a topological edge (e.g., the midline of a corridor, or near the wall of a larger space) until reaching the neighborhood of another distinctive place.

The use of control strategies makes it possible to eliminate random error and unpredictable environmental detail, and to enable the robot to treat a continuous error-prone world in terms of a discrete, error-free, topological description. There is a large repertoire of control strategies suitable for different types of environments or sensorimotor interactions. The method is not restricted to the use of any particular control strategy, but applies generally to the architecture that selects a suitable control strategy for the specific robot and environment, and uses the strategy to build the topological description.

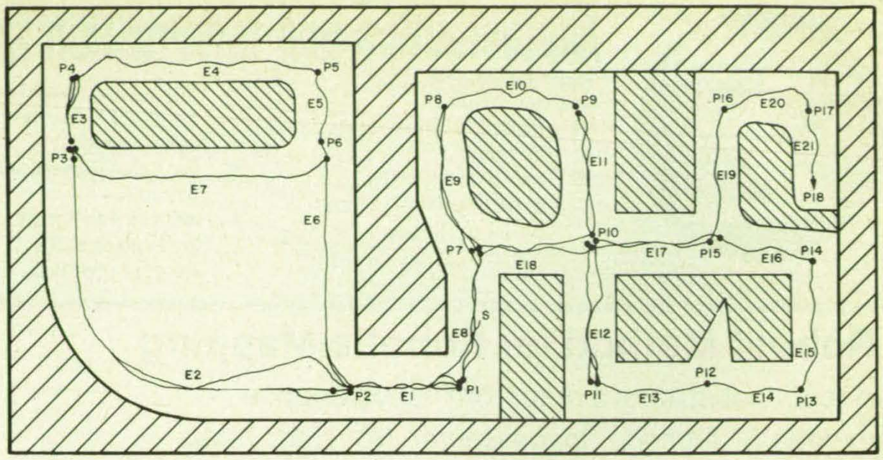

This **Exploration Trace** summarizes the results of a simulation of the exploration of a two-dimensional (room-and-corridor) environment by a robot equipped with range sensors. The numbered points denoted by "P" and the numbered curved lines denoted by "E" represent distinctive places and local travel edges, respectively.

The topological description serves as a substrate for more sophisticated and detailed models of the environment. The metrical model can be accumulated and refined by standard data-analysis techniques, because the short-term travel needs of the robot are not critically dependent on a possibly inaccurate metrical model. The assumption that the robot is the only changing element of an otherwise constant environment can be relaxed to include such things as doors that may be open or closed, or people who walk quickly through a space while it is being explored. The method allows for study and improvement of the handling of such systematic errors as sensor failure, the acoustic peculiarities of sonar rangefinders, or differing reflective properties of wall surfaces.

This work was done by Benjamin J. Kuipers and Yung-Tai Byun of the University of Texas at Austin for **Johnson Space Center**. *For further information, Circle 107 on the TSP Request Card.* *MSC-21468*

Fast Transform Decoding of Nonsystematic Reed-Solomon Codes

Decoding is speeded by making certain computations unnecessary.

NASA's Jet Propulsion Laboratory, Pasadena, California

An algorithm that decodes nonsystematic Reed-Solomon codes is simpler and faster than some prior algorithms developed for this purpose have been. The algorithm is particularly suitable for implementation in very-large-scale integrated circuits. This is an important development because Reed-Solomon codes are error-detecting and error-correcting codes that are used in deep-space communications, military communications, and compact-disk recording.

The derivation of the algorithm begins with the observation that the Reed-Solomon codes constitute a subclass of redundant residue polynomial codes. It has been shown previously that a redundant residue polynomial code can be decoded by use of the Chinese remainder theorem together with the Euclidean algorithm, without having to solve the error-locator and error-evaluator polynomials. The reconstruction of the corrupted (by errors and/or erasures) information polynomial $F'(x)$ from the received symbols is an essential intermediate step of the decoding process, the objective of which is to reconstruct the uncorrupted information polynomial $F(x)$. The disadvantage of the prior algorithm for decoding a redundant residue polynomial code is that, for a code word of length n, the reconstruction of $F'(x)$ involves n polynomial multiplications followed by the operation modulo $M(x)$, where $M(x)$ is a product of n polynomials. These operations require much computation and thereby decrease the speed of decoding.

In the present algorithm, a fast, efficient Fermat number transform is used to compute $F'(x)$ in a manner analogous to that of computation of the syndrome in a conventional decoding scheme. The Fermat number transform eliminates the polynomial multiplications and reduces the number of other multiplications in the reconstruction of $F'(x)$ to $n \log(n)$. Next, the Euclidean algorithm is used to evaluate $F(x)$ directly, without going through the intermediate steps of solving the error-locator and error-evaluator polynomials.

The algorithm (see figure) can be summarized as follows:

1. Compute the inverse Fermat number transform of the received code word to obtain $F'(x)$.
2. If the degree of $F'(x) < k$ (where k = the number of information symbols), then $F(x) = F'(x)$; otherwise, go to the next step.
3. Compute the erasure-locator polynomial, $D_1(x)$. If the degree of $F'(x)D_1(x) \leq$ the degree of $M(x)$, then set $p_{-1}(x) = 0$, $p_0(x) = 1$, $r_{-1}(x) = M(x)$, and $r_0(x) = F'(x)D_1(x)$; otherwise, set $p_{-1}(x) = 1$, $p_0(x) = 0$, $r_{-1}(x) = F'(x)D_1(x)$, and $r_0(x) = M(x)$.
4. To determine the error-locator polynomial $D_2(x)$ and $F'(x)D(x)$ (where $D(x) = D_1(x)D_2(x)$), apply the Euclidean algorithm to $M(x)$ and $F'(x)D_1(x)$. The initial values of the Euclidean are defined in step 3. The iterative procedure of the Euclidean algorithm terminates at the

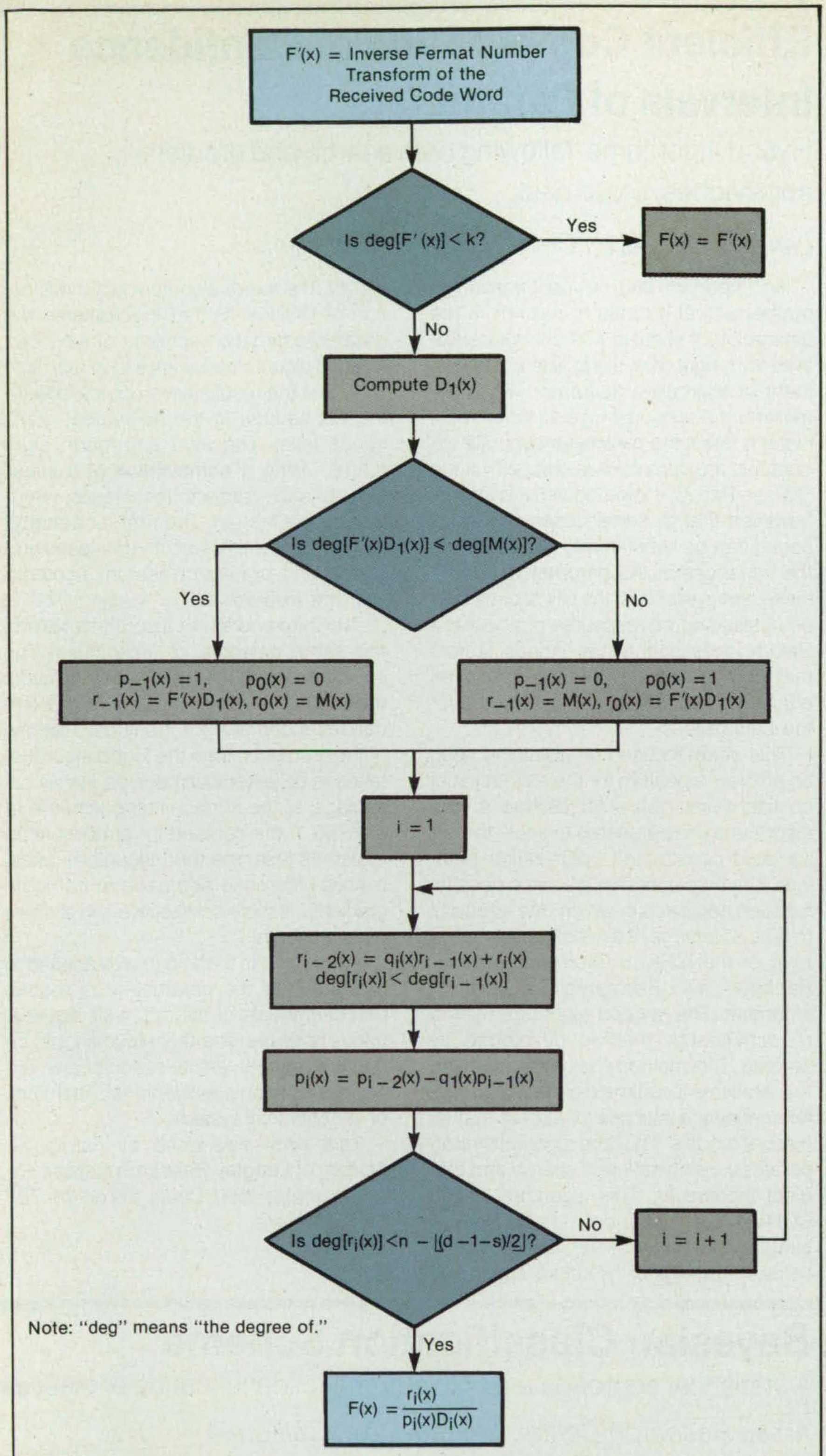

The **Fast Transform Decoding Algorithm** reconstructs the information polynomial $F(x)$, provided that the numbers of errors and erasures do not exceed the correcting capacities of the code.

value of i for which the degree of $r_i(x) < n - \lfloor(d-1-s)/2\rfloor$ (where $\lfloor x \rfloor$ denotes the greatest integer $\leq x$).

5. Compute $F(x) = r_i(x)/p_i(x)D_1(x)$ for the i, $r_i(x)$, and $p_i(x)$ reached at the end of the iterative procedure in step 4, where $p_i(x)$ is defined in the figure.

This work was done by Trieu-Kie Truong and Kar-Ming Cheung of Caltech, A. Shiozaki of Osaka Electro-Communication University, and Irving S. Reed of the University of Southern California for **NASA's Jet Propulsion Laboratory**. *For further information, Circle 126 on the TSP Request Card.*

NPO-18039

Efficient Computation of Confidence Intervals of Parameters

Hybrid algorithms, following both search and gradient approaches, prove best.

Langley Research Center, Hampton, Virginia

An important step in identification of mathematical models of aircraft is the estimation of stability and control derivatives from flight data, along with an assessment of estimation accuracy. When the maximum-likelihood (ML) estimation technique is used, the parameter-estimate accuracies are commonly assessed via the Cramer–Rao (CR) lower bound. It is known, however, that in some cases the lower bound can be substantially different from the variances of the parameters. Under these circumstances, the CR bounds may be misleading as measures of accuracy. Before investigating the various factors that contribute to estimation errors, an efficient algorithm should be selected for the calculations.

This study focused on obtaining such an efficient algorithm for the estimation of confidence intervals of ML estimates. Four algorithms were selected to solve the associated constrained optimization problem. The first algorithm follows a penalty-function approach in which one attempts to take advantage of a subalgorithm in the form of the MNRES (Modified Newton–Raphson with Estimated Sensitivities) algorithm. The second algorithm uses a random-search method developed by Mereau. This method has been one of the few available to estimate general parameter confidence intervals for aircraft mathematical models. The third algorithm incorporates a combination of search and gradient techniques. This algorithm, called CONMINS, is commonly used at NASA Langley Research Center as part of the software package of the central computing facility. The fourth algorithm is a modification of CONMINS that incorporates the gradient-estimation scheme of MNRES.

Each algorithm was applied to real flight data, and the results were compared with the CR bounds at the 95-percent confidence level. The third and fourth algorithms, using a combination of a linear search and gradient techniques, were clearly the fastest. The first, or penalty-function, algorithm was third in speed and the second, or random-search, algorithm was the slowest.

The third and fourth algorithms fall into the same category of techniques. The choice between the two algorithms favors the fourth algorithm. If a particular problem causes a demand for many calculations of the gradients, then the fourth algorithm tends to be faster inasmuch as it takes advantage of the surface-fitting scheme of MNRES. If the demand for gradient information is less, the third algorithm, using a finite-difference approach to compute gradients, is more competitive and at times possibly faster.

Although this technique was applied to estimation of the parameters of mathematical models of aircraft, wide application is possible. The technique should be applicable in the identification of any fairly large and complex electrical, chemical, or mechanical system.

This work was done by Patrick C. Murphy of **Langley Research Center**. *For further information, Circle 139 on the TSP Request Card.*
LAR-14341

Bayesian Classification Scheme

A statistical approach leads to automatic identification of classes.

Ames Research Center, Moffett Field, California

A scheme derived via a statistical approach automatically identifies classes in a set of data. The scheme is applicable to real-valued, discrete (e.g., binary or normal) or continuous (real-valued) data presented in the form of parameter vectors that represent the attributes of objects. It determines the most probable number of classes, the probabilistic descriptions of the classes, and the probability that each object is a member of each class. It incorporates partial prior knowledge of some classes that may be present, striking a balance between the tendency to put each datum in a class by itself and the tendency to put all data in the same class.

The scheme is based on the theory of finite mixtures, in which each datum in a set of I data is assumed to be drawn from one of J classes. The jth class, C_j, is described by a class distribution function, $p(x_i \mid x_i \in C_j, \theta_j)$, which gives the probability distribution of the parameters of a datum (components of a vector) that belongs to that class. The jth class distribution is described by a class parameter vector, θ_j.

For a single-attribute normal distribution, θ_j consists of the class mean, μ_j, and variance, σ_j^2.

The probability of an object being drawn from class j is called the class probability π_j. Thus, the probability of a given datum coming from a set of classes is the sum of the probabilities that it came from each class separately, weighted by the class probabilities.

$$p(x_i|\boldsymbol{\theta},\boldsymbol{\pi},J) = \sum_{j=1}^{J} \pi_j\, p(x_i|x_i \in C_j,\theta_j) \qquad \text{(a)}$$

Provided that the data are unordered and independent of each other, the likelihood of measuring an entire data base is the product of the probabilities of measuring each datum.

$$p(\mathbf{x}|\boldsymbol{\theta},\boldsymbol{\pi},J) = \prod_{i=1}^{I} p(x_i|\boldsymbol{\theta},\boldsymbol{\pi},J) \qquad \text{(b)}$$

For given values of the class parameters, one can calculate the probability that object i belongs to class j by use of Bayes's theorem:

$$p(x_i \in C_j|x_i,\boldsymbol{\theta},\boldsymbol{\pi},J) = \frac{\pi_j\, p(x_i|x_i \in C_j,\theta_j)}{p(x_i|\boldsymbol{\theta},\boldsymbol{\pi},J)} \qquad \text{(c)}$$

The problem of identifying a finite mixture is broken into two parts: determining the classification parameters for a given number of classes and determining the number of classes. Rather than seek the class parameter vectors, $\boldsymbol{\theta}$, and the class probabilities, $\boldsymbol{\pi}$, one seeks the full posterior probability distribution of them. The posterior distribution is proportional to the product of the prior distribution of the parameters $p(\boldsymbol{\theta},\boldsymbol{\pi}|J)$ and the likelihood function $p(\mathbf{x}|\boldsymbol{\theta},\boldsymbol{\pi},J)$.

$$p(\boldsymbol{\theta},\boldsymbol{\pi}|\mathbf{x},J) = \frac{p(\boldsymbol{\theta},\boldsymbol{\pi}|J)p(\mathbf{x}|\boldsymbol{\theta},\boldsymbol{\pi},J)}{p(\mathbf{x}|J)} \qquad \text{(d)}$$

The pseudolikelihood $p(\mathbf{x}|J)$ is simply the normalizing constant of the posterior distribution, obtained by integrating out the classification parameters — in effect, treating them as "nuisance" parameters:

$$p(\mathbf{x}|J) = \iint p(\boldsymbol{\theta},\boldsymbol{\pi}|J)p(\mathbf{x}|\boldsymbol{\theta},\boldsymbol{\pi},J)\,d\boldsymbol{\theta}\, d\boldsymbol{\pi} \qquad \text{(e)}$$

To solve the second half of the classification problem (determining the number of classes), one calculates the posterior distribution of the number of classes J. This is proportional to the product of the prior distribution $p(J)$ and the pseudolikelihood function $p(\mathbf{x}|J)$.

$$p(J|\mathbf{x}) = \frac{p(J)p(\mathbf{x}|J)}{p(\mathbf{x})} \qquad \text{(f)}$$

In principle, one can determine the most probable number of classes by evaluating $p(J|\mathbf{x})$ over the range of J for which the prior $p(J)$ is significant. In practice, the multidimensional integrals of equation (e) are computationally intractable, and one must search for the maximum of the function and approximate it about that point. The search and approximate integration are performed by the AutoClass algorithm. The complete problem involves starting with a random number of classes, searching to find the best class parameters for that number of classes, approximating the integral to find the relative probability of that number of classes, and then repeating the procedure with a possibly different number of classes. The number of classes J used in each repetition is chosen to be a random variation on the J's of the best previous repetitions; i.e., the ones with the highest approximated pseudolikelihoods $p(\mathbf{x}|J)$.

AutoClass uses a Bayesian variant of Dempster's and Laird's EM algorithm to find the best class parameters for a given number of classes [the maximum of equation (d)]. To derive the algorithm, one differentiates the posterior distribution with respect to the class parameters and equates the derivative to zero. This yields a system of nonlinear equations that are solved iteratively. At the end of these iterations, classes with a negligible probability π_j can be ignored, since models in which a class has negligible probability are always less probable than are models that simply omit that class.

A robust Lisp implementation of AutoClass was applied to the IRAS low-resolution spectral database, and found many new and interesting classes; results are available in NASA Reference Publication 1217.

This work was done by John Stutz of **Ames Research Center**, *Peter Cheeseman of RIACS, Will Taylor and Robin Hanson of Sterling Software, and Matthew Self of NEXT. For further information, Circle 71 on the TSP Request Card.*
ARC-12797

Method Accelerates Training of Some Neural Networks

Three-layer networks can be trained faster under some circumstances.

Lyndon B. Johnson Space Center, Houston, Texas

A procedure that accelerates the training of an artificial neural network under some circumstances is based on a modified version of the back-propagation method. The procedure is applicable to a three-layer (input, hidden, and output layers) network. The synaptic-connection weights obtained at the end of the procedure are compatible with (though not necessarily the same as) those obtained by unmodified back propagation. Preliminary studies indicate that the synaptic-connection weights produced by this procedure offer some statistical advantages over those produced by unmodified back propagation.

The procedure can be used to train the network in less time than in an unmodified back-propagation procedure, provided that the following two conditions are satisfied: (1) the numbers of neurons in the layers are such that the majority of the work is done in the synaptic connections between the input and hidden layers, and (2) the number of neurons in the input layer is at least as great as the number of training pairs of input and output vectors.

The procedure is as follows:

1. Initialize the synaptic-connection weights between the hidden and output layers in the usual manner to avoid numerical traps near zero and infinity. Use these weights to initialize the activation matrix.
2. Use the unmodified back-propagation procedure to update the synaptic-connection weights and calculate the presynaptic error signals, e_j (j =1 to n_2, where n_2 = the number of neurons in the hidden layer).
3. Update the coefficients $c_{j,k}$ from the tth to the t+1st iteration by
$$c_{j,k}(t+1) = c_{j,k}(t) - \alpha e_j$$
where the $c_{j,k}$ are used to compute the vector $\mathbf{W}_j$ of synaptic-connection weights between the jth neuron in the hidden layer and the neurons of the input layer according to
$$\mathbf{W}_j = \sum_k c_{j,k}\mathbf{V}_k$$
where $\mathbf{V}_k$ is the kth input vector, and α is a positive constant called the "learning rate."
4. Update the entire activation matrix from the tth to the t+1st iteration by
$$A_{k',j}(t+1) = A_{k',j} - \alpha p_{k',k}e_j$$
where $A_{k,j}$ denotes the activation of the jth hidden element in response to the kth input vector, j ranges from 1 to n_2, k' ranges from 1 to the number of training pairs of input and output vectors, and $p_{k',k}$ is the matrix of inner products of all pairs of input vectors.

The major attraction of this procedure lies in its ability to reduce the cost of training in some cases. In addition, the vectors of synaptic-connection weights produced by this procedure are guaranteed to lie in a subspace that is orthogonal to the anticipated noise components.

This work was done by Robert O. Shelton of **Johnson Space Center**. *For further information, Circle 99 on the TSP Request Card.*

This invention is owned by NASA, and a patent application has been filed. Inquiries concerning nonexclusive or exclusive license for its commercial development should be addressed to the Patent Counsel, Johnson Space Center [see page 18]. Refer to MSC-21625.

Books and Reports

These reports, studies, handbooks are available from NASA as Technical Support Packages (TSP's) when a Request Card number is cited; otherwise they are available from the National Technical Information Service.

Decoupling Control for Oblique-Wing Airplane

Control interactions would be decoupled by feedforward and feedback.

A NASA technical memorandum proposes a procedure for the mathematical synthesis of control signals proportional to the commanded deflections of the rudder, elevators, and ailerons of an oblique-wing airplane. The procedure is designed to generate signals that compensate for the aerodynamical and inertial cross-coupling among the yawing, pitching, and rolling motions in the oblique-wing configuration; that is, with a properly designed control system, the command for each such motion produces only that motion and not the other two.

The synthesis is based on the concept of real-model following, according to which the controls force the airplane to respond as an ideal mathematical model of the airplane would respond to commands from the pilot. The model dynamics are simulated in the flight computer, and the airplane-control signals are generated from a combination of commands, model states, and measured airplane attitude angles and rates of change of these angles. In essence, the pilot controls the computer, and the computer controls the airplane.

The feedforward gains chosen are those that would cause the airplane to follow the model perfectly under conditions reported in a previous paper. Even though perfect-model-following conditions are not attainable in practice, the use of perfect-model-following feedforward gains can restrict the error between the model and the airplane to a small region of state space.

The feedback gains are obtained through eigensystem assignment, based on the interpretation of performance specifications in terms of desired closed-loop eigenvalues and eigenvectors. The experimental data on the handling qualities of the airplane can be used to obtain the desired locations of the poles in the complex-frequency plane. Using rules derived by previous authors, eigenvalues and the associated eigenvectors are selected and partitioned into specified and unspecified components.

Multiple Pages Intentionally Left Blank

The procedure was used to synthesize control signals in a computer simulation, based on linearized equations of motion, of the oblique-wing airplane. The simulated system was then tested in terms of the response to the application of a 1-degree elevator (pitch) or aileron (roll) command for 2 seconds. The open-loop (controls applied without decoupling) response to the pitch command included a significant yaw rate and roll angle, indicating significant cross-coupling. Similarly, the open-loop response to the roll command included pitch and yaw rates. However, in the closed-loop (decoupling) condition, cross-coupling was nearly eliminated, and the system followed the desired model closely.

This work was done by Robert W. Kempel and Joseph W. Pahle of **Ames Research Center** *and Gurbux S. Alag of Western Michigan University. Further information may be found in NASA TM-86801 [N86-26339], "Decoupling Control Synthesis for an Oblique-Wing Aircraft."*

Copies may be purchased [prepayment required] from the National Technical Information Service, Springfield, Virginia 22161, Telephone No. (703) 487-4650. Rush orders may be placed for an extra fee by calling (800) 336-4700.
ARC-11751

Progress Toward Automated Cost Estimation

Continuing efforts to integrate ACE with CAD are described.

A report discusses continuing efforts to develop a standard system of automated cost estimation (ACE) combined with computer-aided design (CAD). The obvious advantage of such a system is that time can be saved and accuracy enhanced by automating the extraction of quantities from design drawings, the consultation of price lists, and the application of cost and markup formulas. An integrated CAD/ACE system would not only make it easier to arrive at cost-effective designs but would also decrease the cost of the cost-estimation process itself.

Following introductory remarks, the report summarizes the background and history of CAD/ACE from the year 1963 to the time of the report (April 1990). The story begins with the use of computers in designing, planning, and scheduling the construction of the Vertical Assembly Building at Kennedy Space Center — the largest building in the world at the time of construction. It continues through early efforts to introduce computer cost-estimating systems, the lessons learned in those efforts, and the evolution of criteria for the development of an ideal integrated CAD/ACE system.

The history includes specific examples of the use of computers in estimating the costs of large projects, with ever increasing refinement and attention to detail, illustrating the development of increasingly sophisticated CAD/ACE. Examples of present cost-estimating practices and computer cost-estimating systems illustrate the current state of the art. Anticipated future practices and computer systems being developed to implement them are described briefly.

The report concludes with a summary list of problems, difficulties, and challenges in the further development of CAD/ACE. The list includes such items as the need for (and obstacles to) standardization, the difficulties of extracting ACE data from CAD data, training users, the need to make CAD/ACE easier to use, the high initial cost, the need for customization, and the need for a totally integrated CAD/ACE software and hardware.

This work was done by Joseph A. Brown of **Kennedy Space Center**. *To obtain a copy of the report, "The Challenges in Development of Automatic CAD for Government and Aerospace Construction Cost Estimating Systems," Circle 1 on the TSP Request Card.*
KSC-11578

New on the Market

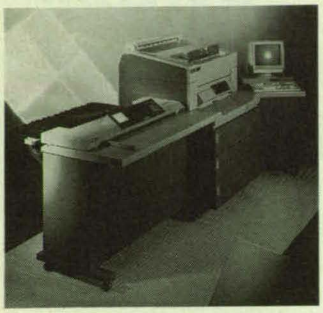

The industry's first **laser copier/plotter** system has been introduced by Océ-Bruning Inc., Itasca, IL. The multifunctional 7700D features high copy quality at 400 DPI, fast throughput of 12 D-size copies per minute, and up to 999 copies from a single scan. It can plot CAD drawings from a variety of host output formats including HPGL, CALCOMP 906/907, and VERSATEC RASTER. An advanced image editing system provides on-line cut and paste options, including mirror imaging and image overlay, deleting, and shift.
Circle Reader Action Number 782.

Digital Equipment Corp., Maynard, MA, has announced the Alpha **open computing architecture**. Intended to serve as the foundation for the company's computing technology into the next century, Alpha is a 64-bit RISC architecture optimized for speed, engineered to support multiple operating systems, and designed to increase performance by a factor of 1000 over its anticipated 25-year life. Digital has released the first Alpha product, the 21064-AA microprocessor, a .75 micron CMOS-based super-scalar, super-pipelined process using dual instruction issue and a 150 MHz cycle time.
Circle Reader Action Number 800.

BICC-VERO Electronics, Hamden, CT, has introduced a cost-effective six-layer **VMEbus monolithic backplane** for high-volume, medium-to-high performance applications. All-stripline construction provides low crosstalk levels, good protection against ground bounce, and a 125A capability on the 5 v planes.
Circle Reader Action Number 796.

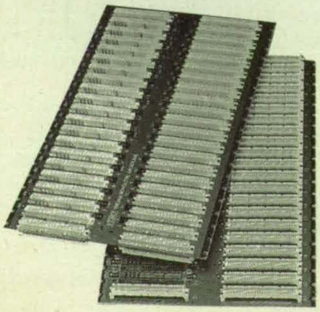

The new I-Step **motor controller** developed by Anorad Corp., Hauppauge, NY, uses a smoothed trapezoidal velocity profile and resonant frequency instability compensation to maximize torque and velocity. Available in single- and multi-axis configurations, the module combines a programmable indexer with a high-efficiency, bi-polar PWM drive that operates directly from 115 or 240 vac. Advantages include use of a software language to allow step/servo interchangeability and dual servo amplifiers to control the two-phase step motor.
Circle Reader Action Number 784.

Vicon Industries Inc., Melville, NY, has introduced a 24-hour time-lapse **videocassette recorder**. It features two time-lapse recording modes (12 and 24 hours) and two continuous modes (two and six hours), all of which offer audio recording and playback. The screen displays time, date, day, recording mode, alarm number and incidents, and power outages.
Circle Reader Action Number 786.

A novel measurement technology from Rosemount Inc., Burnsville, MN, uses **infrared radiometry** to detect windshear and clear air turbulence (CAT) encountered by aircraft. The Windshear/CAT Prediction System uses forward-looking infrared to measure air temperature and water vapor concentrations in front of the aircraft. It provides warning of windshear events, including wet and dry microbursts, and CAT four to six minutes before an encounter.
Circle Reader Action Number 780.

Interpoint Corp., Redmond, WA, has announced a line of **DC-DC converters** with a power density rating of 70 watts per cubic inch. The converters provide up to 100 watts of output power in a case measuring just 2.5" x 1.5" x .38". An advanced magnetics control system called Asymmetrical Power Transfer minimizes losses in the transformer.
Circle Reader Action Number 778.

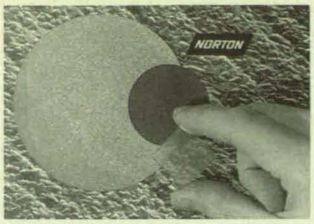

Freestanding "white" **diamond wafers** are available from Norton Co., Northboro, MA, in sizes up to 4 inches in diameter and 1 millimeter thick. White diamond, the purest form of diamond manufactured by the chemical vapor deposition process, offers improved optical and thermal management performance characteristics. The wafers are suited for infrared and microwave windows applications, where transparency is desired, and for heat sinks and electronic substrates, where thermal conductivity is critical.
Circle Reader Action Number 798.

The PGL ToolKit from AnSoft Inc., Laurel, MD, is a set of **graphics libraries** for generating high-resolution printer output. The software provides support for six major programming languages: C, BASIC, Pascal, FORTRAN, Clipper, and ASSEMBLY, as well as 32-bit support for C and FORTRAN. The libraries can stand alone or be integrated with screen graphics libraries such as Borland BGI and Microsoft Graphics. PGL ToolKit sells for $195.
Circle Reader Action Number 788.

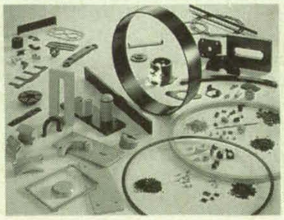

Du Pont's new Vespel ST **polyimides** offer ultra-high operating temperatures, low friction and wear, and excellent creep resistance. They can operate to 315° C, with excursions to 540° C. The parts have higher tensile strength, better hydrolytic stability, and greater chemical resistance than the previous generation of polyimides and can be applied in aircraft engines, industrial machinery, glass bottle production, and laboratory instruments.
Circle Reader Action Number 774.

The first **optical tape recorder** has been announced by Metrum Information Storage, Denver, CO. The new HD-1000 can store 1 terabyte (1000 gigabytes) of data on a single reel of optical tape, equivalent to the storage capacity of 5000 magnetic tapes or 2000 5-1/4" optical disks. Potential applications include telemetry and satellite downloading, storing and transcribing large data files, remote sensing, and medical and geophysical imaging.
Circle Reader Action Number 792.

Applied Electron Corp.'s Quantrad Sensor Division, Santa Clara, CA, has designed an innovative **liquid analyzer** for the detection and spectroscopic identification of radioactive particles in liquids. The system employs proprietary silicon detector technology and a unique sensor design that allows alpha-particle-emitting radionuclides to attach themselves to the face of the detector, yielding spectroscopic identification of the radioactive isotope. The system features a multichannel analyzer workstation operating under Microsoft Windows 3.0 for data acquisition and analysis.
Circle Reader Action Number 790.

Export Hotline, an information service to help US businesses launch or expand their **export sales,** has been introduced by AT&T and several multinational corporations. Supported by the US Department of Commerce, the 24-hour fax information retrieval system offers access to a database of current information on 50 key industries of all major US trading partners. The typical report is 5-10 pages long and includes details on trade issues, investment incentives and barriers, key contacts, and shipping. The only expense to the user is the fax charge.
Circle Reader Action Number 794.

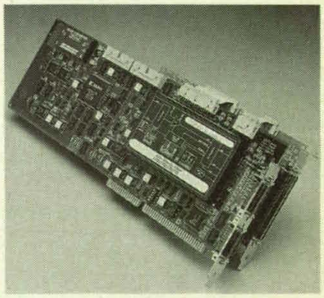

The DT2839 **analog and digital I/O board** and DT2896 **96-channel expander board** from Data Translation Inc., Marlboro, MA, are optimized for sampling from 1 to 224 input channels at very high speeds (224 kHz to 1 MHz). They can be configured to sample 32 inputs at an aggregate rate of 416 kHz for aerospace, automotive, and neuroscience applications. Control features include analog threshold triggering to start acquisition and variable scan to automatically sample different channels at different rates.
Circle Reader Action Number 776.

New on the Market

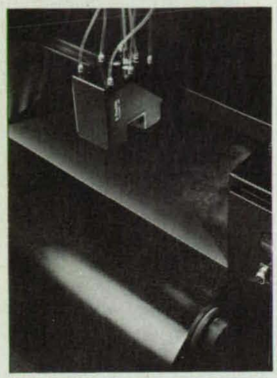

A new series of low-cost **infrared line scanners** from Raytek Inc., Santa Cruz, CA, provides uniform temperature analysis and closed-loop control of continuous flow processes. The Thermalert Multipoint series features accurate and dependable noncontact sensing, measuring up to 256 points per scanned line, 10 lines per second, across a 90 degree field of view. It is suited for temperature maintenance in continuous flow web processing of plastics, glass, metals, or textiles.
Circle Reader Action Number 768.

GW Instruments, Somerville, MA, has announced two new **speech and sound analysis** products: SoundScope/16, which turns a Macintosh II series computer into a CD-quality 16-bit stereo sound workstation; and SoundScope/8, a low-cost, 8-bit version for use with entry-level Macintosh computers. Both allow the user to record, play, edit, and view time waveforms and spectrograms, compute frequency spectra and linear predictive coding, add pertinent notes, and create custom displays.
Circle Reader Action Number 760.

Sony Corp. of America, Park Ridge, NJ, has introduced an extremely small and lightweight four-channel **GPS receiver** for military applications. The IPS-360 PYXIS™ receiver calculates 3D position fixes indicating the user's precise latitude, longitude, altitude, and velocity. It operates in real time anywhere in the world.
Circle Reader Action Number 770.

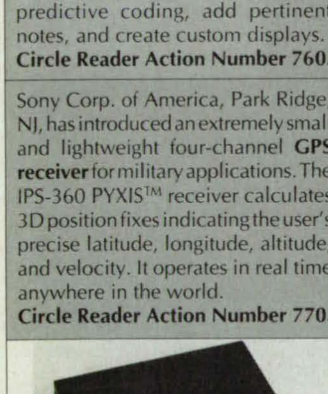

HEM Data Corp., Southfield, MI, has released Snap-Master Analysis software for Microsoft Windows 3.0 and 3.1. A stand-alone **analysis package** for engineers and scientists, it includes arithmetic, trigonometric, logarithmic, and statistical functions, as well as auto- and cross-correlation, smoothing, three types of differentiation, and five types of integration. Snap-Master's "Equation Builder" allows the user to construct simple or complex equations by pointing and clicking on the information needed. A simple tabular format assists the user in defining and storing constants, equations, and algorithms.
Circle Reader Action Number 772.

The PCI-20501C **data acquisition boards** from Intelligent Instrumentation, Tucson, AZ, are the first to provide multifunction analog and digital I/O capabilities on one EISA-standard board. Features include eight single-ended, 12-bit analog inputs; 1 MHz sample rate; 16 digital I/O channels; and two DMA channels capable of one million transfers per second. The boards are suited for complex process automation, machine-health monitoring, vibration analysis, and audio processing.
Circle Reader Action Number 766.

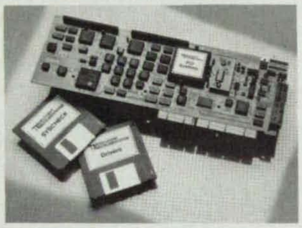

Hewlett-Packard Co., Palo Alto, CA, has released **software that can quadruple in-circuit throughput** on HP 3070 board-test systems without additional hardware. The new software, called HP Throughput Multiplier, allows users to test multiple, loaded printed-circuit boards simultaneously. Cost and time savings are achieved through a modular board-test system architecture that permits four testheads in a single system.
Circle Reader Action Number 764.

The CHASE NFPS1 **near-field probe set** from IBEX Group Inc., Somerville, NJ, is a complete diagnostic electromagnetic interference (EMI) probe kit for electrical and mechanical applications. The kit features three handheld probes, two magnetic and one electric, covering the frequency range of 9 kHz to 1 GHz. Used in conjunction with a spectrum analyzer or measuring receiver, these probes locate and qualify EMI sources, yielding repeatable results.
Circle Reader Action Number 762.

New Literature

Vacuum fluorescent, liquid crystal, and DC plasma displays are featured in a product selection guide from IEE, Van Nuys, CA. It contains charts illustrating differences between popular **display technologies** such as cost, power requirements, and ruggedness. Also covered are IEE's interactive touch panels, mini-terminals, and data interfaces.
Circle Reader Action Number 720.

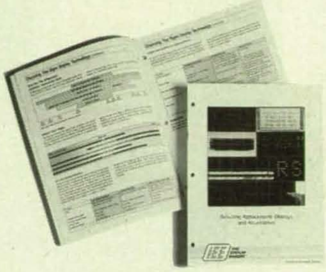

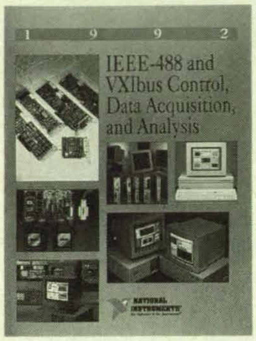

National Instruments, Austin, TX, has published its 1992 catalog of software and hardware products used to develop **test, measurement, and instrumentation systems** for automating aerospace engineering and manufacturing applications. The 544-page catalog offers plug-in PC data acquisition boards, GPIB and VXI/MXI instrumentation interfaces, and signal conditioning accessories for incorporation into custom systems on PC/XT/AT, Macintosh, Sun, DEC, and other platforms. Also featured is the company's application software, including LabVIEW 2, Lab Windows, and Measure.
Circle Reader Action Number 712.

EAR Specialty Composites, Indianapolis, IN, has published an overview of the materials and technology used to **solve noise, vibration, and impact energy problems** in OEM product designs. The eight-page brochure outlines strategies for energy-control problems ranging from limiting excessive noise and vibration in trucks to meeting high shock absorption and cushioning requirements in sporting goods.
Circle Reader Action Number 708.

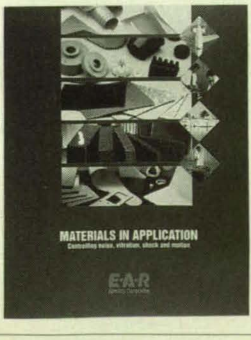

The new GPM series of **DC servo motors** is showcased in a brochure from IMC Magnetics Corp., Westbury, NY. The motors use a high-performance printed armature to achieve a thin profile package, high start/stop rates, and no cogging throughout the motor's speed range. The brochure provides mechanical, thermal, and electrical performance specifications for models ranging from 1" long/32 watts to 1.3" long/164 watts.
Circle Reader Action Number 706.

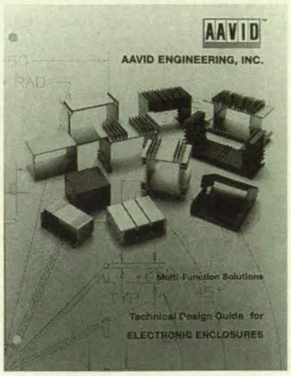

A new brochure offering technical assistance in designing aluminum **electronic enclosures** has been released by Aavid Engineering Inc., Laconia, NH. The publication offers methods of reducing packaging costs, improving product appearance, and extending system life. Layouts for multi-functional enclosures emphasize mechanical and thermal characteristics.
Circle Reader Action Number 710.

The ***Fiber Optic Data Communications Forecast*** released by ElectroniCast Corp., San Mateo, CA, predicts strong growth for the industry through the 1990s. North American consumption of fiber optic components in data communications is expected to expand 13% per year, from $453 million in 1991 to $823 million by 1996. The study addresses declining military deployment of fiber optic data links, increasing use of FDDI networks and high data rate lines, and trends in cable value share and distribution channels.
Circle Reader Action Number 726.

Free subscriptions to *Linear Technology* magazine are available from Linear Technology Corp., Milpitas, CA. The latest issue provides advice on designing with the new LT1158 low-voltage, half-bridge N-channel **MOSFET driver IC**. It also discusses micropower A/D converters, high-efficiency regulators, a 12-bit data acquisition system, and a DC-accurate Butterworth lowpass filter that requires no on-board clock.
Circle Reader Action Number 716.

A full-color brochure describes **aerospace manufacturing services** available from Parkway Products Inc., Cincinnati, OH, including injection molding, secondary machining, assembly, and composite bonding. Parkway specializes in molding jet engine and flight hardware assemblies.
Circle Reader Action Number 702.

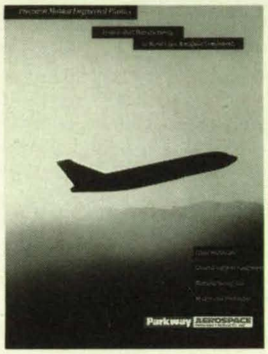

A short-form catalog of **automation components**, published by Aromat Corp., New Providence, NJ, features laser analog sensors, triple-beam photoelectric sensors, multi-function timers, counters, limit switches, relays, and starters. Operating speed, resolution, dimensions, and operating power and life are described, along with examples of applications and installation instructions.
Circle Reader Action Number 722.

Tolo Inc., Santa Ana, CA, has released a brochure highlighting its capabilities to design and fabricate metallic and nonmetallic aerospace structures. Tolo's manufacturing technologies include six-axis, robotically-controlled, high-pressure abrasive waterjet equipment for precision cutting; automatic and robotic welding machines; and superplastic forming capabilities.
Circle Reader Action Number 724.

A 38-page catalog from Solitech, St. Louis, MO, features a full line of **electronic power and logic controls**, including SCRs up to 1200 amps/600 volts and microprocessor-based sequencers and solid-state relays up to 100 amps/480 volts. Solitech also offers sub-panel mount on/off or proportional controls with optional digital displays, and RTD and thermistor sensors.
Circle Reader Action Number 704.

A free brochure from Illbruck Inc., Minneapolis, MN, details the features and applications of ProSPEC Pyramid **acoustical foam**. The foam is a cost-effective means of controlling sound in noisy office and industrial plants. Available in 2' x 2' sheets and 2" to 6" thicknesses, the foam offers a seamless appearance and is easy to apply.
Circle Reader Action Number 714.

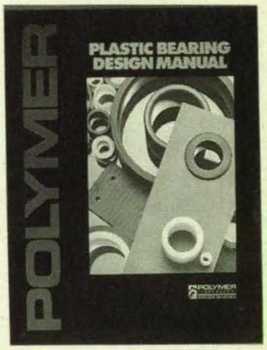

Polymer Corp., Reading, PA, has released a 20-page **plastic bearing design** manual. A training tool and design worksheet, the manual offers a basic review of thermoplastic design considerations. Property data and standard stock shapes of Polymer Corp. bearings and wear materials are included.
Circle Reader Action Number 718.

Literature from Wiltron Co., Morgan Hill, CA, introduces three RF models to the 5400A family of **scalar measurement systems**. The new models provide synthesizer/sweeper accuracy and frequency coverage from 1 to 1000 MHz, 1 to 2000 MHz, and 1 to 3000 MHz. The 20-page publication includes specifications and shows how this scalar analyzer provides a cost-effective solution for high-volume production testing.
Circle Reader Action Number 728.

Subject Index

(Continued on page 105)

(Continued from page 105)

(Continued on page 106)

Subject Index *(continued from page 105)*

ADVERTISERS INDEX

***RAC** stands for **Reader Action Card.** For further information on these advertisers, please circle the RAC number on the Reader Action Card in this issue. This index has been compiled as a service to our readers and advertisers. Every precaution is taken to insure its accuracy, but the publiser assumes no liability for errors or omissions.

NASA Tech Briefs, ISSN 0145-319X, USPS 750-070, copyright © 1992 in U.S., is published monthly by Associated Business Publications Co., Ltd., 41 E. 42nd St., New York, NY 10017-5391. The copyrighted information does not include the (U.S. rights to) individual tech briefs which are supplied by NASA. Editorial, sales, production and circulation offices at 41 East 42nd Street, New York, NY 10017-5391. Subscription for non-qualified subscribers in the U.S., Panama Canal Zone, and Puerto Rico, $75.00 for 1 year; $125.00 for 2 years; $200.00 for 3 years. Single copies $10.00. Foreign subscriptions one-year U.S. Funds $150.00. Remit by check, draft, postal, express orders or VISA, MasterCard, and American Express. Other remittances at sender's risk. Address all communications for subscriptions or circulation to NASA Tech Briefs, 41 East 42nd Street, New York, NY 10017-5391. Second-class postage paid at New York, NY and additional mailing offices.
POSTMASTER: please send address changes to NASA Tech Briefs, 41 East 42nd Street, Suite 921, New York, NY 10017-5391